3.

Characterizing the Physical Oceanography of Coastal Waters Off Rhode Island, Part 2: New Observations of Water Properties, Currents, and Waves

Prepared for the Rhode Island Ocean Special Area Management Plan 2010

By

David S. Ullman and Daniel L. Codiga

University of Rhode Island, December 21, 2010

Executive Summary

This report, Part 2 of the physical oceanography characterization, complements Part 1 by presenting new field observations to improve understanding of under-sampled system attributes. Vessel-based surveys spanning the region (Block Island Sound (BIS), Rhode Island Sound (RIS), and offshore) each season capture three-dimensional structure of water properties (temperature, salinity, oxygen, chlorophyll, turbidity) and geographic variations in euphotic depth. Moored instruments reveal temporal variability in water column temperature, salinity, and velocity on timescales from hours to months at four sites: south and southeast of Block Island, on the offshore portion of Cox Ledge at the southern RIS boundary, and in central RIS. A suite of wave parameters measured at those sites, and a fifth site farther offshore, quantifies wave conditions.

Temperature and salinity surveys corroborate the main seasonal and geographic patterns deduced in Part 1. Central RIS stratification undergoes the widest seasonal swings: a sharp mid-depth thermocline due to solar insolation in summer, and homogenous conditions in winter due to surface cooling and wind mixing. In central BIS stronger tidal currents limit peak stratification in the summer, but during winter and spring estuarine exchange with Long Island Sound sustains stronger stratification than in RIS. Shallow areas of BIS and eastern RIS with strong tidal currents remained well mixed. During December 2009 both the survey and moorings revealed a deep intrusion of anomalously warm salty water normally found near the shelf break 100km south. Energetic weather-band currents included strong deep flow advecting the intrusion toward central RIS through the channel between Block Island and Cox Ledge. The intrusion vividly demonstrated a significant deviation from climatological average salinity/temperature ranges.

Monthly-mean currents at the mooring sites provided important additional support for the system-wide circulation patterns put forth in Part 1; observed tidal currents were in very good agreement with earlier findings. Oxygen concentrations were lowest (5-6 mg l^{-1}) in deep north central RIS during periods of stronger stratification, June and September. Chlorophyll levels were highest during September, in BIS and eastern RIS, with maxima typically in subsurface layers. In summer and fall the euphotic depth varied sharply, from ~10 m or less to the north and west of the BIS estuarine outflow water mass boundary to ~40 m offshore of it, and was reduced by high turbidity in December. Waves showed modest geographic variations, with typical significant wave heights of 0.5-2.5 m, typical peak wave periods of 5-10 seconds, and a generally persistent northward component of peak wave direction.

Table of Contents

List of Figures

List of Tables

Abstract

This report, Part 2 of the physical oceanography characterization, complements Part 1 by presenting new field observations to improve understanding of under-sampled system attributes. Vessel-based surveys spanning the region (Block Island Sound (BIS), Rhode Island Sound (RIS), and offshore) each season capture three-dimensional structure of water properties (temperature, salinity, oxygen, chlorophyll, turbidity) and geographic variations in euphotic depth. Moored instruments reveal temporal variability in water column temperature, salinity, and velocity on timescales from hours to months at four sites: south and southeast of Block Island, on the offshore portion of Cox Ledge at the southern RIS boundary, and in central RIS. A suite of wave parameters measured at those sites, and a fifth site farther offshore, quantifies wave conditions.

Temperature and salinity surveys corroborate the main seasonal and geographic patterns deduced in Part 1. Central RIS stratification undergoes the widest seasonal swings: a sharp mid-depth thermocline due to solar insolation in summer, and homogenous conditions in winter due to surface cooling and wind mixing. In central BIS stronger tidal currents limit peak stratification in the summer, but during winter and spring estuarine exchange with Long Island Sound sustains stronger stratification than in RIS. Shallow areas of BIS and eastern RIS with strong tidal currents remained well mixed. During December 2009 both the survey and moorings revealed a deep intrusion of anomalously warm salty water normally found near the shelf break 100km south. Energetic weather-band currents included strong deep flow advecting the intrusion toward central RIS through the channel between Block Island and Cox Ledge. The intrusion vividly demonstrated a significant deviation from climatological average salinity/temperature ranges.

Monthly-mean currents at the mooring sites provided important additional support for the system-wide circulation patterns put forth in Part 1; observed tidal currents were in very good agreement with earlier findings. Oxygen concentrations were lowest (5-6 mg l^{-1}) in deep north central RIS during periods of stronger stratification, June and September. Chlorophyll levels were highest during September, in BIS and eastern RIS, with maxima typically in subsurface layers. In summer and fall the euphotic depth varied sharply, from ~10 m or less to the north and west of the BIS estuarine outflow water mass boundary to ~40 m offshore of it, and was reduced by high turbidity in December. Waves showed modest geographic variations, with typical significant wave heights of 0.5-2.5 m, typical peak wave periods of 5-10 seconds, and a generally persistent northward component of peak wave direction.

1 Purpose and Scope

The purpose of this report is to present new observations collected to characterize water properties, currents, and waves in the Rhode Island Special Area Management Plan (OSAMP) region. This is Part 2 in a two-part series and complements the review of previously gathered information in Part 1 (Codiga and Ullman 2010). These new observations expand on prior investigations through use of modern measurement techniques and by exploring geographic areas that have, as described in Part 1, received almost no previous attention. For water properties, the emphasis is on geographic (Figure 1) and vertical structure, and seasonal changes. For currents, the emphasis is on descriptions of tidal fluctuations, weather-band variability (changes on timescales of about 1 to 10 days), as well as monthly means and longer-term means. The analysis examines and compares time series of vertical profiles of water properties and currents from four locations (Figure 2), chosen to be representative of the range (across the SAMP region and its important bounding water bodies) of water depths, tidal currents, distance from shore, and distance from freshwater input. Surface wave parameters are described from those sites, and one site farther offshore (Figure 2). The reader is referred to Part 1 (see, in particular, Figures 1 and 2 of Codiga and Ullman 2010) for overall context, including descriptions of the geographic and bathymetric setting, and a map with geographic place names labeled.

In addition to temperature, salinity, and density, the water properties analysis includes measurements of dissolved oxygen, Chlorophyll fluorescence, turbidity, and euphotic zone depth based on vertical profiles of photosynthetically active radiation measurements; while the latter four quantities are described briefly here, for more complete discussion of their implications to biological and sediment transport processes the relevant companion OSAMP reports should be consulted. Similarly, while our analysis presents wind measurements, it does so solely for context in interpreting currents; for a comprehensive description of winds reference should be made to the OSAMP studies dedicated to winds. Tidal and weather-band fluctuations in sea level are addressed here but the durations of the observations do not permit us to address climatic change in sea level, which is taken up in a separate OSAMP document. Finally, it should be noted that the treatment of wave observations here is cursory because a companion OSAMP report includes a more thorough investigation of wave processes based on both these observations and an intensive modeling effort.

2 Introduction

Temperature and salinity characteristics across sizable portions of the OSAMP domain, particularly eastern Rhode Island Sound (RIS), are historically severely under-sampled. This was made clear by the review of available observations in Part 1, and was a primary motivation for the seasonal series of vessel-based conductivity-temperature-depth (CTD) surveys completed and described here. In order to capture vertical structure and geographic patterns, the surveys include profiles spanning the water column at stations covering the entire OSAMP domain with nominal spacing of 8-12 km (Figure 1). The station grid is nearly identical to that used in Part 1 for explorations of historical observations and model outputs, so facilitates direct comparisons. The goal of the surveys was to characterize the seasonal cycle, so one 2-3 day survey was completed in each of September 2009, December 2009, March 2010, and June 2010. In addition to temperature and salinity the surveys measured water properties relevant to biological and sediment transport processes: dissolved oxygen, Chlorophyll fluorescence, turbidity, and photosynthetically active radiation. The maps and sections presented here using these quantities are a considerable advance over previously available observations.

A series of deployments of moored instrumentation captured temporal variability of temperature, salinity, currents and waves on timescales from hours to seasons, in order to complement the broad geographic coverage but minimal temporal resolution and of the vessel-based water property surveys. Moored instruments sampled five sites (Figure 2, Table 1).

At two sites, moorings instrumented with a suite of water-column sensors (temperature, salinity, currents), accelerometers to measure wave properties, and meteorological sensors (winds, temperature, pressure) were maintained continuously year-round starting in October 2009. The deployments were carried out by University of Maine under subcontract, as part of the Northeastern Regional Association of Coastal Ocean Observing Systems (NERACOOS), and data were delivered and distributed in real time. These two moorings are denoted MD-S and MD-F; MD indicates Multi-Disciplinary (both oceanographic and meteorological parameters were sampled), S indicates the site is in RI state waters south of Block Island, and F indicates the site is in federal waters in southeastern RIS. The MD-S site was south of Block Island by about 8 km; the MD-F site was south of eastern RIS at a latitude similar to that of MD-S.

To provide improved understanding of geographic variations of temporal evolution of in water-column structure of physical oceanographic characteristics (temperature, salinity, currents, wave attributes), moored instruments were deployed at two additional sites that complement

MD-S and MD-F. One site was located about 10 km southeast of MD-S, to help characterize the transition toward deeper water. The second site was located about 15 km north-northwest of MD-F, to help understand how properties change inshore of MD-F towards central RIS. At these complementary sites, only physical oceanographic parameters were sampled, hence they are referred to as PO-S and PO-F respectively. Note that, despite its name, the PO-S site is not in state waters. The PO-S and PO-F moorings were maintained for two deployments, one in late Fall 2009 (denoted FA09) and one in late Spring 2010 (denoted SP10), since year-round sampling was not possible given budgetary and logistical constraints. As these instruments were not intended for real time sampling, they recorded and stored data internally.

At a fifth site the Army Corps of Engineers established a Datawell directional wave buoy, denoted the Block Island Wave Buoy (BIWB) although it is located offshore from central RIS. It has operated continuously since October 2009 and its real-time data stream is managed by the Coastal Data Information Program (CDIP) at Scripps Institution of Oceanography.

3 Methods

3.1 Vessel-Based Water Properties Surveys

Four vessel-based surveys, at approximately 3-month intervals covering the seasonal cycle, were carried out from the University of Rhode Island's research vessel Hope Hudner. The station grid (Figure 1) extends across eastern Block Island Sound (BIS), RIS, and the offshore area to the south. Surveys took 2-3 days to complete (see Table 2 for the survey dates) and were made without regard to tidal phase. During the December 2009 survey, not all stations were occupied due to weather conditions; the omitted stations are clear in the maps presented below.

At each station, vertical profiles of electrical conductivity (C), temperature (T), pressure (P), oxygen concentration (O_2), chlorophyll fluorescence, turbidity, and photosynthetic active radiation (PAR) were obtained using a hand-lowered package. The sensors included a SeaBird Electronics SBE 19plus CTD, with T, C, and O_2 (SBE 43) sensors located within a pumped duct; a Turner Designs 2-channel SCUFA 2000-007 Fluorometer measuring chlorophyll and turbidity; and a BioSpherical QSP2300 PAR sensor.

The data were processed using SeaBird's data processing software (SBE Data Processing), including corrections for sensor alignment, conductivity cell thermal mass, and the response time of the O_2 sensor. Salinity was computed from the measured C, T, and P data, and all variables were averaged into 1 dbar (~1m) vertical bins. Chlorophyll fluorescence measurements were converted to chlorophyll concentrations using a generic calibration. Turbidity, a measure of the scattering of light by suspended particles in the water, was estimated from measurements of the 90^{o} scattering of light from the fluorometer's light source using the manufacturer's calibration. The vertical profiles of PAR were used to estimate the light extinction coefficient by fitting the observed data to an exponential function: $I(z) = I_0 e^{-kz}$, where $I(z)$ is light intensity at depth z, I_0 is the intensity at the surface (z=0), and k is the extinction coefficient (units m^{-1}). For profiles where the CTD was not shaded by the survey vessel at the surface, the fits were performed using observations from the surface down to a depth at which the sensor response was observed to roll off. When the CTD was shaded near the surface, the upper 5-10 m of the profile was omitted from the fit. The depth of the euphotic zone was estimated as the depth at which the light intensity was 1% of the surface value (I_0).

3.2 MD-S and MD-F Moored Instrumentation

On the MD-S and MD-F moorings the subsurface instrumentation (Table 1) included three CTDs, a 2m-deep Aanderaa 3429 current/temperature sensor recording once per hour, and a downward-looking Teledyne RD Instruments 600 kHz acoustic Doppler current profiler (ADCP) that sampled each meter from 5 m deep to within 3-4 m of the seafloor using 6-second ping interval for 8 minutes once an hour. The CTDs were SeaBird Electronics 37 Series; one mounted on the buoy sampling each 30 minutes, one on the mooring wire in the upper water column, and one on the wire nearest the seafloor, the latter two sampling each 60 minutes and sending their data inductively to a coupler at the top of the wire rope. Wave parameters were measured by a Summit 34103A accelerometer package on the buoy operating at 2 Hz for a 17-minute interval each 30 minutes. The meteorological package included redundant Gill WindSonic wind sensors at 4m above sea level, and a Campbell 107L temperature sensor and Setra 270 barometric pressure sensor both at 3m above sea level.

3.3 PO-S and PO-F Moored Instrumentation

During each period (FA09 and SP10) a mooring instrumented with 7 CTD sensors distributed through the water column was deployed at each of the two sites, with an upward-looking ADCP in a bottom frame deployed close nearby (within nominally 200 m). The CTDs, measuring pressure as well as temperature and conductivity, consisted of a Falmouth Scientific Instruments NXIC bracketed to the buoy, sampling at 6 Hz for about 10 seconds each 90 seconds, and six SBE-37SM Microcats on the wire rope below sampling once each 16 seconds. After passing the data through a 3 point running median filter to remove spurious values, the CTD data were averaged into 4-minute ensembles.

Each ADCP was a Teledyne RD Instruments 600 kHz deployed and recovered in a Mooring Systems Incorporated bottom frame. They measured currents each meter from about 2-3 m off the seafloor to about 3-4 m below the surface, with pings each 6 seconds and 20-minute ensemble averaging interval. The ADCP measured wave orbital motions and computed significant wave height, peak wave period, and peak wave direction, using a 20-minute burst of 1 Hz sampling each 2 hours.

Sea level perturbations η [units: m] were estimated using bottom pressure p_{bot} [units: dbar] measured by the ADCPs, under the assumption of a water column with constant density ρ [units: kg m^{-3}], as $\eta = p_{bot}/(\rho g)$ for gravitational acceleration g = 9.8 m s^{-2}. For the analysis of subtidal sea level the raw bottom pressures were adjusted, by adding 0.01 x p_{atm} meters to account for the inverse barometer effect, using the average of the atmospheric pressure p_{atm} [units: mbar] measured by the MD-S and MD-F buoys. Subtidal bottom pressure and atmospheric pressure were each treated as deviations relative to their respective record mean.

3.4 BIWB Moored Instrumentation

The BIWB is a Datawell directional buoy measuring significant wave height, peak wave period, and peak wave direction, based on 17-minute bursts of sampling each 30 minutes. Details of the processing are provided at the CDIP website (cdip.ucsd.edu).

3.5 Analysis techniques

Tidal analysis was carried out using the t-tide software package (Pawlowicz et al. 2002) and methods as described in Codiga and Rear (2004). Sub-tidal currents, sea level from bottom pressure, winds, and wave directions were calculated by sub-sampling to 12-hourly values after applying a 25-hour half-width triangle-weight low-pass filter.

4 Results: Water Properties

4.1 Maps and Sections of Water Properties from Vessel-Based Surveys

We present the observations in two forms: (1) maps showing variables at a given depth below the water surface or height above the bottom, and (2) vertical sections along the approximately north-south and east-west lines shown in Figure 1. Although the data are treated as if the stations were sampled synoptically, it should be borne in mind that 2-3 days were required to complete the surveys. Therefore during the course of the sampling some unresolved changes in water properties occurred due to temporal evolution of the processes controlling them, including advection by tidal and subtidal currents.

4.1.1 Temperature

During the late summer (September) hydrographic survey (Figures 3, 4, and 6), near-surface horizontal temperature gradients are generally small. This is in contrast to the observation of a moderately strong temperature front ($\Delta T \sim 1\text{-}2$ °C) separating cooler BIS waters from warmer RIS and offshore waters in the satellite-derived sea surface temperature (SST) climatology developed in Part 1 using all available observations from 2002-2007 (Codiga and Ullman, 2010). The reason for this lack of gradient in the survey data is not clear, but it is possible that the survey period (which was calm, sunny, and hot) was unrepresentative of typical conditions whereby vertical mixing is strong enough to mix heat downwards, thus cooling the surface nearer to BIS. Strong near-bottom horizontal gradients occur generally aligned with the 40 m isobath on the south side of Cox Ledge (southern end of lines NS6 and NS7) and the 30 m and 40 m isobaths south of Block Island. A deep thermocline (~30 m or deeper) is observed in central RIS and in the areas offshore of RIS and BIS, whereas in BIS and north-central RIS there is little vertical temperature structure. Vertical temperature differences range from less than 1.5 °C along the northern edge of the survey region to around 7 °C in the offshore region south of RIS. At the offshore end of line NS7, a thin layer of warm (18-19 °C) water is observed just above the thermocline (~30 m depth). Examination of the corresponding salinity section (Figure 9) shows that this water is saltier than the water above and below, suggesting that this feature is an intrusion of outer shelf water similar to those observed in earlier surveys (e.g. Churchill 1985).

Whereas the late summer survey observed warmer surface water temperatures than deep temperatures, during the early winter (December) survey (Figures 3, 4, and 6), the temperature gradient is reversed with coolest water near the surface and warmest water at depth. Vertical temperature differences range from near zero in BIS and the shallower northern and eastern parts of RIS to 4-5 °C at the offshore end of line NS3 south of Block Island. Near-surface temperatures generally decrease towards the north and east where the shallow water column tends to cool most rapidly in late fall. However, as during summer, near-surface horizontal temperature gradients are weaker than those at depth. Near the bottom, highest gradients occur in the region south of Block Island and in central RIS associated with the edges of a warm patch centered on the deep channel extending northeast into central RIS. Water temperatures at depth in this patch, which appears to be contiguous with offshore deep waters south of Block Island , are greater than 15 °C. Temperatures in this region are anomalously high compared to temperatures during fall (≤13 °C) and winter (≤6 °C) at the seafloor in the hydrographic climatology and the model output examined by Codiga and Ullman (2010). As will be discussed in the next section, this water is also anomalously salty, suggesting outer shelf origin.

During the late winter (March) survey (Figures 3, 5, and 7), the range of observed temperature over the whole region is quite small (range of 2-4 °C over the entire region at all depths) reflecting the homogenization of temperature due to strong surface cooling in winter (and possibly the offshore retreat of the anomalously warm deep water observed in late autumn). Coldest water during this survey was located near the bottom in northeast RIS while warmest temperatures were observed near the surface in the western half of the survey region. The relatively warm surface layer in BIS and western RIS was less than 10 m thick and likely associated with outflow from Long Island Sound (LIS).

The late spring hydrographic survey in June (Figures 3, 5, and 7) shows the re-emergence of strong thermal stratification in the region. Vertical surface to bottom temperature differences range from 2-3 °C in BIS and northeastern RIS to ~10 °C at the offshore edge of the survey region. Surface temperatures in BIS are ~2 °C cooler than surface waters offshore and in RIS, consistent with the SST climatology of Codiga and Ullman (2010). As was seen in the September survey, large gradients in near-bottom temperature occur, but during this survey the high-gradient region is shifted to shallower areas (roughly the 30 m isobath). This shift is probably explained by the shallower surface mixed layer during the June survey compared to September. In this interpretation, the high near-bottom gradients are found where the thermocline intersects the bottom.

4.1.2 Salinity

The salinity field during the September survey (Figures 8, 9, and 11) is dominated by the low-salinity outflow from LIS. Near-surface salinities increase from less than 31 PSU in central/western BIS to greater than 31.5 PSU in central RIS and greater than 32 PSU in offshore areas. Near-bottom salinities increase by roughly the same amount (~1.5 PSU) over the same areas with some indication that the horizontal gradient steepens in the southwest corner of the survey region where the coastal current associated with the LIS outflow onto the continental shelf is known to lie (Ullman and Codiga 2004). Vertical salinity stratification is strongest in northwest BIS where surface to bottom differences of up to 2 PSU occur, and weakest to the east and offshore (except for the westernmost portion of the offshore zone which is influenced by the aforementioned coastal outflow). The shallow area east of Montauk Point, station 31 along line NS1 (Figure 1), is vertically well-mixed during this survey (and appears to be so during the later ones as well). Although salinity generally increases with depth (and distance eastward), the highest salinities in the entire region occur in the thin intrusive feature identified in the temperature data (see section 4.1.1) at about 30 m depth at the offshore end of line NS7. The maximum observed salinity in this intrusion (which is also warmer than water above and below) is approximately 33.5 PSU, which according to the shelfbreak front climatology of Linder and Gawarkiewicz (1998) is outer shelf water found on average on the inshore side of the shelfbreak front, about 100 km offshore.

In the December survey (Figures 8, 9, and 11), observed near-bottom salinities in areas of the survey region with water depth greater than about 35 m are extremely high. Salinity in the deep channel north and west of Cox Ledge is greater than 34 PSU and the peak salinity of greater than 34.5 is observed at the offshore end of line NS3. Note that the offshore station of line NS4 was not sampled during this survey and it is possible that the high salinity core is larger than it appears in Figure 8. Nonetheless, the deep water observed in the December survey is clearly anomalous (compare with peak near-bottom salinities of 33.25 PSU in the fall and winter hydrographic climatology; Codiga and Ullman, 2010). In fact the shelf break front climatology of Linder and Gawarkiewicz (1998) puts the 34.5 isohaline in the center of the front over the shelf break, intersecting the bottom on average at approximately the 100 m isobath. Minimum surface salinity of less than 31 PSU was observed in the December 2009 survey in west/central BIS. This value is approximately the same as the minimum value observed in the September survey, although the areal extent of the low salinity region appears to be somewhat reduced. Examination of the hydrographic climatology surface salinity in west/central BIS (Codiga and Ullman 2010) shows that the observed December values are approximately equal to the climatological values in fall and fresher (by several tenths of a PSU) than the winter values.

Strongest near-surface horizontal salinity gradients in the December survey are observed on the shelf southwest of Block Island (as in September) and also in northeastern RIS. In northeast RIS, on lines NS7 and NS8, a surface-layer front with cross-frontal salinity difference of approximately 0.5 PSU over 10 km is observed (Figure 9). The front weakens slightly in the RIS sections to the west (NS4 – NS6). Vertical surface-bottom salinity differences during the December survey ranges from several tenths of a PSU in BIS (and nearly zero at the station east of Montauk) to ~3 PSU in the offshore regions influenced by the high salinity intrusion discussed above. There is a suggestion, in the upward bowing of deep isohalines in sections EW3 and EW4 (Figure 11), that the deep saline water mass over the northwest corner of Cox Ledge and in the channel to the northwest is being modified by vertical mixing.

The March survey found the deep salinity in the deep central RIS and offshore regions to be greatly reduced from the December values (Figures 8, 10, and 12) indicating the presumed outer shelf water has retreated offshore or been advected alongshore out of the survey region. Maximum salinity during the March survey was ~32.5 PSU while the freshest water, at the surface in west/central BIS, was less than 29.5 PSU, reflecting the increased river inflows during late winter. Near-surface salinities increase rapidly towards eastern BIS and the front between the freshest water and RIS and shelf surface water extends from eastern BIS southwest onto the shelf to the southwest of Block Island. The sloping front on the shelf south of BIS intersects the bottom roughly between the 30 m and 40 m isobaths, consistent with findings of Codiga (2005) based on the sharp front in velocity. Vertical salinity stratification in BIS is much stronger during March 2010 than during the previous surveys, with surface-bottom salinity differences of ~2 PSU there. Salinity stratification weakens towards the east, with surface-bottom differences of less than 1 PSU in eastern RIS. However, even in eastern RIS, there is evidence of a slightly freshened (S ~ 31 PSU) lens of relatively low salinity water at the northern edge of the survey region.

During the June survey (Figures 8, 10, and 12), the observed salinity range is slightly reduced from that encountered in the March survey. Minimum observed salinity in west/central BIS was about 0.5 PSU saltier (~30 PSU), while maximum salinity at depth offshore is approximately the same (32-32.5 PSU). Eastern BIS and central RIS are fresher (by ~0.5 PSU) in June as compared with March, suggesting an expansion of the region influenced by the outflow from LIS. Horizontal as well as vertical gradients of salinity are somewhat reduced in June compared to March. There is a weak signal of freshening along the edge of the survey region in northeast RIS. As was observed in prior surveys, the shoals east of Montauk are well-mixed, but during the June survey, the mixed area extends all the way to Block Island.

4.1.3 Density stratification

Vertical stratification in water density is an important dynamical characteristic of the water column in the sense that vertical mixing is influenced by the degree of stratification present (conversely, vertical mixing impacts the stratification in the sense that increased mixing produces, over time, a less stratified water column). Vertical stratification was computed for each CTD cast by differencing the deepest (typically 1-3 m above the bottom) and shallowest (1 m depth) density values. This definition of stratification is the most straightforward, however, it should be borne in mind that there is some tendency for this quantity to be higher for deeper CTD casts. Figure 13 shows maps of the density difference for each of the 4 CTD surveys.

Stratification during the September survey was strongest in the deep offshore region, especially in the area south of BIS where density differences of 2-3 kg m^{-3} were observed. Weakest stratification (< 1 kg m^{-3}) occurred in the northeast portion of RIS, in northern and western BIS, and southeast of Block Island. A zone of rapid spatial variation in the vertical stratification was found just south of the entrance to BIS, the area where the LIS/BIS outflow front is observed in surface temperature and current data (Ullman and Codiga 2004; Codiga 2005). In general, during September, vertical stratification is influenced by both salinity and temperature in the western portion of the OSAMP region, with the influence of salinity decreasing towards the east.

In December, stratification was generally weak, with density differences everywhere less than 1.25 kg m^{-3}. Highest values occurred in the deeper offshore region and lowest values (essentially zero) were observed around the periphery of BIS and RIS as well as on Cox Ledge. Vertical density differences during December were dominated by salinity variations, as the vertical temperature gradient (Figure 4) during this period was destabilizing (warmer water at depth). As discussed in Section 4.1.2, the near-bottom salinity at depth at the deep offshore stations was anomalously high during this particular December, suggesting that the vertical stratification in this survey may not be typical.

Stratification during the March survey remained negligible in the southeast part of the OSAMP region (Cox Ledge). Relatively high stratification (1.5-2 kg m^{-3}) was detected at two stations in BIS. This results primarily from decreased near-surface salinity (see Figure 10) presumably due to increased freshwater runoff via LIS, but also from warming of the near surface waters. The entire western portion of the domain, with the exception of a well-mixed area extending from northern Block Island to Montauk Point, is moderately stratified, with vertical differences of at least 1 kg m^{-3}. As distance from western BIS increases, the effect of thermal stratification increases while that of salinity decreases.

At the time of the June survey, strong stratification was present in the deep offshore area and in central RIS, with density differences of 2-3 kg m^{-3}, due primarily to temperature differences. BIS and northeast RIS were weakly stratified (density difference of less than 1 kg m^{-3}). Although the latter region, and the area between Block Island and Montauk Point, is essentially well-mixed throughout the year, the stratification in northwest BIS is generally weaker during the rest of the year than observed during the March 2010 survey, presumably because the outflow of low-salinity water from the Connecticut River via LIS peaks in spring.

4.1.4 Dissolved Oxygen

Dissolved oxygen levels during the September survey (Figures 14, 15, and 17) generally decrease with depth. The near surface concentration in west/central BIS is in the range 7-8 mg l^{-1} and increases towards the east, reaching 8-9 mg l^{-1} in surface waters of eastern RIS. These values are at or slightly above the 100% saturation level (not shown). Near-bottom oxygen concentration is generally 6-7 mg l^{-1} except for a portion of north/central RIS (northern part of lines NS5 and NS6) where concentrations fall to around 5 mg l^{-1}(approximately 50% saturation).

In December oxygen concentrations in the bottom water of north/central RIS are increased above the levels observed in September (Figures 14, 15, and 17). Concentrations during December are above 6 mg l^{-1} (~75% saturation). Lowest concentrations during the December survey occur near the bottom in the deep channel of central RIS, the area of apparent deep intrusion of outer shelf water. Surface oxygen levels in December are everywhere above 8 mg l^{-1}. During the March survey when water temperatures are at a minimum, oxygen concentrations are uniformly high throughout the water column with values above 10 mg l^{-1} (approximately 100% saturation) everywhere (Figures 14, 16, and 18).

The June survey found dissolved oxygen concentrations (Figures 14, 16, and 18) reduced significantly over the March values, in part due to the increase in water temperatures. The region of low concentration in north/central RIS appears to be redeveloping, with concentrations of 6-7 mg l^{-1} (~75% saturation) observed at the north end of line NS5. A significant feature during the June survey is a subsurface oxygen maximum with concentrations above 9 mg l^{-1} occurring in bands of order 10 m thick in the southern, offshore region of the survey. The location of the most intense of these maxima is typically at depths of 20-30 m, although there are places where the maximum is found at depths of 10-20 m. As will be discussed in Section 4.1.5, subsurface maxima in Chlorophyll concentration were detected in the June survey and it is likely that the oxygen maxima observed here result from phytoplankton photosynthesis.

4.1.5 Chlorophyll

Near-surface chlorophyll concentrations (derived from fluorometric measurements) during the September survey are below 4 μg l^{-1} throughout the survey region (Figures 19, 20, and 22). Highest values occur around Block Island and lowest concentrations (less than 1 μg l^{-1}) are found in the southern and eastern portions of the survey region. The vertical sections (Figures 20 and 22) show that chlorophyll concentrations are often elevated at mid-water depths. These subsurface maxima, with concentrations reaching ~10 μg l^{-1} in places but usually 5-6 μg l^{-1}, are detected at various depths, ranging from near the bottom on lines NS8 and NS9 to approximately 10 m depth along lines NS1 – NS3. In general, phytoplankton biomass as measured by chlorophyll concentration tends to be highest in northwestern RIS and BIS and also in eastern RIS.

Chlorophyll levels in December (Figures 19, 20, and 22) are somewhat lower than were found during the September survey. Near-surface levels are below 3 μg l^{-1}, but the region of highest concentration has shifted to central and eastern RIS. In most parts of the survey region, chlorophyll is low throughout the water column in December, although a weak subsurface maximum (3-4 μg l^{-1}) was detected at several stations in central RIS.

In March, very low chlorophyll concentrations were observed throughout the survey region (Figures 19, 21, and 23). Surface values are less than 1 μg l^{-1}, and concentrations at depth are generally lower than 2 μg l^{-1}, except in northeast RIS. In that region, near bottom chlorophyll levels of 3-4 μg l^{-1} are observed.

Surface chlorophyll concentrations during the June survey (Figures 19, 21, and 23) remained at low levels, less than 1 μg l^{-1} over most of the region and only 1-2 μg l^{-1} around Block Island and in isolated areas along the northern and western periphery of the survey region. In much of the region, especially central and southern RIS and BIS, a subsurface chlorophyll maximum was observed, with concentrations of up to approximately 5 μg l^{-1} at depths of 20-30 m.

Chlorophyll concentrations measured in this study are comparable to those of previous studies in the Mid-Atlantic Bight, for example those summarized by O'Reilly et al. (1987). Typical seasonally and depth averaged values of their data in the BIS/RIS region were in the range of 1-3

$\mu g\ l^{-1}$. It should be noted that we saw no evidence of a winter-spring phytoplankton bloom, although such an event could have easily been missed if it occurred between our quarterly surveys.

4.1.6 Turbidity

Water turbidity is a measure of the scattering of light by suspended particulate matter. The turbidity calibration used here provided turbidity values in nephelometric turbidity units (NTU), a standard measure of this quantity. Estimates of water turbidity from the fluorometer were below 1 NTU during the September survey (Figures 24, 25, and 27). Highest values (0.75-1.0 NTU) were detected in BIS and near the bottom in the shallowest areas along the northern edge of the survey region. Values in the middle of the water column in central RIS are lower (~0.5 NTU). High near surface turbidity approaching 1 NTU was detected at station 47 near the offshore end of line NS7. Adjacent stations did not exhibit a similar elevation suggesting either an instrument malfunction or the presence of a very small scale feature. The lack of a corresponding signal in either the Chlorophyll concentration (Figure 20) or the depth of the euphotic zone (Figure 29, to be discussed in Section 4.1.7) suggests the former explanation.

Turbidity values during the December survey (Figures 24, 25, and 27) were significantly higher than during September. Highest values (1.25-1.5 NTU) were detected in northeastern RIS. Moderately high turbidity (0.75-1.0 NTU) was observed in west/central BIS with decreasing turbidity towards the east.

During the March survey, turbidity was low throughout the survey region, with values below 0.75 NTU everywhere (Figures 24, 26, and 28). Highest turbidity (above 0.5 NTU) was detected in northern RIS and in BIS, with offshore values generally low.

Near-surface turbidity in June was generally very low, with values in the range of 0.25 – 0.5 NTU (Figures 24, 26, and 28). Near bottom turbidity was elevated to 0.5-0.75 NTU in west/central BIS and in the far northeast corner of the survey region.

4.1.7 Euphotic Zone Depth

The estimated depth of the euphotic zone during the September survey was quite variable, ranging from ~10 m to 40 m (Figure 29). Highest values occur in central RIS and in the offshore areas and lowest values in BIS and in the far eastern portion of the survey region. The boundary between the BIS region of shallow euphotic zone depth and the region of deeper light penetration to the south and east is quite sharp and extends continuously from Pt. Judith southward along the east side of Block Island and then to the southwest corner of the survey region. During the December survey, the euphotic zone depth is generally less than 20 m, with a general increase in the offshore direction, although without the sharp frontal boundary observed in September. In March, the depth of the euphotic zone is everywhere greater than 20 m with some increase offshore. During June, the map of the euphotic zone depth resembles the September map, with low values (less than 20 m) in BIS and around the periphery of RIS and higher values offshore (30-40 m).

4.2 Temperature and Salinity Time Series from Moored Instruments

The PO moorings were deployed in mid-September 2009 with planned recovery in mid-December 2009. However, adverse weather conditions prevented this operation until mid January (see Table 1 for details on the mooring deployments). The PO moorings were re-deployed in mid-March 2010 and were recovered in mid-June 2010. The MD-F and MD-S moorings were deployed in early October, 2009 for a planned 1-year deployment; for the preparation of this report, data were downloaded from the start of the deployment to July 15, 2010. In this context, for convenience two time periods are discussed: Fall/Winter, September 15, 2009 – February 15, 2010; and Spring/Summer, February 15 – July 15, 2010.

Based on real-time data from a tracking device on the PO-S CTD mooring, in the final days of November during the Fall/Winter deployment the buoy was relocated, over the course of a couple hours, to a position about 1 km southwest from where it was deployed. Upon recovery in January the mooring showed clear signs that it had been dragged, likely by a trawler. Although the surface and 3 subsurface instruments were severely damaged during the incident, all provided useful data up to the time it occurred. One instrument (nominally at a depth of 7 m) was moved on the mooring wire to a final depth of ~3 m below the surface during the incident, where it continued to record good data. The lengths of the data records from the various instruments on the PO moorings during the Fall/Winter deployment can be seen in the instrument pressure records shown in Figure 30. Except for the 3 m depth CTD at PO-F, which malfunctioned in early November 2009, and the damaged instruments mentioned above, the MicroCat CTDs on the PO moorings filled their onboard memories in late December (28 Dec., 17:00 UTC); the CTD on the surface buoy at PO-F continued to sample until the January recovery.

Near the end of the Spring/Summer period, the salinity at both PO moorings at 1 m depth (FSI NXIC CTD) began to diverge significantly from the values measured at 3 m depth. Examination of CTD casts near these moorings during the June spatial survey suggested that the NXIC salinities were not correct. We concluded the problem was caused by biofouling of the NXIC conductivity cell. For this reason, the 1 m depth salinity records at the PO moorings were truncated in late May.

The pressure records from the CTDs at moorings PO-F and PO-S (Figures 30 and 31 for the Fall/Winter and Spring/Summer deployments respectively) provide information on the vertical motion of the instruments in response to waves and currents. The instruments are seen to experience correlated upward excursions of up to 2-3 m on time scales of days. The magnitude of the depth excursions appears to increase with the nominal depth of the instruments suggesting that strong currents and/or wind caused the mooring wire to tilt. Because the vertical excursions are relatively small compared to the nominal instrument spacing, in the analysis that follows, no attempt has been made to correct for the vertical motion of the sensors. The CTDs on moorings MD-F and MD-S were not equipped with pressure sensors, so no such analysis could be performed for these records.

In the discussion that follows it is valuable to refer to Connecticut River discharge (Figure 32), which is the dominant river source to LIS and generally representative of regional runoff, hence a good indicator of freshwater influence on the SAMP region.

4.2.1 Fall/Winter 2009 Deployment

This subsection discusses the time series of temperature and salinity during the Fall/Winter period from MD-S (Figure 33), PO-S (Figure 34), MD-F (Figure 35), and PO-F (Figure 36), and their vertical gradients (Figures 37 and 38). In mid-September 2009 when the PO-F and PO-S moorings were deployed, the water column at both sites was stratified, with warm, lower salinity water overlying cooler, saltier water. At both sites, the upper portion of the water column (down to at least 20 m at site PO-F) was fairly well mixed, with clear differences apparent between the deepest instruments (35 m) and the near surface units (Figures 34 and 36). This indicates that the seasonal pycnocline was quite deep at this time, as noted in Part 1 to be typical based on the hydrographic climatology. At both moorings, the period of vertical stratification abruptly ends in mid-October when the water column becomes well-mixed (see Figure 38). This event coincides with the occurrence of a strong northeasterly wind event (Section 5.2 below), which has been shown by Lentz et al. (2003) to be much more effective at achieving vertical mixing than similar strength wind events from other directions. The MD-S and MD-F moorings were located in shallower water than the corresponding PO moorings. The vertical stratification at these moorings is much less intense than at the deeper PO moorings, nonetheless the stratification abruptly disappears at the time of the northeaster.

After the destratification event in mid-October, the water column continues to cool and remains essentially isothermal (in the vertical) until late November. During this period, the deeper moorings (PO-F and PO-S) as well as the MD-S mooring experience moderately large fluctuations (~1 PSU) in salinity. The largest signal is observed at the deeper sensors where salinity is observed to increase for several days to two weeks, only to decrease again. The near-surface response is weaker but is generally in the opposite sense; that is a decrease in near-surface salinity occurs at the same time as an increase in deep salinity. Although there are relatively high Connecticut River discharge events during this time period (Figure 32), it is difficult to relate specific events to the observed near-surface salinity fluctuations. This is because of the lag time between upstream discharge and the arrival of freshened water in BIS, and also because the movement of this water within the OSAMP region depends a great deal on wind forcing.

A dramatic hydrographic transition occurs in late November at all mooring sites. At this time, the deep salinity abruptly increases by approximately 2 PSU at PO-S (Figure 34) with lesser increases observed at the other moorings (Figures 33, 35, and 36). Contrary to what was observed in the previous events, in this case, the increase in deep salinity is accompanied by an increase in deep temperature as well. There is also a small decrease in near-surface salinity at this time at all locations except for MD-F. The duration of this event is 3-4 weeks at PO-S and somewhat less at the other locations. At PO-S, there is a brief period, about 2 weeks after the onset of the event, during which time the deep salinity decreases and the near-surface salinity increases, suggestive of a vertical mixing event, but also consistent with differential advection (deep saline water offshore and low salinity surface water onshore). Similar variability is seen at the other sites as well. The mixing or relaxation event is quickly followed by the return of the deep saline water. At PO-S, the peak salinity during this event is nearly 35 PSU, whereas the peak at PO-F is approximately 34 PSU. This is clearly the same outer shelf/slope water seen during the December CTD survey as discussed in the previous subsections.

Comparison of the hydrographic time series from PO-S (Figure 34) with wind observations from MD-S (Section 5.2 below) suggest that the intrusions of deep outer shelf water are correlated with periods of intense northwesterly wind. Such events occurred in late November, mid-December, and late December 2009. The response of currents to these wind stress bursts appears to be qualitatively similar to that of the classical upwelling circulation. Near surface currents at PO-S are eastward while near-bottom currents are northward to northeastward (onshore). This suggests that the rapid increase in deep salinity observed during these three periods results from onshore advection of outer shelf water. Strong northwesterly winds are a common occurrence in winter in the OSAMP region but the observation of outer shelf/slope water so far inshore is not, so far as we know. It is possible that the foot of the shelfbreak front (on average located at the shelfbreak approximately 100 km south of PO-S) was anomalously far inshore during late fall of 2009 thus bringing the slope water source closer to the OSAMP region, allowing it to be rapidly advected into the region. Further investigation of this phenomenon is warranted.

4.2.2 Spring/Summer 2010 Deployment

This subsection discusses the time series of temperature and salinity during the Spring/Summer period from MD-S (Figure 39), PO-S (Figure 40), MD-F (Figure 41), and PO-F (Figure 42), and their vertical gradients (Figures 43 and 44). The MD-S and MD-F moorings continued to obtain observations throughout the winter of 2010. At the time the PO moorings were redeployed in mid-March 2010, temperatures at the MD moorings had just begun to rise from the wintertime minimum values of 2-3 °C (Figures 39 and 41). The water column was still approximately isothermal in the vertical at both stations. At station MD-S (Figure 39), moderate salinity stratification was present, a result of this station's location closer to the major local freshwater source, Long Island Sound. At station MD-F (Figure 41) there was no vertical salinity stratification, thus there was no appreciable vertical density stratification.

During the Spring/Summer period, temperature increases steadily at all sites (Figures 39, 40, 41, and 42). During the period that the PO moorings were operational (mid-March – mid June), the surface temperature increased by approximately 15 °C, while the near-bottom temperature increased by only about 5 °C. The fact that the surface temperature increase is roughly similar at all sites suggests that the observed change in temperature during the spring is predominantly forced by surface heat fluxes which do not vary appreciably over the OSAMP region. Although the general increase in temperature is the dominant feature observed, the increase is not monotonic. There are a number of periods, of duration about 1 week, during which temperatures decrease. These decreases tend to occur simultaneously at all sites. In some cases, for example mid-April and late-April at PO-F (Figure 42) and to a lesser extent at the other sites (Figures 39, 40, and 41), near-surface cooling is accompanied by warming of deeper water suggestive of the signature of vertical mixing in the presence of vertical temperature stratification.

At all sites, thermal stratification, as shown by estimates of the vertical temperature gradient (Figures 43 and 44), slowly increases from March to mid-May at which time the rate of stratification increases significantly. After mid-May, the large temperature difference between sensors at 7 m and 20 m depth at stations PO-S and PO-F (Figures 40 and 42) indicates the presence of a thermocline in this depth range. During this time period, large fluctuations in temperature at 12 m depth are observed, consistent with the presence of this instrument within the thermocline. The fluctuations are largely of tidal period (not shown), indicating the presence of an internal tide at moorings PO-S and PO-F.

Contrary to the situation during Fall/Winter when the largest salinity fluctuations occurred at depth, during the Spring/Summer deployment, surface salinities undergo large fluctuations, with near-bottom salinity varying much less intensely during this period. Fluctuations (at both tidal timescales and on timescales of days to weeks) are most intense at stations MD-S and PO-S and are weaker at MD-F and PO-F. In early April 2010, a large drop in near-surface salinity (~3 PSU) was detected at stations MD-S (Figure 39) and PO-S (Figure 40). Surface salinity remained low at these sites for approximately 2 weeks. Weaker signals of near-surface freshening occurred at MD-F (Figure 41) and PO-F (Figure 42) 1-2 weeks after appearing to the west at MD-S and PO-S.

With highest Connecticut River discharge occurring in spring (Figure 32), it is likely that the observed variability in near-surface salinity is due to the movement of low salinity surface plumes associated with outflow from LIS. The 1-2 week lag in the arrival of the low-salinity water at MD-F and PO-F in the east is consistent with a propagation speed of O(0.05 m s^{-1}), which is consistent with our knowledge of the residual circulation (Part 1, and Section 5 below). During 2010, Connecticut River discharge peaked in late March to early April with discharge nearly double the 80-year mean peak value (the peak in 2010 occurred approximately 3 weeks earlier than the mean). At the same time, Rhode Island experienced the "Great Flood" of 2010 wherein several rivers draining into Narragansett Bay were at 100-year levels. Thus the freshening observed during spring 2010 is likely to be anomalously strong compared to an average year.

Over the entire spring 2010 period, salinities at all locations experience a general decrease of 0.5-1 PSU. This general freshening of the shelf during spring is consistent with prior work by

Mountain (1991) who computed the seasonal cycle in the volume of shelf water (defined as water with salinity < 34 PSU) on the southern New England shelf and found that the shelf water volume peaked in late spring/early summer.

Water density during the spring period decreases steadily with time. This is predominantly a result of the heating of the water column, but a part is due to the above mentioned water column freshening. Short-term (days to weeks) fluctuations in near-surface density occur in early and mid spring in response to the near-surface freshening events. Because the episodic freshening events are confined to the upper part of the water column, these events produce an increase in vertical density stratification. This is observed most strongly at MD-S and PO-S, with weaker effects at MD-F and PO-F (Figures 43 and 44). In addition to the freshening events, vertical density gradients at all sites slowly increase during the spring as a result of heating of the near surface waters (as discussed above, the near-surface warms more than the deep waters; see the vertical temperature gradient plots in Figures 43 and 44).

4.2.3 Monthly Mean Hydrographic Profiles

To provide a more complete picture of the seasonal cycle in hydrography in the region, we present monthly mean vertical hydrographic profiles at each of the four sites (Figures 45 and 46). The profiles do not represent multi-year means but only averages over those months during which the PO and MD moorings were deployed. There is no profile for August, since there were no data available from that month in either 2009 or 2010. It should also be borne in mind that some of the averages are not full monthly averages. For instance, if the mooring was deployed or recovered in mid-month, then only data from part of that month was available. In addition, the instrument damage caused by the trawler impact at PO-S during the fall/winter 2009 deployment reduced the available data at some depths.

Vertical profiles during September 2009 are available only for the PO moorings, which were deployed on September 15, 2009. The upper 2/3 of the water column at this time is nearly isothermal. The thermocline at this time in early autumn is very deep, with near bottom waters 2-3 °C cooler than in the upper mixed layer. Weak salinity stratification is present at this time, with surface-bottom differences of approximately 1 PSU. The halocline at PO-S is shallower (10-20 m depth) than that at PO-F (20-30 m depth), although the mean salinity at PO-S is higher than at PO-F. October profiles at the PO moorings are similar to those in September. The corresponding profiles at the MD moorings (composed of only the last 2/3 of the month) are more vertically well-mixed. During November 2009, the water column at all sites is almost completely well-mixed, with the exception of a slight increase in salinity with depth at PO-S. In December 2009, temperature remains nearly well-mixed at all sites except PO-S. At PO-S, the monthly mean near-bottom temperature is approximately 3 °C warmer than the near surface temperature, in part due to the onshore excursion of deep, warm, saline offshore water which was discussed previously. Salinity profiles at PO-S, MD-S, and to a lesser extent PO-F exhibit an increase in salinity with depth that is associated with the offshore intrusion discussed above. The effects of the intrusion at MD-F, as noted previously are weak, thus this process does not noticeably affect the mean profile.

During January and February 2010 profiles are only available at the MD moorings, where they are thermally well-mixed. At MD-S, there is approximately a 0.5 PSU increase of salinity from surface to bottom, presumably due to the relative proximity of this site to the LIS source of low-salinity water. Salinity stratification at MD-S increases somewhat in March (nearly 1 PSU surface to bottom difference), while the PO moorings (deployed in mid-March) exhibit somewhat weaker salinity stratification (0.5 -1 PSU over ~35 m). Surface water temperatures during March have increased slightly compared to February, but there is only 1-2 °C difference, surface to bottom, at the PO moorings and even less at the MD moorings which are in shallower, more tidally energetic areas. In April 2010, significant thermal and haline stratification has developed. At MD-S and PO-S, surface salinity is ~2 PSU lower than deep salinities, with the low salinity layer at PO-S concentrated in the upper half of the water column (the salinity profile at MD-S is linear, but there are only 3 sensors at this site, so surface intensification of the stratification cannot be ruled out there). The eastern stations (MD-F and PO-F) exhibit weaker vertical salinity stratification (~0.5 PSU) due to their greater distance from the primary local freshwater source (LIS). At all sites during April, temperatures at the surface are 2-3 degrees higher than at depth.

From May 2010 through July 2010 (at which time only the MD profiles are available), thermal stratification gradually strengthens while salinity stratification weakens. In June, mean surface to bottom temperature differences of 7-9 °C are found at the deeper sites (MD-F and the PO moorings). A shallow thermocline is present (5-15 m depth) at PO-S and to a lesser extent at PO-F (the thermocline location cannot be resolved at the MD moorings). Surface to bottom salinity differences during June are reduced to approximately 1 PSU, with a deeper and weaker halocline than was present during the peak runoff period in April. Due to the increasing effects of thermal stratification and the remnant of strong spring salinity stratification, density stratification is highest during June and July, with surface to bottom differences of ~3 kg m^{-3} present in July at station MD-F.

5 Results: Currents and Sea Level

5.1 Tidal Motions

Characteristics of tidal heights and tidal currents across the OSAMP region were described in some detail by Codiga and Ullman (2010) using hydrodynamic model output and previously available observations; the reader is referred to Part 1 for background information regarding which constituents are most energetic, and the role of surrounding water bodies such as LIS in shaping the response. This section presents new measurements from moored instruments. For the MD-S and MD-F sites (Figure 2), data from October 2010 through June 2010 are used. For the PO-S and PO-F sites in this section the FA09 records are used and not the SP10 records; FA09 records are 4 months long and so better suited for the harmonic analysis than the 3 month long SP10 records, which, for tidal quantities, give very similar results in any case. The seven tidal constituents (M_2, K_1, N_2, O_1, S_2, M_4, and L_2) that are dominant in the new observations are, as expected, the same as those seen in previous analyses.

Tidal current ellipses for each of the seven constituents (Figure 47), based on observed vertical-mean currents, reveal distinct patterns at each site. The relative importance of the constituents, including dominance by M_2, is similar at all four sites. Currents rotate clockwise in time for all constituents at all sites, except for the M_4 constituent at three of the sites. The magnitudes and orientations of the ellipses vary from site to site; for example, M_2 ellipses are largest at MD-S, where the major axis is oriented in a NW-SE direction, and at PO-F, where the ellipse is more round. Overall, the geographic variations and many other detailed aspects of the observed current ellipse characteristics from these four sites are in very good agreement with those reported in Codiga and Ullman (2010).

The vertical variations of tidal ellipse characteristics across the water column, for the dominant M_2 constituent, are clear from plots of the four current ellipse parameters at each of the four sites (Figure 48). In general, as the seafloor is approached amplitudes decay, major axes turn slightly clockwise, and ellipses flatten; the vertical extent off the seafloor in which these changes occur varies from 5-10 m, where currents are most energetic, to less than 5 m. These features are characteristic of theory for frictional tidal boundary layers over a flat seafloor influenced by background rotation (e.g. Soulsby 1990). Codiga and Rear (2004) analyzed ADCP records from the inner shelf south of Block Island Sound, including one record from a site a few km ENE of PO-S where the vertical structure was very similar to that presented here, and demonstrated they compare favorably to the theory. Patterns that diverge from the theory occur in locations influenced by sharp topographic features. For example, at PO-S the minor axis decreases over most of the water column instead of in a 5-10 m near-bottom layer as the theory would suggest, which is likely because the bottom slopes steeply offshore at this site. Owing to the lack of characteristic reversals of velocity in depth, it can be concluded that if energetic internal tides are occurring, they are at sufficiently higher frequencies (as seen, for example, by Colosi et al. (2001) on the shelf to the south of Martha's Vineyard) and/or sufficiently intermittent (see discussion of high energy tidal fluctuations in mid-depth temperature and salinity time series in Section 4.2.2) to not be apparent in this harmonic analysis.

Tidal sea level observations can be estimated using the bottom pressure observations collected by the PO-S and PO-F ADCPs. The superposition of the seven main tidal constituents in harmonic fits (Figure 49) to sea level for these two locations reveals several important features. At both sites there is a distinct spring-neap cycle characterized by neap periods which alternate in their amplitudes, such that every second neap period is typically significantly weaker. During spring conditions, peak-to-peak amplitudes are typically 1.1-1.3 m at PO-S and 1.2-1.4 m at PO-F; during neap conditions they are about 0.5-0.6 m. The diurnal inequality changes as the spring-neap cycle progresses, and is maximal during spring conditions. In addition to the minor differences in overall amplitudes between the two sites, small differences are apparent in the relative importance of diurnal and semidiurnal constituents, as expected due to their geographic variations (detailed in Codiga and Ullman 2010).

5.2 Subtidal Current and Wind Time Series

The component of current, sea level, and wind variability at lower frequencies than tidal is referred to as "subtidal". Subtidal variables are computed by application of a low-pass filter and subsampling to 12-hour resolution, as explained in the methods section. Subtidal currents, also denoted "residual flow", may have smaller magnitude than tidal currents, but because they do not reverse as regularly as tidal currents they have a more important influence on the long-term pathways for transport of water and waterborne materials.

Time series of subtidal currents from each site are presented as a pair of stickplot figures, one for the Fall/Winter period and one for the Spring/Summer period (MD-S in Figures 50 and 51; PO-S in Figures 52 and 53; MD-F in Figures 54 and 55; and PO-F in Figures 56 and 57). The black vectors in the plots show the currents at a series of depth levels, to depict the water column structure. The blue vectors along the tops of the plots show the winds measured by the MD-S mooring (on the MD-S and PO-S plots) and the MD-F mooring (on the MD-F and PO-F plots).

The winds at MD-S and at MD-F were generally very similar to each other, as expected given that their separation is smaller than the typical scale of weather systems. As is characteristic of the region (e.g., Codiga 2005), the wind had seasonal-mean direction generally southeastward in winter when it was strongest, and generally northeastward in summer when it was weakest. These longer-term trends were overcome by events on the days-weeks timescale of passing weather systems, which cause the wind to take on a wide range of directions for up to a few days at a time, also a regional wind characteristic.

Certain general features of subtidal currents are similar at all four sites. Current magnitudes are typically in the range of about 10 to 25 cm s^{-1}, with minima of a few cm s^{-1} and maxima of about 40 cm s^{-1}. Current variations on timescales of days to weeks are dominantly influenced by wind events. Within a few hours of a change in the wind direction, currents generally become aligned with the component of the wind in the direction of the large-scale coastline nearby (discussed below). The strongest currents tend to occur when the wind is strongest, and when it persists in the same direction for a longer duration; thus subtidal current magnitudes are distinctly stronger in winter and weaker in summer. Variations of subtidal currents as a function of depth tend to be modest and tend to occur over scales of about 5 to 10 m or more.

At the MD-S site, subtidal currents (Figures 50 and 51) are typically in the range of 15 to 30 cm s^{-1}, the most energetic among the four sites. The direction toward which they flow typically varies from toward the west-southwest, to the opposite direction toward the east-northeast. These directions align with the large-scale southern New England coastline, set predominantly by the southern shore of Long Island, indicating the currents at this location are constrained to move roughly parallel to this direction. The timing of the shifts of currents between these opposing directions is tied closely to variations in the wind; winds with a southward component tend to cause south-southwestward currents. Vertical variations of the currents across this 26-m deep water column are generally modest and typically consist of amplitudes that decrease weakly from surface to bottom. Prominent exceptions to these patterns did occur, however. For example, for several days during late December, late February, and mid-April there was strong flow directed east-southeast that was more sharply concentrated in the upper 5-10 m of the water column. These events were very likely tied to pulses of the LIS outflow driven by river runoff events (Figure 32), though there is not a direct correspondence between currents and specific river flow pulses, for reasons discussed above.

In the upper half of the 44-m deep water column at the PO-S site, some 10 km southeast of MD-S, subtidal currents (Figures 52 and 53) had many similarities to those at MD-S, the main difference being that current amplitudes were generally up to a few cm s^{-1} weaker than at MD-S. Current directions at PO-S closely matched those at MD-S, indicating the tendency for alignment with the regional coastline extends offshore at least to the PO-S site. Prominent differences of PO-S from MD-S occur in the deeper water column, from about 20 to 44 m. At these depths a component of flow east-northeastward can strengthen considerably during southeastward wind events, when near-surface currents are east-southeastward. Examples of this are in mid-December and early-mid May. This flow pattern is characteristic of coastal upwelling circulation in which the wind drives shallow flow offshore (in addition to alongshore) and deep water has a compensatory component of motion onshore. These pulses of deep water shoreward can have profound influence on water properties. As discussed in Section 4 above, they can deliver shelf-break water, from points some 100 km to the south, to central RIS, resulting in salinities that far exceed the seasonal extremes found in multi-year climatologies.

Another distinction of subtidal currents in the PO-S record compared to MD-S occurs in early April, when flow in the upper ~10 m is strongly offshore at PO-S but not at MD-S. This could be the signature of a pulse of freshened near-surface water out of LIS. The plume associated with this outflow sometimes extends across a broad area encompassing both MD-S and PO-S, and sometimes is confined nearer to Montauk Point where it exits the southwestern corner of BIS. Wind fluctuations cause the spatial extent and shape of the outflow and freshened plume to vary significantly, which could explain the occurrence of offshore currents near the surface at PO-S but not at MD-S simultaneously. There is some evidence during the early April offshore flow at PO-S that near-surface salinity decreases at PO-S are significantly more pronounced than at MD-S, which is consistent with this hypothesis. A similar period of strong offshore flow confined to the upper ~10 m at PO-S occurs during early October.

At the 34-m deep MD-F site near the southernmost extent of eastern RIS, subtidal currents (Figures 54 and 55) are weaker, and aligned in different directions, than those at MD-S and PO-S. At MD-F, subtidal current magnitudes are typically in the range of about 5 to 20 cm s^{-1}. The weaker response is likely due in part to the fact that this site is further from the nearby shorelines and thus responds less strongly to wind forcing; it is also likely due to the fact that the LIS outflow does not reach this site under typical conditions, hence does not contribute to the variability here. The predominant directions of motion are toward the west-northwest and opposite that, toward the east-southeast. These are not aligned closely with the local isobaths of Cox Ledge, but rather are aligned with the larger-scale coastline leading from Martha's Vineyard toward southern Rhode Island. Other than a weak decrease in amplitudes from surface to bottom, the vertical structure of subtidal currents at MD-F deviates from vertical uniformity in modest ways. A prominent example is that in the late spring and summer months, the upper half of the water column has significantly more energetic currents, a characteristic of RIS when strong stratification sets in (discussed in Part 1, Codiga and Ullman 2010).

Finally, subtidal currents at the 44-m deep PO-F site (Figures 56 and 57) in central RIS about 15 km to the north of MD-F are the weakest of the four sites. Current amplitudes typically range from less than 5 cm s^{-1} to about 15 cm s^{-1}. These smaller amplitudes are likely because the site is farthest north within RIS and hence the most sheltered from offshore winds. Furthermore, among the four sites, the orientation of currents at PO-F has the broadest range of directions. The direction of currents at PO-F tends to be quite dissimilar from that at MD-F, indicating that these two sites respond to wind forcing in substantially different ways. A likely contributing factor to this phenomenon is the presence of Cox Ledge, the shoal that extends west-southwestward from Martha's Vineyard and forms a submerged outer edge of RIS. The PO-F site is in the deepest central RIS, onshore of Cox Ledge, while the MD-F site is on the outer portion of Cox Ledge. At PO-F, deep water will tend to be steered parallel to Cox Ledge, while the upper water column need not be. Vertical structure at PO-F includes weather-band events with shallow and deep flows that tend to be opposed to each other, with the shallow movement in the direction of the wind, particularly in fall and winter. Examples of this occur in early October and mid-December. This is characteristic of a wind-driven coastal upwelling/downwelling response. As at MD-F, in the late spring and summer the subtidal currents in the upper water column at PO-F were also more energetic, as is typical of stratified conditions.

5.3 Mean Flow and Subtidal Principal Axes Current Ellipses over Monthly Intervals

Monthly-mean subtidal currents, and principal axes ellipses of the monthly subtidal variability about them, have been calculated and plotted for each site, at a series of depths on a single timeline spanning the 11 months of sampling (Figure 58 for MD-S; Figure 59 for PO-S; Figure 60 for MD-F; and Figure 61 for PO-F). Monthly-mean currents (red arrows in Figures 58 to 61) highlight the longer-term mean flows that persist when weather-band fluctuations on the days-weeks timescale are averaged out. Monthly mean currents range from a few cm s^{-1} to about 25 or 30 cm s^{-1}, and are generally strongest during the summer months, when they are concentrated in the upper water column; only during summer months do monthly-mean current amplitudes significantly exceed typical wind-driven subtidal variability (the January and March results at PO-F, and to a lesser extent PO-S, appear to be an exception but they are based on 13 and 12 days, respectively, so are considered unrepresentative).

At MD-S (Figure 58, red vectors), during the fall and winter the upper water column monthly means are 5-10 cm s^{-1} with a southward component, while at depth they are weaker and have a northward component. This pattern is suggestive of a coastal upwelling response during this period of strong offshore winds. During spring and summer the monthly means take their peak values of up to 25 cm s^{-1} west-southwestward in the upper water column and are about 5-10 cm s^{-1} in the same direction near the bottom. In March the near-surface flow is distinctly offshore, in contrast to that deeper than about 5 m, likely a signature of the peak spring LIS outflow. The seasonal cycle of monthly means at PO-S (Figure 59) shares many traits with that at MD-S, but at PO-S the amplitudes are generally weaker (about 5 to 15 cm s^{-1}) and the deeper onshore flow in winter is more developed.

At MD-F (Figure 60, red vectors) monthly means range from a few cm s^{-1} to 10-15 cm s^{-1}, and are more vertically uniform. Here, currents tend toward the west-southwest in fall and spring, toward the southeast in winter, and toward the west-northwest in summer, when amplitudes near the surface exceed those at depth significantly. Finally, monthly means at PO-F (Figure 61; excluding January and March because they average too few days to be representative) are weakest, reaching about 10 cm s^{-1} maximum. In the upper water column they are very weakly eastward in fall and winter, then slightly stronger in the west-northwestward direction and concentrated in the upper water column in spring and early summer. At depth they are persistently east-northeastward, consistent with the influence of the steep adjacent contours of the onshore side of Cox Ledge in that direction.

The monthly-mean flows observed are, as a whole, largely consistent with the residual circulation patterns discussed in Part 1 (Codiga and Ullman 2010). This is particularly true with regard to the offshore/onshore components of shallow/deep flow in the winter, and the summer presence of the RIS Current flowing around the periphery of RIS counterclockwise that contributes to strong southwestward flow to the east and south of Block Island.

Key features of subtidal current variability noted above are also summarized effectively by the monthly principal axes (blue ellipses, Figures 58 to 61). At MD-S and PO-S (Figures 58 and 59) the subtidal ellipses are narrow and elongated in the west-southwest/east-northeast direction, and deviate from vertically uniformity mainly in that there is a weak Fall/Winter surface to bottom amplitude reduction and a sharper decrease in amplitude in the deeper water column during Spring/Summer. At MD-F (Figure 60) the ellipses are smaller, slightly less elongated, and generally oriented west-northwestward/east-southeastward; during the summer they become more round and smaller at depth. At PO-F (Figure 61), ellipses are the smallest and the least elongated, with modest deviations from uniform vertical structure.

5.4 Subtidal Sea Level

Magnitudes and temporal characteristics of sea level variations at subtidal timescales of days to weeks in the OSAMP area, in particular RIS, have not to our knowledge been closely examined before. Estimated sea level fluctuations were calculated from the subtidal component of the bottom pressure time series recorded by the ADCPs at the PO-S and PO-F sites and adjusted for the inverse barometer effect. The focus here is fluctuations on timescales of days to weeks, and estimated sea level is computed as a deviation from the record mean, so variability on timescales longer than a few weeks cannot be addressed. Furthermore, water-column density changes have not been accounted for in these sea level estimates but may be an important contributor to their variability.

The estimated subtidal sea level fluctuations at PO-S and PO-F (Figure 62) are very similar to each other, in magnitude and temporal variability (differences of about 0.02-0.05 m typically and about 0.08 m maximum), and to subtidal Newport, RI sea level observations (not shown). This indicates that the main contributing processes occur on scales comparable to the OSAMP region. Sea level fluctuations are typically between about -0.2 and +0.2 m, with peak values occurring in winter that reach magnitudes of up to 0.5 m, and values in summer infrequently rising above magnitude 0.15 m. The temporal variability is closely related to meteorological conditions, including both atmospheric pressure and winds, as expected given that multiple atmospheric processes can contribute to sea level fluctuations. Further analysis will be required to identify the relative contributions to the signal from various processes (see, e.g., Ullman and Codiga 2004) including steric changes, water-column density changes, local circulation processes such as the setdown/setup due to upwelling/downwelling response to wind forcing, and remote driving factors potentially including several-day period coastal trapped waves (e.g. Wang 1979) that may propagate to the site from a non-local generation area such as the sharp bend in the large-scale coastline near Cape Cod.

6 Results: Waves

Wave parameter time series from all five sites (MD-S, PO-S, MD-F, PO-F, and BIWB) are presented together with each other and with wind observations, for ease of comparison, during the Fall/Winter (Figure 63) and Spring/Summer (Figure 64) periods. Significant wave height (H_{sig}) is the average wave height, trough to crest, of the largest 33% of waves. Peak wave period (T_{peak}) is the period of the most energetic waves in the spectrum; the peak wave direction is the direction towards which the most energetic waves are traveling.

Significant wave heights (red traces in Figures 63 and 64) at the five sites share very similar ranges and temporal variations. The typical range is from about 0.5 to 2.5 m. Minimal amplitudes of less than 0.5 m occur a few times a month for durations of less than about a day during winter, and more often, for up to several days at a time, during summer. Values higher than about 2.5 m occur during events that typically last about 3-8 days from start to finish, and are characterized by a steep growth to a peak at about 3.5 to 5 m (the maximum observed during the sampling period was slightly more than 6m), followed nearly immediately by a steep decay. These events are clearly tied to wind variations (blue vectors in Figures 63 and 64), and they are more energetic and slightly more common during the winter months. Within these general ranges the BIWB site had the highest significant wave heights, by a modest amount, over MD-S and MD-F which were comparable to each other. The PO-S site had slightly lower values than MD-S, indicating that the closer proximity of MD-S to the shoal to the south of Block Island plays a role in increasing wave heights there. Values were lowest at the PO-F site, likely because its position farthest onshore is most sheltered and it is also not close to near-coastline shoaling areas where waves would be expected to amplify such as apparently occurs at MD-S.

Just as for significant wave heights, the peak wave periods (green traces in Figures 63 and 64) at the five sites share very similar ranges and temporal variations. Typical values are about 5 to 10 seconds; minima are about 2.5 seconds and maxima are about 14 seconds. Temporal variations are dominated by events during which the peak wave period rises rapidly, over about a day or less, to a peak value between about 8 and 12 seconds, and persists there for about 2-5 days before decaying over a few days. The timing of events in peak wave period is closely linked to the timing of events in significant wave height; however, during each event the elevated peak wave periods persist significantly longer than the elevated significant wave heights.

Peak wave direction (black vectors, Figures 63 and 64) was measured at PO-S, PO-F, and BIWB. At all three sites the peak wave direction was dominantly northward, consistent with the arrival of wave energy from offshore toward the south where the available fetch is longest. At PO-S and PO-F wave directions were very similar to each other, with a northwestward (most common) or northeastward orientation that varied on the timescale of the events described above for significant wave height and peak wave period; there was not a strong pattern for a preferred direction (northeast vs northwest) of waves during high wave height events, indicating that during individual events waves can arrive from points southwest or southeast. At the BIWB site, the peak wave direction was far more variable, particularly in winter, with some periods of westward, eastward, and southward directed waves. This is consistent with the fact that this site is least sheltered and hence waves local to it can respond more nearly uniformly to wind fetch from all directions.

In summary, waves at the five sampled sites typically have significant wave height from 0.5 to 2.5 m, peak wave period from 5 to 10 seconds, and peak wave direction from the south or southeast. Temporal variations are dominated by wind events on timescales of several days. During intense winter wind events, significant wave heights increase rapidly over a few hours or a day and reach up to 6 m or more, then after a short duration at the peak level they decrease about as rapidly as they grew; peak wave periods also rise during these events, reaching up to 14 seconds, and typically remain elevated for a longer duration of up to a few days before decaying. The MD-S site south of Block Island has wave heights slightly larger than at PO-S farther south, probably due to its closer proximity to the shoal south to Block Island. The most offshore site, BIWB, has modestly higher wave heights and more variable peak wave directions.

7 Summary and Conclusions

These observations have (a) provided important additional evidence to support the integrated view presented in Part 1 (Codiga and Ullman 2010) regarding temporal and spatial patterns in temperature, salinity, stratification, and tidal and subtidal currents across the OSAMP region; (b) facilitated more thorough characterizations of these quantities in previously unsampled areas, at previously under-examined timescales of days to months, and with respect to deviations of an individual year from climatological conditions; (c) generated a more complete view than previously available of the seasonal cycle across the OSAMP area of dissolved oxygen, chlorophyll, and turbidity patterns in three dimensions, and of the euphotic depth; and (d) led to better quantitative understanding of spatial and temporal patterns in the standard suite of surface wave parameters.

Temperature, salinity, and stratification from the seasonal vessel-based surveys have confirmed many of the geographic features deduced in Part 1. During summer the stratification peaked in strength, largely due to temperature; it was strongest along the offshore southern edge of the OSAMP area, also strong in central RIS, while weaker in BIS and the northern and eastern periphery of RIS where tidal currents are stronger and/or water depths shallower. In fall stratification was again strongest offshore, but comparable in strength in RIS and BIS. In spring BIS was most stratified, due to its proximity to the influence of exchange flow with LIS. In winter, temperature had a destabilizing influence and stratification was weakest. Northeastern RIS and the shoal region just east of Montauk Point were effectively unstratified throughout the year. In central RIS, relatively weak tidal currents and weak influence of LIS freshening result in a seasonal cycle with stratification that is very strong in summer and very weak in winter when surface cooling and wind mixing is intense. In BIS, the stronger tidal currents preclude summer stratification as strong as in RIS, but the influence of exchange with LIS sustains stronger stratification than in RIS during spring and to a lesser extent winter.

There were, however, significant deviations in the 2009-2010 seasonal vessel-based surveys from typical conditions expected based on the hydrographic climatology analyzed in Part 1. A prominent example was that during the December survey a deep layer of water with anomalously high salinity (nearly 35 PSU) and temperature (more than 15°C) was observed to the south of BIS and RIS, and extending into RIS via the deep channel between Cox Ledge and Block Island. These values were sufficiently high to be well outside the extreme limits of the climatologies (both that presented in Part 1 and that of Linder and Gawarkiewicz, 1998), and implied that the salty and warm water was an intrusion originating near the shelf break or slope, some 100 km to the south.

The mooring time series temperature and salinity records revealed intense variability on days to weeks. In general, during Fall/Winter the deeper water column was more variable, due to the deep surface mixed layer which is expected based on the climatology, and due to interactions between the OSAMP area and the shelf to its south. In contrast, during Spring/Summer the upper water column was more variable, particularly toward the west, due to the freshening influence of shallow estuarine outflow from LIS that strengthens and weakens in response to river runoff.

The Fall/Winter observation period began with a nearly homogeneous upper ~30 m that overlaid a strong thermocline, consistent with the climatology. A northeasterly wind event in October homogenized the entire water column at all sites, but later in November the anomalously salty intrusion noted above arrived at depth and, over a period of ~2-3 weeks, built up stratification stronger than expected for a typical year. The intrusion was significantly more evident at the mooring just north of Cox Ledge than at the mooring on the southern portion of the ledge, indicating the importance of this morphological feature in causing the interactions of deep water in RIS with the shelf to the south to occur via the channel extending in to RIS from the west end of the ledge and along its northern edge. The moored CTD observations indicated that the intrusion advanced and may have mixed vertically several times over the course of about 1 month, likely in response to wind fluctuations. Several CTD casts during the December CTD survey on and northwest of Cox Ledge were more well mixed than surrounding stations, with high salinity water appearing to have been mixed upwards (see sections EW3 and EW4 in Figure 11), suggesting the plausibility of this scenario. The combination of horizontal advection and vertical mixing thus appears to be a potentially important mechanism for net cross-shelf transport of water properties that couple the outer shelf and RIS.

The Spring/Summer deployment revealed that vernal warming occurs in alternating periods, lasting from a few to several days, during which the temperature either increases relatively rapidly, remains steady, or decreases slowly. Salinity fluctuations were dramatic in the upper ~12 m, particularly toward the west, and responded to pulses of river flow with irregular lags of days to weeks, as expected. By early June, a sharp pycnocline at about 12 m deep had developed, which exhibited intense oscillations at tidal timescales, suggesting internal tide activity.

Analysis of the tidal component of the moored current meter time series demonstrated that the detailed characteristics of tidal current ellipses in the new observations are in very good agreement with those depicted in Part 1. This includes the rank order of constituents by energy level as well as the nature of geographic changes in the orientation and ellipticity of current ellipses. The vertical structure of tidal current ellipses was in reasonable agreement with expectations based on theory and previous analyses of observations from south of Block Island. Tidal sea level from measured bottom pressure demonstrates the characteristic spring-neap cycle attribute of alternating neap periods with relatively low and relatively high minimum tidal ranges, as well as the tendency for larger daily inequalities during spring tide conditions.

Observed subtidal current variations at days-weeks timescales were pronounced and dominantly shaped by wind variations. South of Block Island they were most intense, typically in the range of 15-30 cm s^{-1}, and generally aligned with the large-scale coastline in the east-northeast/west-southwest direction. Deviations from vertically uniform structure were modest, though anomalously strong deep currents onshore were observed in association with the intrusion of shelfbreak/slope water. Over Cox Ledge subtidal currents were similarly responsive to wind variations although weaker (~10-20 cm s^{-1}), and aligned in a direction along the coastline from Martha's Vineyard toward southern Rhode Island, in general agreement with the hydrodynamic simulation of 2006 discussed in Part 1. The weakest subtidal currents were seen in central RIS (~5-15 cm s^{-1}), where they were also strongly wind-driven but took a more variable range of directions in the upper water column; the flow direction in the deeper water column there was aligned parallel to the adjacent Cox Ledge just south of the site.

Attributes of observed monthly mean currents were in good agreement with expectations for residual circulation based on Part 1, in particular with regard to the offshore/onshore components of shallow/deep flow in the winter, and the summer presence of the RIS Current flowing around the periphery of RIS counterclockwise and contributing to strong southwestward flow just east and south of Block Island. It bears re-emphasizing that the magnitudes of these longer-term mean currents are, except in summer, generally weak compared with wind-driven subtidal variations on days-weeks timescales. They are also weaker than tidal currents over most of the western OSAMP area. Nonetheless these weak residual currents play a major role in determining transport pathways for water and waterborne materials, and hence the distributions of water properties and tracers.

Dissolved oxygen observations from the vessel-based surveys were lowest (~5-6 mg l^{-1}) near the bottom in a small area in northern RIS, south of the mouth of Narragansett Bay, during the June and September surveys when stratification was strongest. These observations (two 2-3 day periods) are not sufficient to ascertain whether hypoxia (the RI Department of Environmental Management applies survival-protective thresholds of 4.8, 2.9, and 1.4 mg l^{-1} for chronic, 24-hr and 1-hr exposures respectively in Narragansett Bay; RI DEM (2006)) did or did not occur during the 2009 and 2010 summer seasons. However, if deep oxygen variability in Narragansett Bay on days-weeks timescales and inter-annually (Codiga et al. 2009) is taken to be representative of RIS characteristics, the measurements suggest that hypoxia could occur in RIS for limited periods during some summers. Projected climate regional climate change suggests wetter, hotter conditions and more storms (Frumhoff et al. 2007); depending on the net influence of these competing trends on stratification, the likelihood and intensity of hypoxia in the OSAMP region could be increased or reduced. Further work is needed to address this issue.

Chlorophyll concentrations from the vessel-based surveys imply extreme spatial patchiness and temporal variability of phytoplankton biomass in the OSAMP region. Integrated across the whole region, highest biomass was observed in the September 2009 survey, with highest chlorophyll in BIS and eastern RIS. In those areas, as well as in central RIS where overall biomass was lower, highest chlorophyll was typically detected in a subsurface layer as opposed to the surface. Although not evident during the December and March surveys, when biomass was very low, similar vertical structure in the chlorophyll field was observed in the June survey. It should be noted that the quarterly surveys provided very crude temporal resolution, and thus the low biomass observed in Spring (March 2010) should not be interpreted as the absence of a Springtime phytoplankton bloom, but more likely that such an event occurred later in Spring.

During the vessel-based surveys the depth of the euphotic zone was found to be highly variable spatially, ranging from 10-40 m. During the high stratification periods (September and June), the euphotic zone was deep in central RIS and the shelf region offshore, and relatively shallow in BIS and in the northern and eastern portions of RIS. The boundary between these zones was typically quite sharp; in the western half of the OSAMP domain it generally mirrors the water mass boundary delineating the southern and eastern edge of the Long Island Sound outflow plume. The euphotic depth in RIS is quite low during December, although chlorophyll values are lower (which would suggest clearer water). High turbidity measurements during this survey suggest that low light penetration might result from the presence in the water column of particles re-suspended from the bottom. Turbidity and phytoplankton biomass were generally low during the March survey, resulting in a deep euphotic zone (> 25 m) throughout almost the entire region.

The significant wave height and peak wave period from five representative sites, and the peak wave direction from three sites, indicate that geographic variations in wave parameters across the southern and central OSAMP region are modest. Typical significant wave heights are 0.5-2.5 m and typical peak wave periods are 5-10 seconds. During wind events of several days duration, significant wave heights can reach 4-6 m within hours, after which they fall off again as rapidly;

peak wave periods become longer, up to 14 seconds, and remain elevated for a few days. Peak wave direction has a persistent northward or northwestward component, except at the farthest offshore site where it is more variable as a result of longer fetch from a wider range of directions.

Acknowledgements

Mooring design and preparation by Jim Fontaine of Exeter Science Services was crucial to the success of the vessel-based surveys and PO mooring deployments; he was also able to miraculously recover data from a damaged CTD whose pressure case had been completely cracked open, allowing the electronics board to soak in seawater for more than a month. We thank Captain Tom Puckett for his superb work on the R/V Cap'n Bert for mooring deployments/recoveries and on the R/V Hope Hudner for the vessel-based surveys, for which Brian Oakley was also very helpful. Candace Oviatt generously provided us with the CTD package for the vessel-based surveys.

References

Churchill, J.H. 1985. Intrusions of outer shelf and slope water within the nearshore zone off Long Island, New York. *Limnol. Oceanogr.* 30(5), 972-986.

Codiga, D.L., L.V. Rear. 2004. Observed tidal currents outside Block Island Sound: Offshore decay and effects of estuarine outflow. *J. Geophys. Res.* 109, doi:10.1029/2003JC001804.

Codiga, D.L. 2005. Interplay of wind forcing and buoyant discharge off Montauk Point: seasonal changes to velocity structure and a coastal front. *J. Phys. Oceanogr.* 35, 1068-1085.

Codiga, D.L., H.E. Stoffel, C.F. Deacutis, S. Kiernan, C. Oviatt. 2009. Narraganset Bay Hypoxic Event Characteristics Based on Fixed-Site Monitoring Network Time Series: Intermittency, Geographic Distribution, Spatial Synchronicity, and Inter-Annual Variability. *Estuaries and Coasts* 32(4), p621 DOI 610.1007/s12237-12009-19165-12239.

Codiga, D.L., D.S. Ullman. 2010. Characterizing the Physical Oceanography of Coastal Waters Off Rhode Island, Part 1: Literature Review, Available Observations, and A Representative Model Simulation. *Appendix to Rhode Island Ocean Special Area Management Plan*, 169 pp.

Colosi, J.A., R.C. Beardsley, J.F. Lynch, G. Gawarkiewicz, C.S. Chiu, A. Scotti. 2001. Observations of nonlinear internal waves on the outer New England continental shelf during the summer Shelfbreak Primer study. *J. Geophys. Res.* 106, 9587-9601.

Frumhoff, P., J. McCarthy, J. Melillo, S. Moser, D. Wuebbles. 2007. Confronting Climate Change in the U.S. Northeast: Science, Impacts, and Solutions. Synthesis report of the Northeast Climate Impacts Assessment (NECIA). *Union of Concerned Scientists, Cambridge, MA*, 160 pp.

Lentz, S., K. Shearman, S. Anderson, A. Plueddemann, J. Edson. 2003. Evolution of stratification over the New England shelf during the Coastal Mixing and Optics study, August 1996-June 1997. *J. Geophys. Res* 108, 3008-3008.

Linder, C.A., G. Gawarkiewicz. 1998. A climatology of the shelfbreak front in the Middle Atlantic Bight. *J. Geophys. Res* 103, 18405-18423.

Mountain, D.G. 1991. The volume of Shelf Water in the Middle Atlantic Bight: Seasonal and interannual variability, 1977-1987. *Cont. Shelf Res.* 11, 251-267.

O'Reilly, J.E., C. Evans-Zetlin, D.A. Busch. 1987. Primary production *In: R. H. Backus (Ed.), Georges Bank, MIT Press, Cambridge*, 220-233.

Pawlowicz, R., B. Beardsley, S. Lentz. 2002. Classical tidal harmonic analysis including error estimates in MATLAB using T-TIDE. *Computers & Geosciences* 28, 929-937.

RIDEM. 2006. Water quality regulations. Office of Water Resources, Department of Environmental Management, State of Rhode Island and Providence Plantations. [http://www.dem.ri.gov/programs/benviron/water/quality/surfwq/index.htm]

Soulsby, R.L. 1990. Tidal-current boundary layers. In: Le Mehaute, B., Hanes, D.M (Ed.), The Sea; Ocean Engineering Science Vol. 9A, Wiley-Interscience, New York, pp. 523-566.

Ullman, D.S., D.L. Codiga. 2004. Seasonal variation of a coastal jet in the Long Island Sound outflow region based on HF radar and Doppler current observations. *J. Geophys. Res.* 109, doi:10.1029/2002JC001660.

Wang, D.-P. 1979. Low frequency sea level variability on the Mid-Atlantic Bight. *J. Mar. Res.* 37, 683-697.

Table 1. Moored instrumentation locations, dates of analyzed records, and sensor information.

	MD-S	MD-F	PO-S	PO-F	BIWB
Latitude	41^{o} 06.045’	41^{o} 07.096’	41^{o} 02.869’	41^{o} 14.970’	40^{o} 58.117’
Longitude	71^{o} 34.174’	71^{o} 01.703’	71^{o} 29.972’	71^{o} 05.297’	71^{o} 07.565
Depth [m]	26	34	44.1	43.5	48.2
Dates	Oct 9, 2009 to July 15, 2010		FA09: Sep 15, 2009 to Jan 14, 2010 SP10: Mar 19, 2010 to Jun 23, 2010		Oct 9, 2009 to July 15, 2010
Sensors: CTD	1, 6, 18m	1, 6, 28m	1, 3, 7, 12, 20, 28, 35m		(none)
Sensors: Currents	Aanderaa 2m; ADCP 5, 6, 7, … 21, 22 m	Aanderaa 2m; ADCP 5, 6, 7, … 30, 31 m	ADCP 4, 5, 6, … 40, 41, 42m	ADCP 4, 5, 6, … 39, 40, 41m	(none)
Sensors: Waves	Accelerometers on discus buoy		Orbital currents from bottom-mounted ADCP		Datawell buoy
Sensors: Meteorology	Winds: 4m Temperature, Pressure: 3m	Winds: 4m Temperature, Pressure: 3m	(none)	(none)	(none)

Notes: See text for abbreviations. The PO-S and PO-F coordinates apply to the bottom-mounted ADCPs; the buoys were within a few hundred meters of them, PO-S buoy at 41^{o} 02.893 71^{o} 30.016 and PO-F buoy at 41^{o} 15.000’ 71^{o} 05.500.

Table 2. Vessel-based hydrographic survey dates.

Survey	Dates	Number of Stations
1 – late summer	2009 Sep. 22, 23, 24	45
2 – late autumn	2009 Dec. 7, 8	38
3 – late winter	2010 Mar. 9, 10, 11	45
4 – late spring	2010 Jun. 16, 18	45

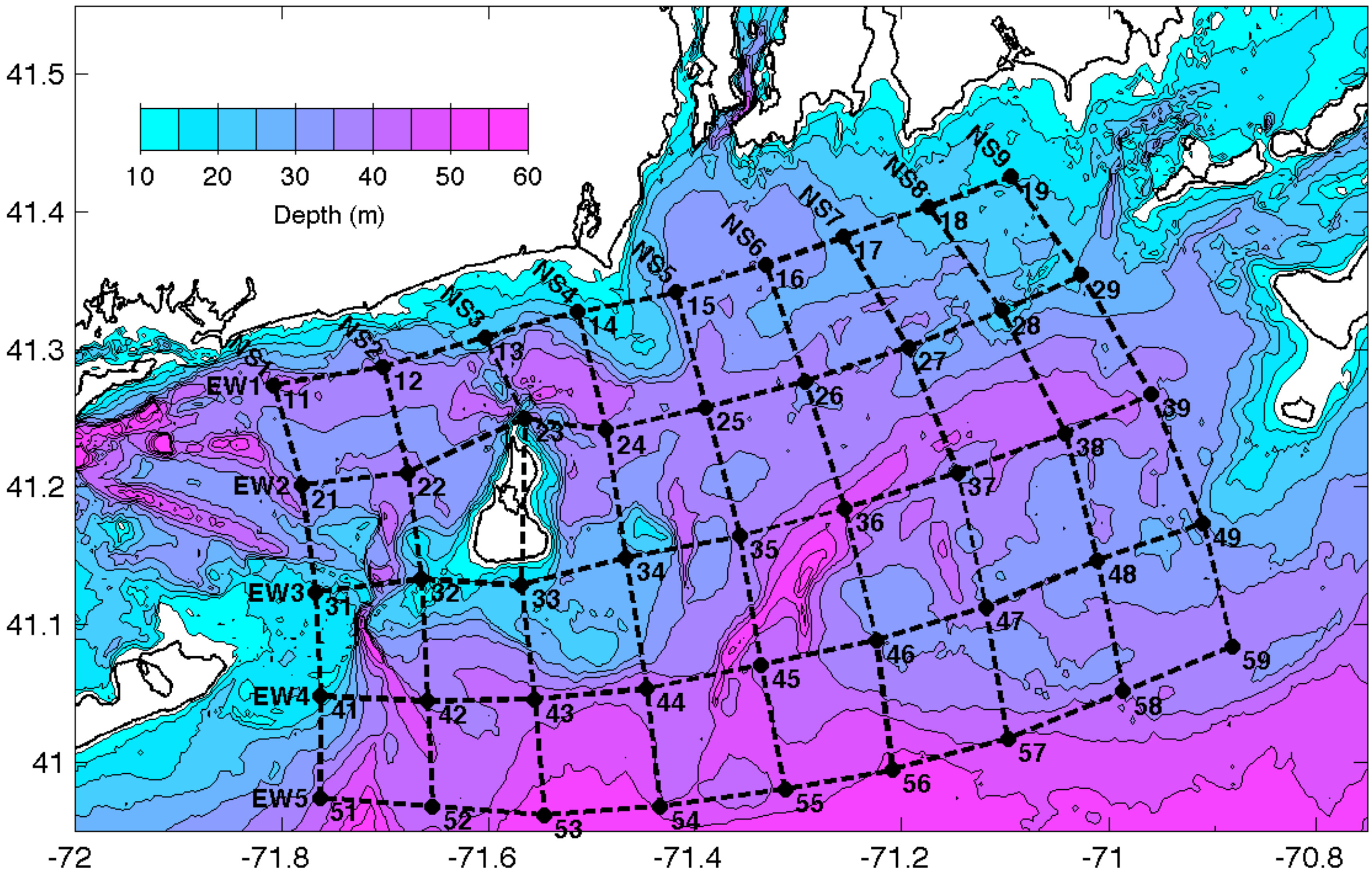

Figure 1. Vessel-based survey station grid superimposed on regional bathymetry.
The dashed lines denote the 9 north-south lines and 5 east-west lines along which vertical sections of hydrographic parameters are presented below.

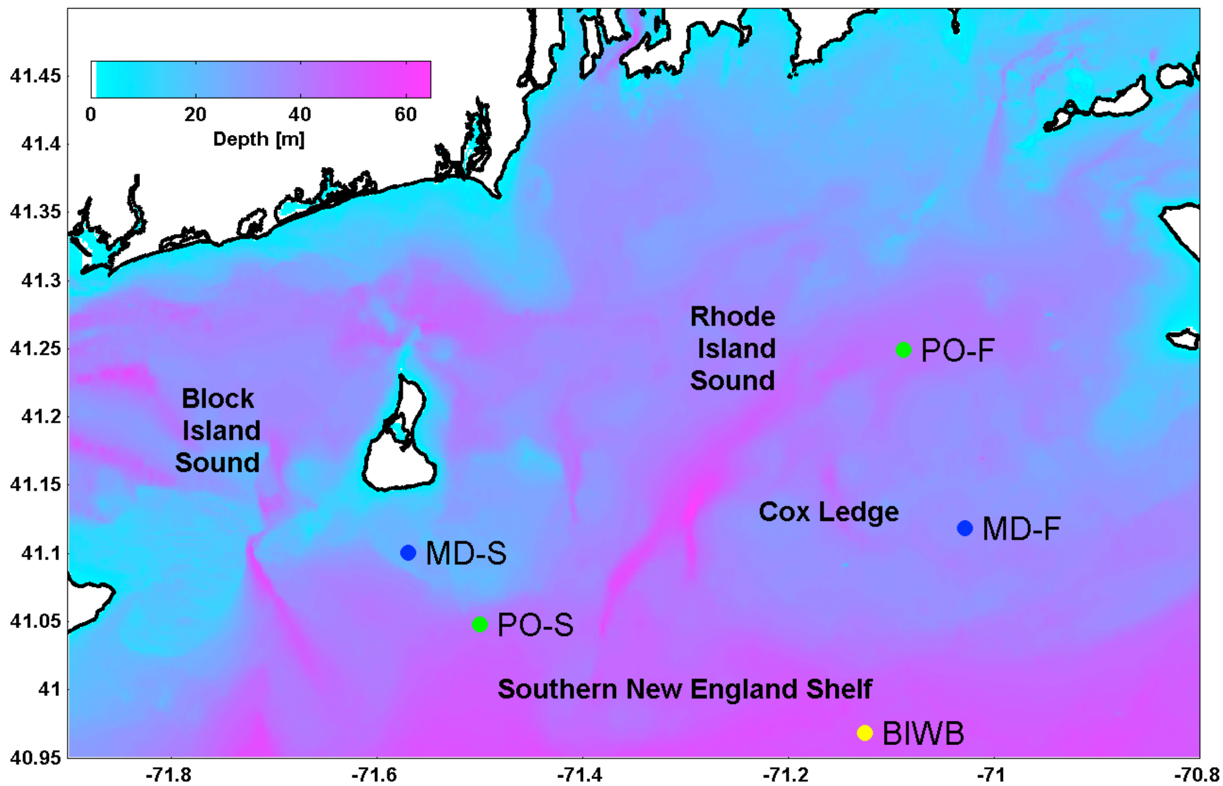

Figure 2. Moored instrumentation sites: MD-S, PO-S, MD-F, PO-F, and BIWB.

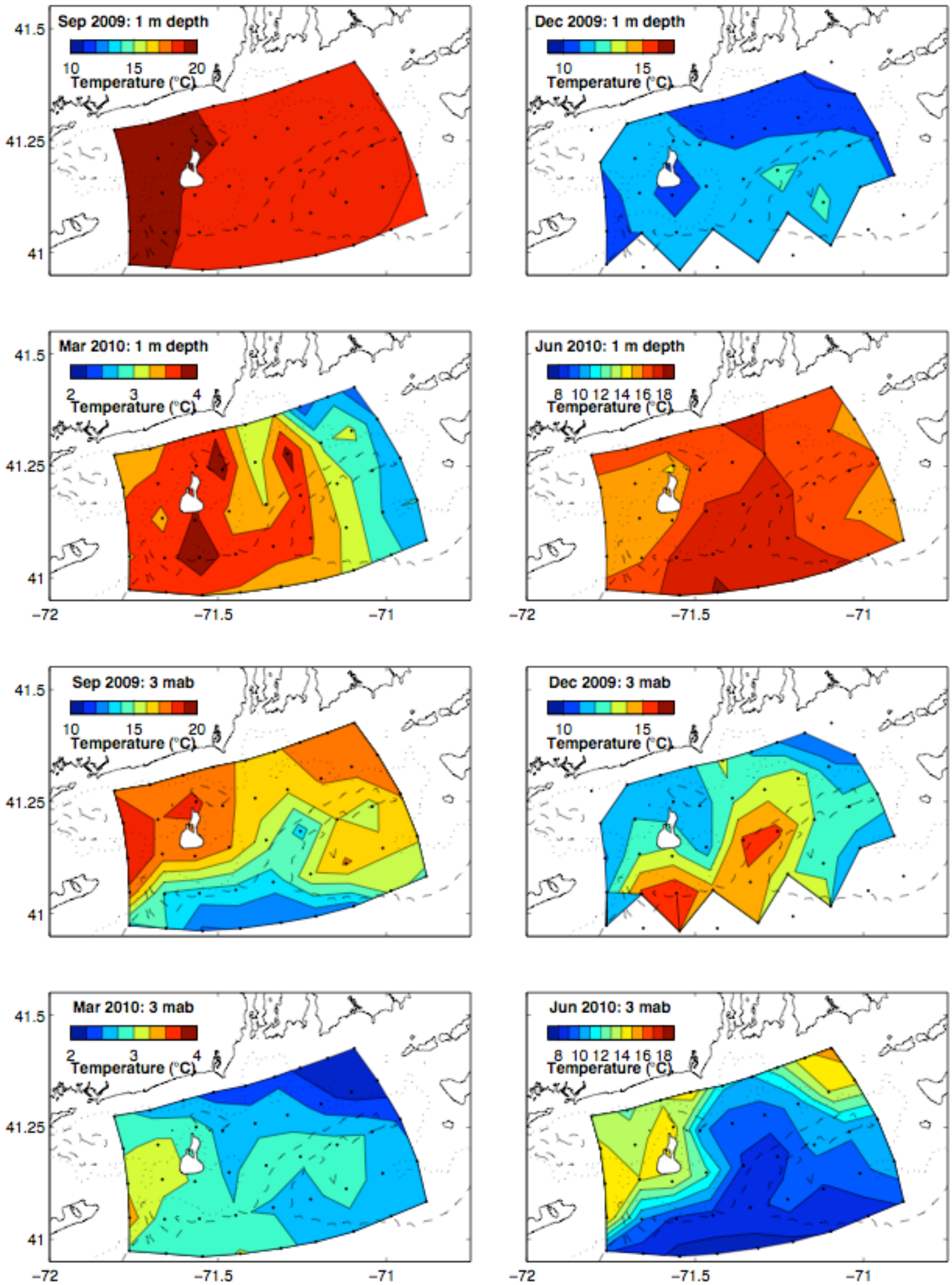

Figure 3. Surveys, Temperature, all seasons: 1 m deep (upper); 3 m above seafloor (lower). The CTD cast locations are denoted by the black dots. The dotted and dashed lines are the 30 m and 40 m isobaths, respectively.

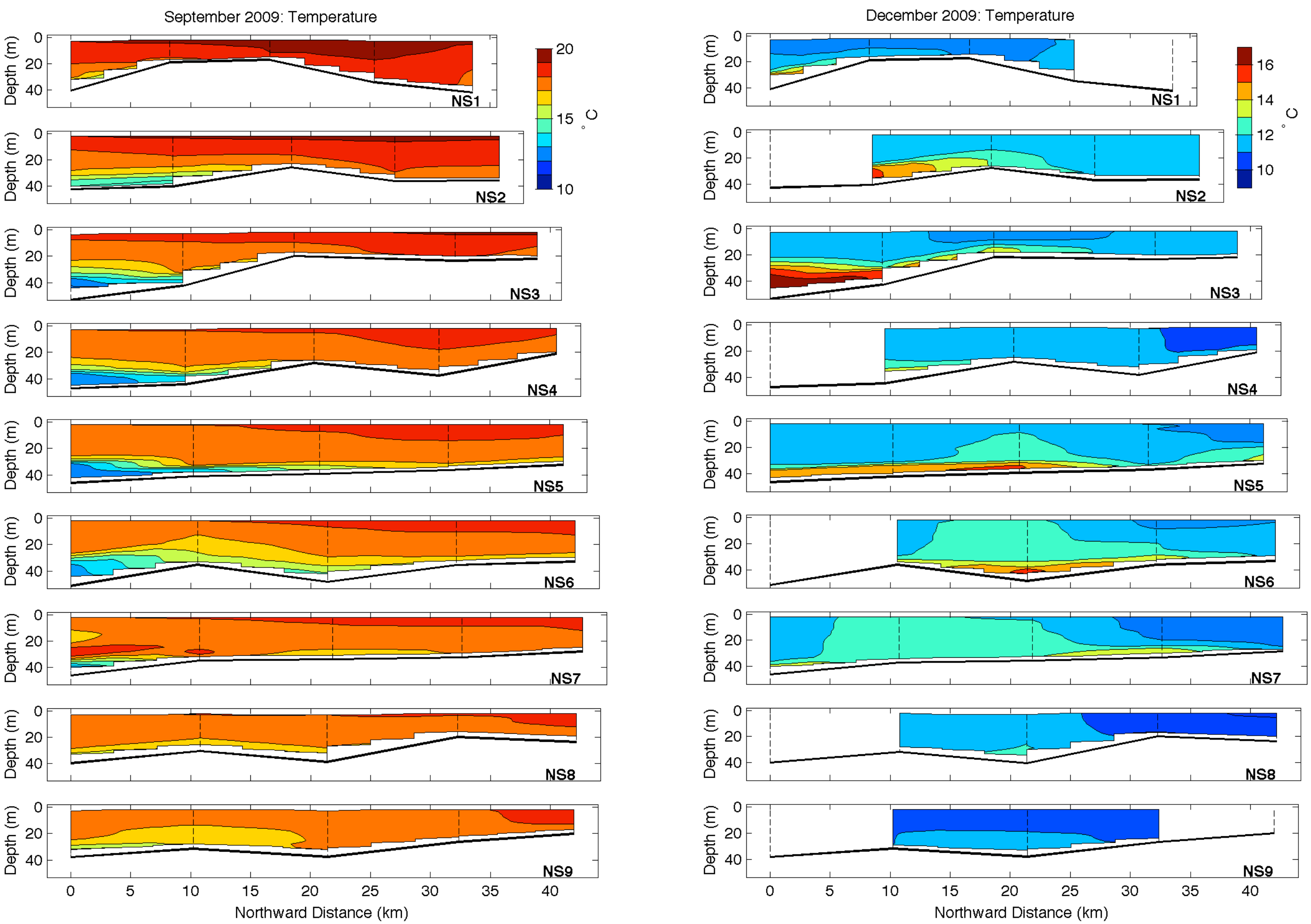

Figure 4. Surveys, Temperature, NS sections: September (left); December (right).
The section numbers are referenced to the map in Figure 1. The dashed lines denote the locations of the CTD casts.

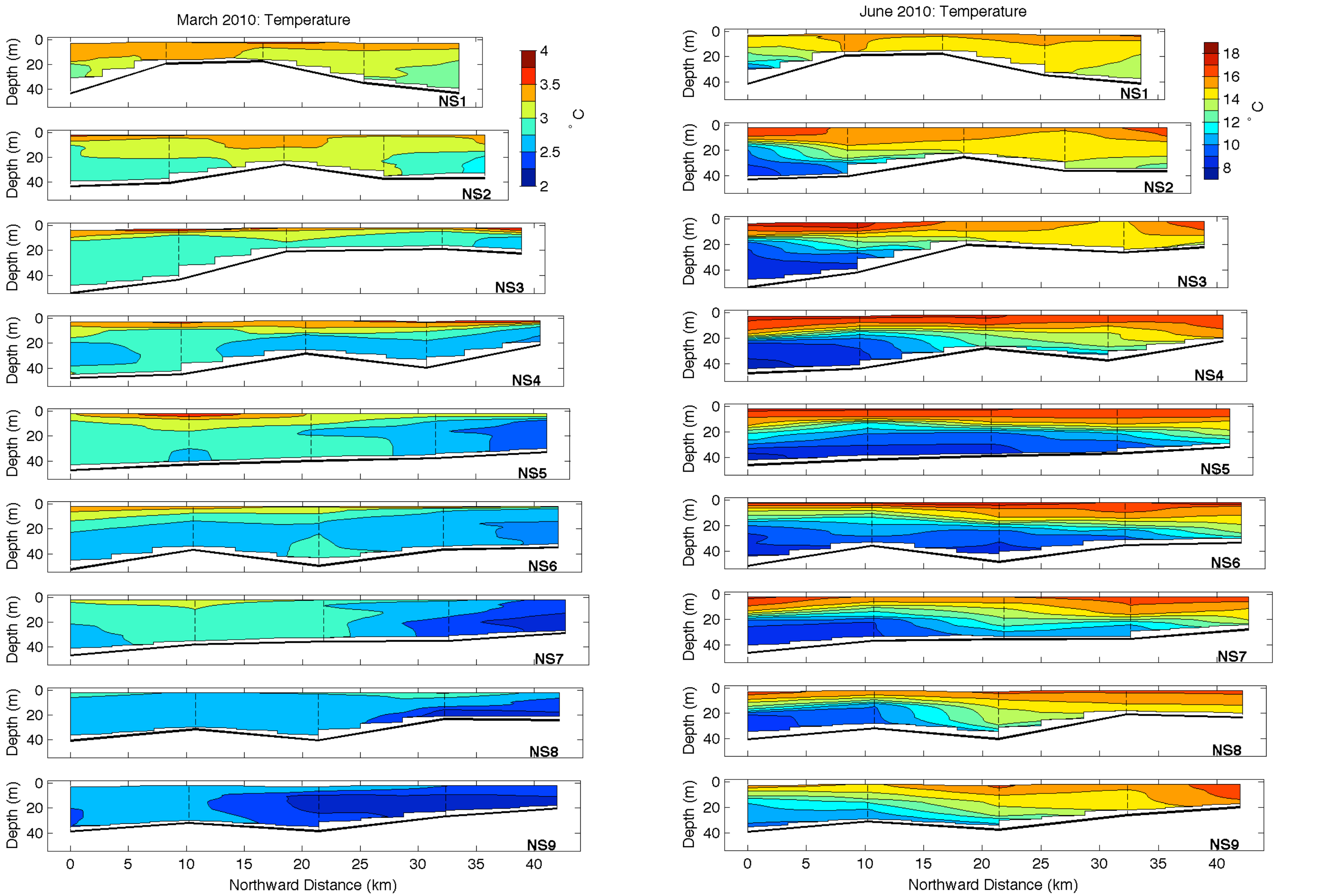

Figure 5. Surveys, Temperature, NS sections: March (left); June (right).
The section numbers are referenced to the map in Figure 1. The dashed lines denote the locations of the CTD casts.

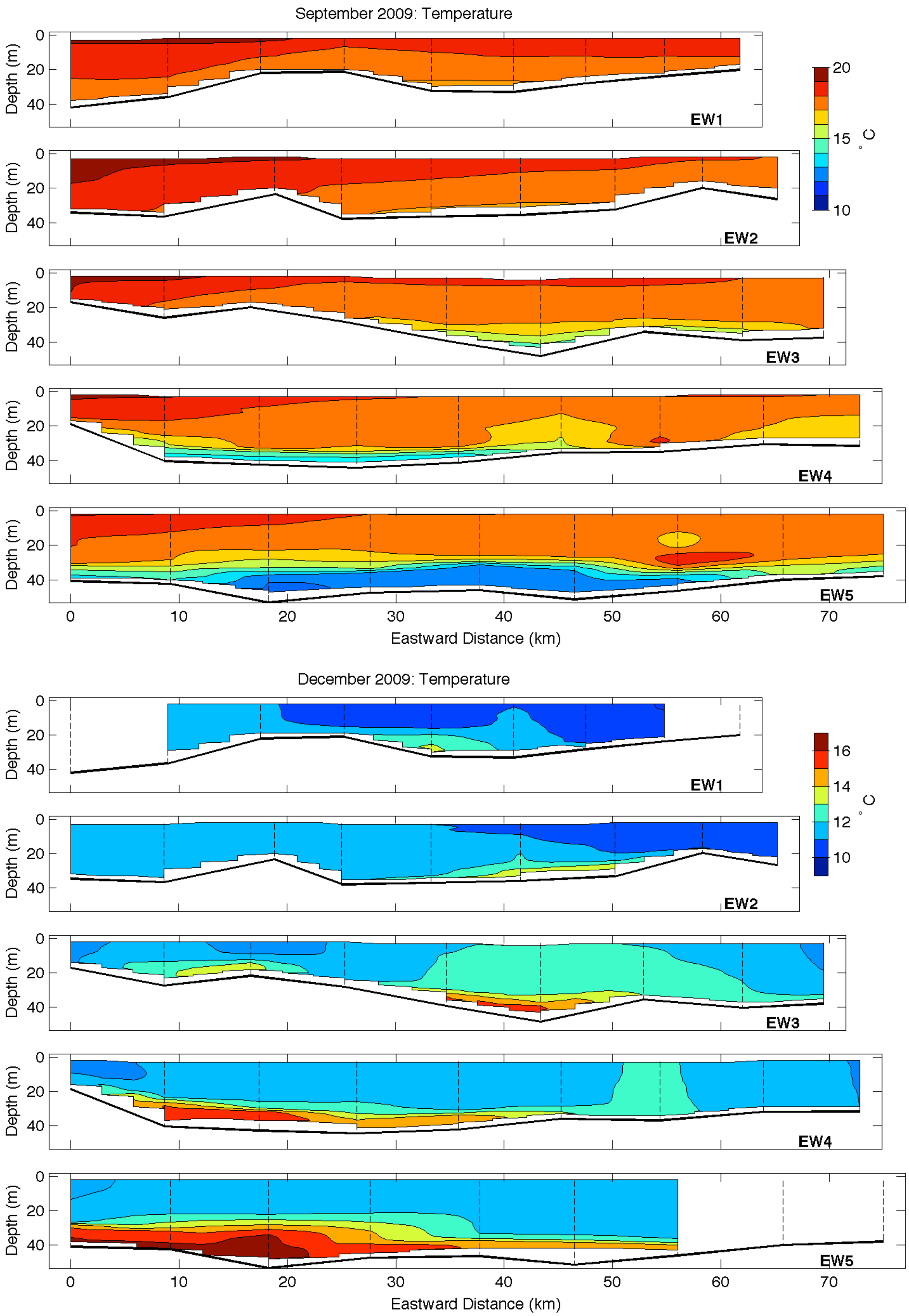

Figure 6. Surveys, Temperature, EW sections: September (upper); December (lower). The section numbers are referenced to the map in Figure 1. The dashed lines denote the locations of the CTD casts.

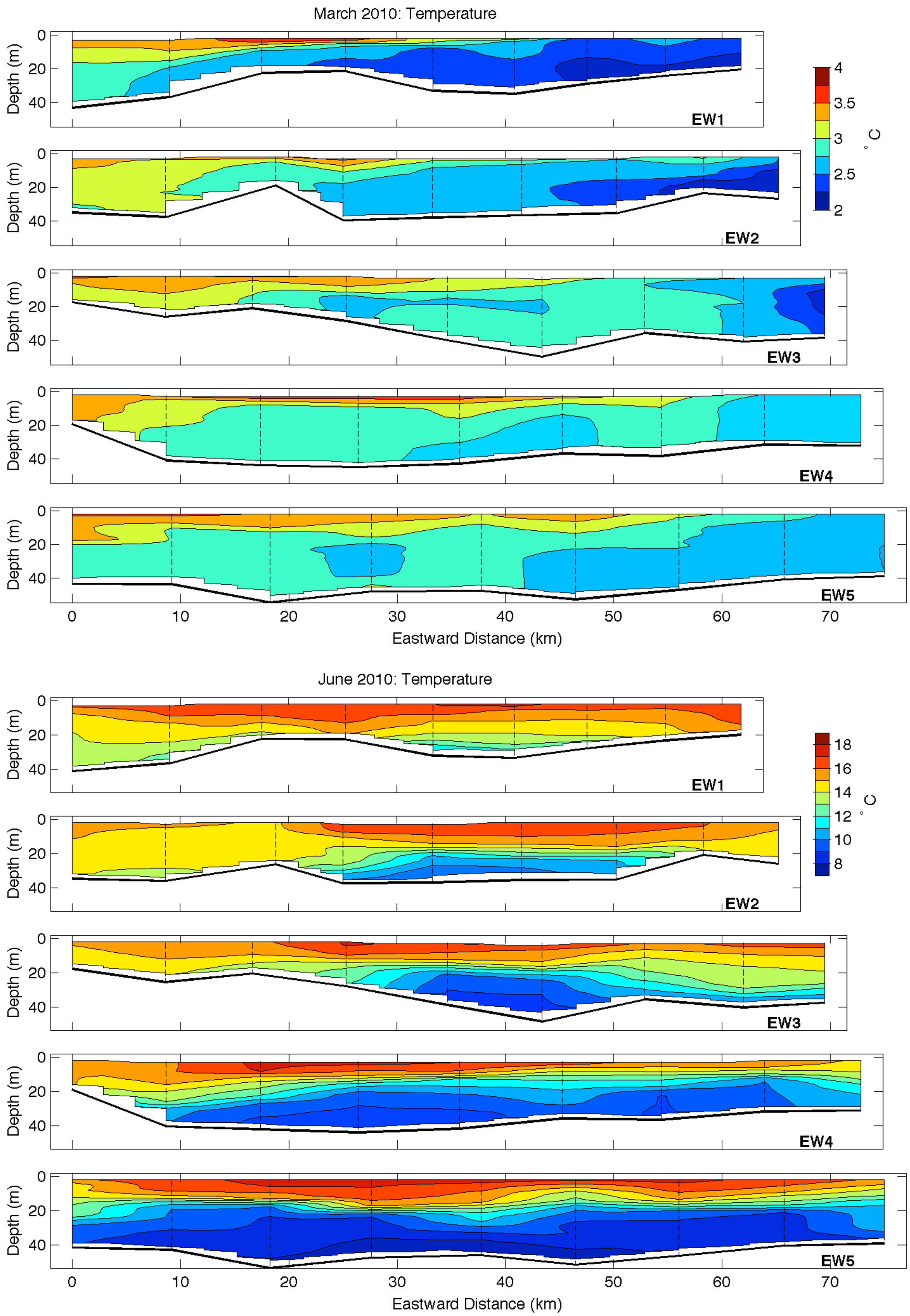

Figure 7. Surveys, Temperature, EW sections: March (upper); June (lower).
The section numbers are referenced to the map in Figure 1. The dashed lines denote the locations of the CTD casts.

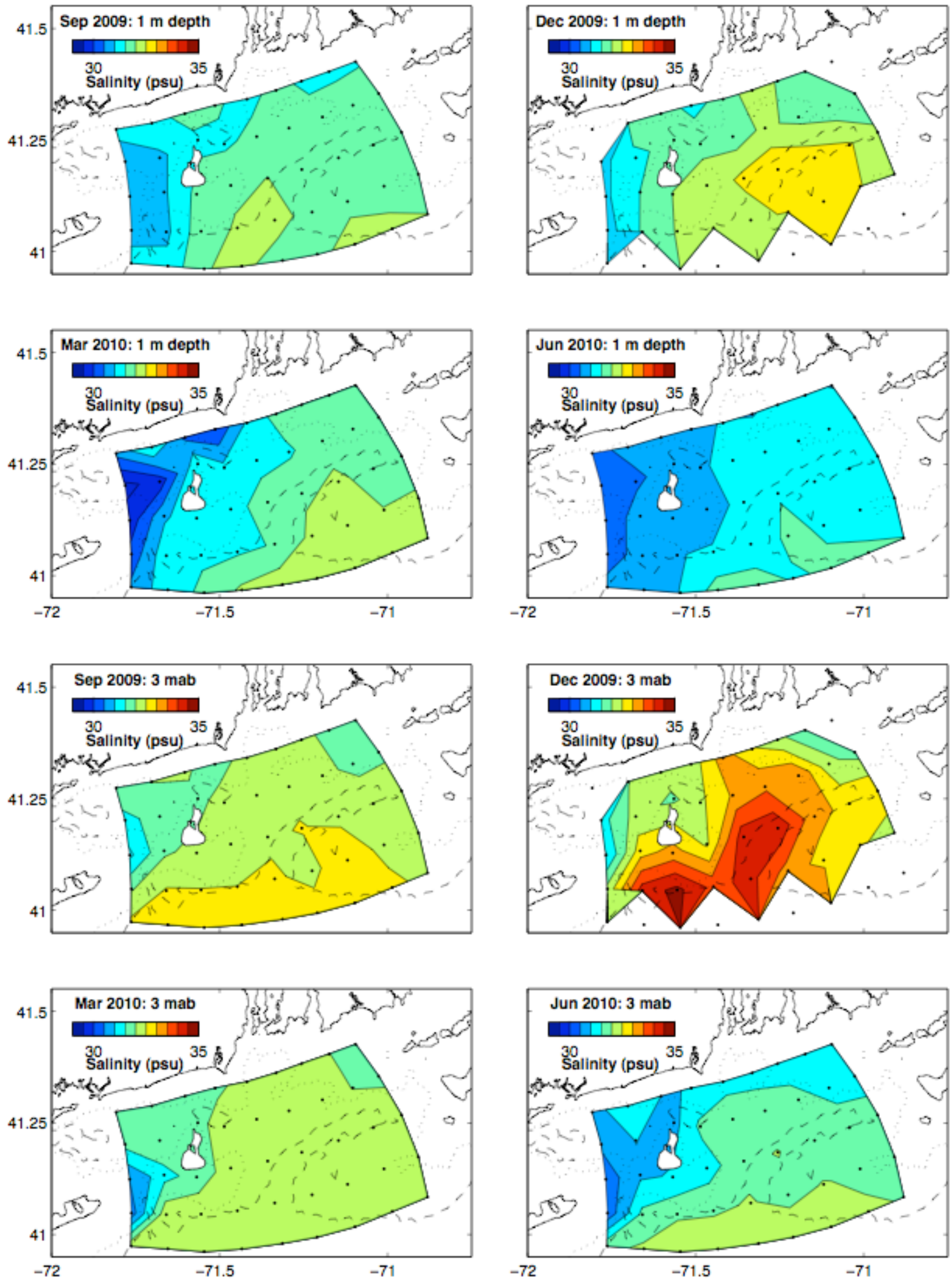

Figure 8. Surveys, Salinity, all seasons: 1 m deep (upper); 3 m above seafloor (lower). The CTD cast locations are denoted by the black dots. The dotted and dashed lines are the 30 m and 40 m isobaths, respectively.

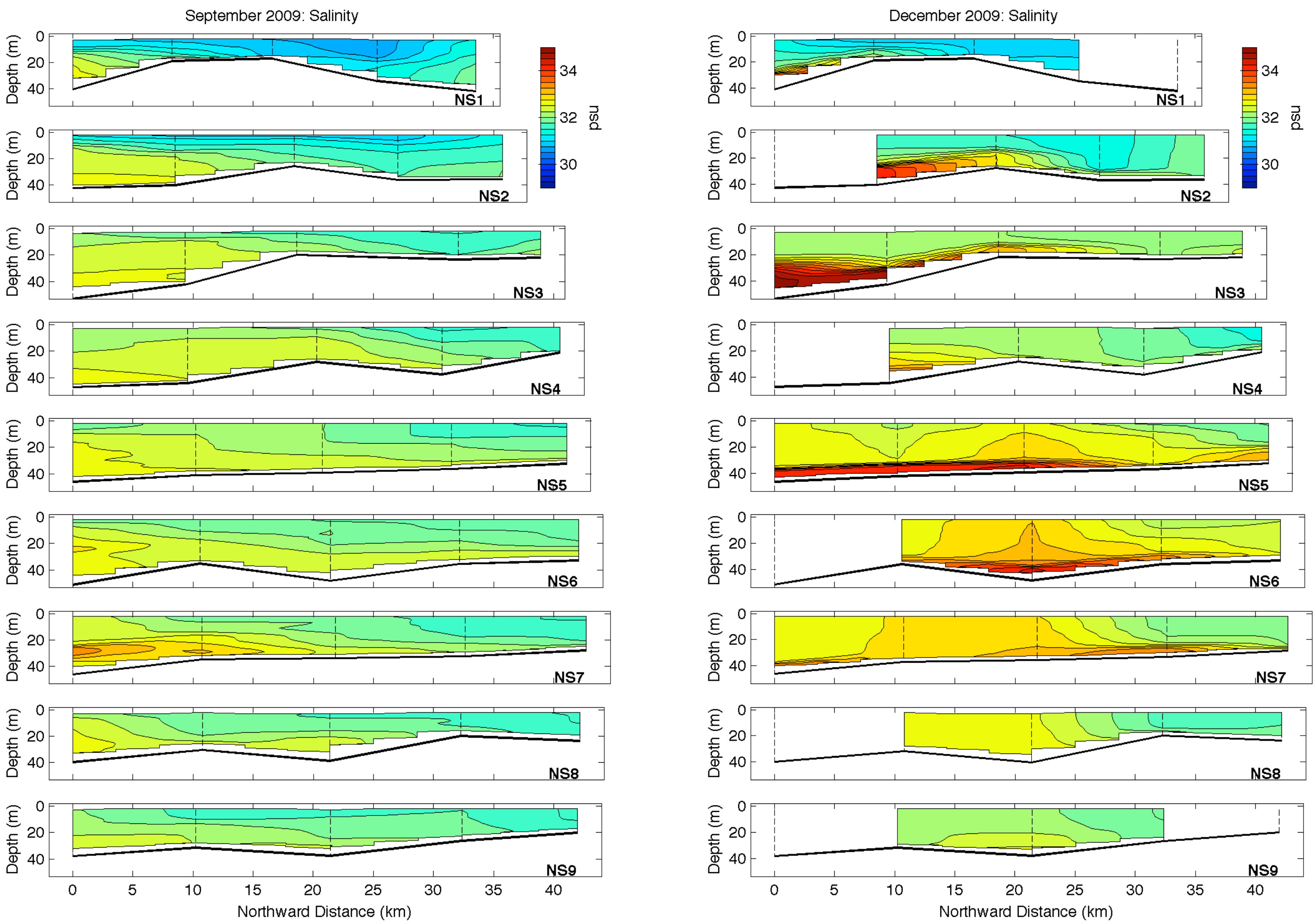

Figure 9. Surveys, salinity, NS sections: September (left); December (right).
The section numbers are referenced to the map in Figure 1. The dashed lines denote the locations of the CTD casts.

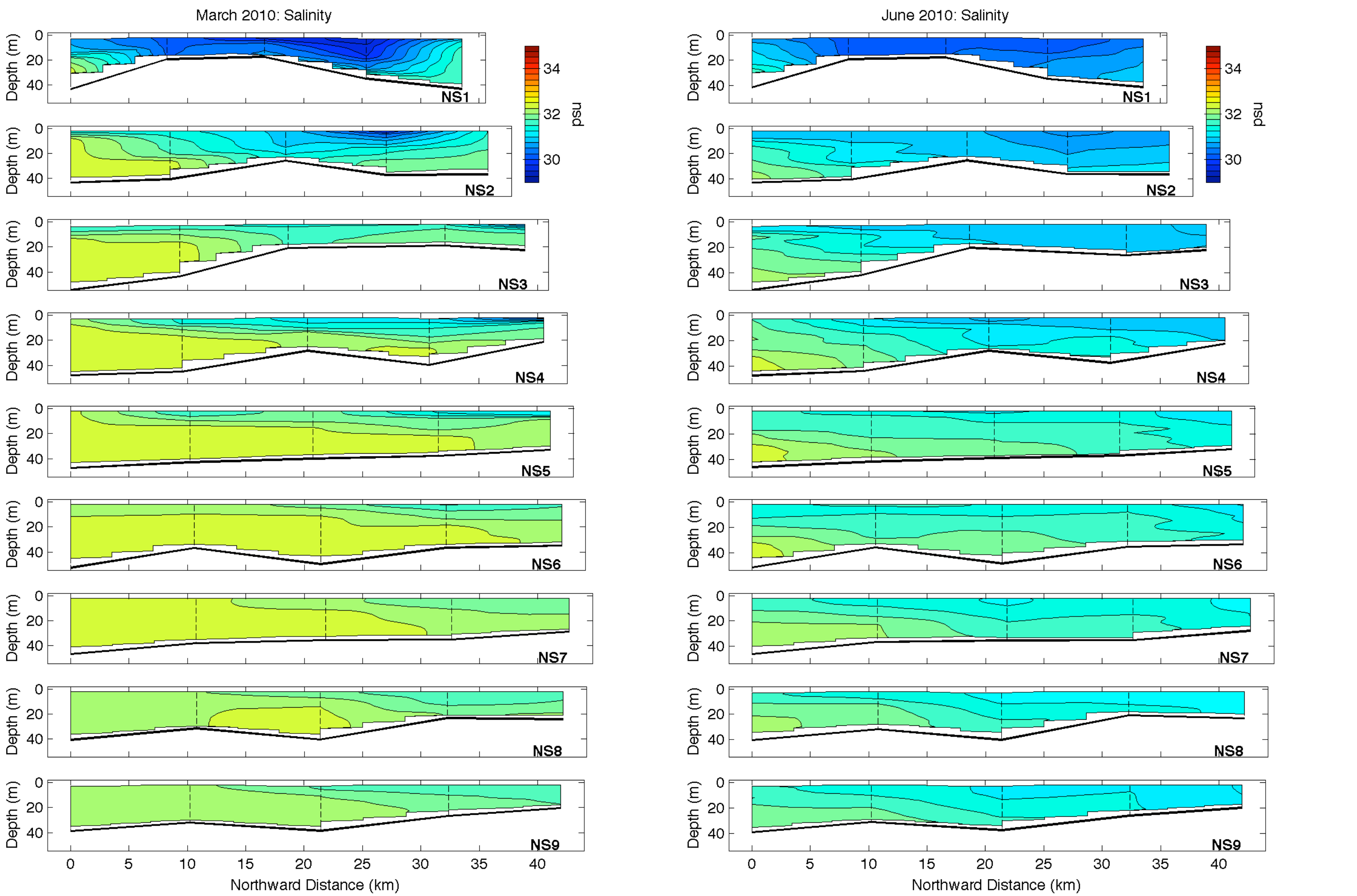

Figure 10. Surveys, salinity, NS sections: March (left); June (right).
The section numbers are referenced to the map in Figure 1. The dashed lines denote the locations of the CTD casts.

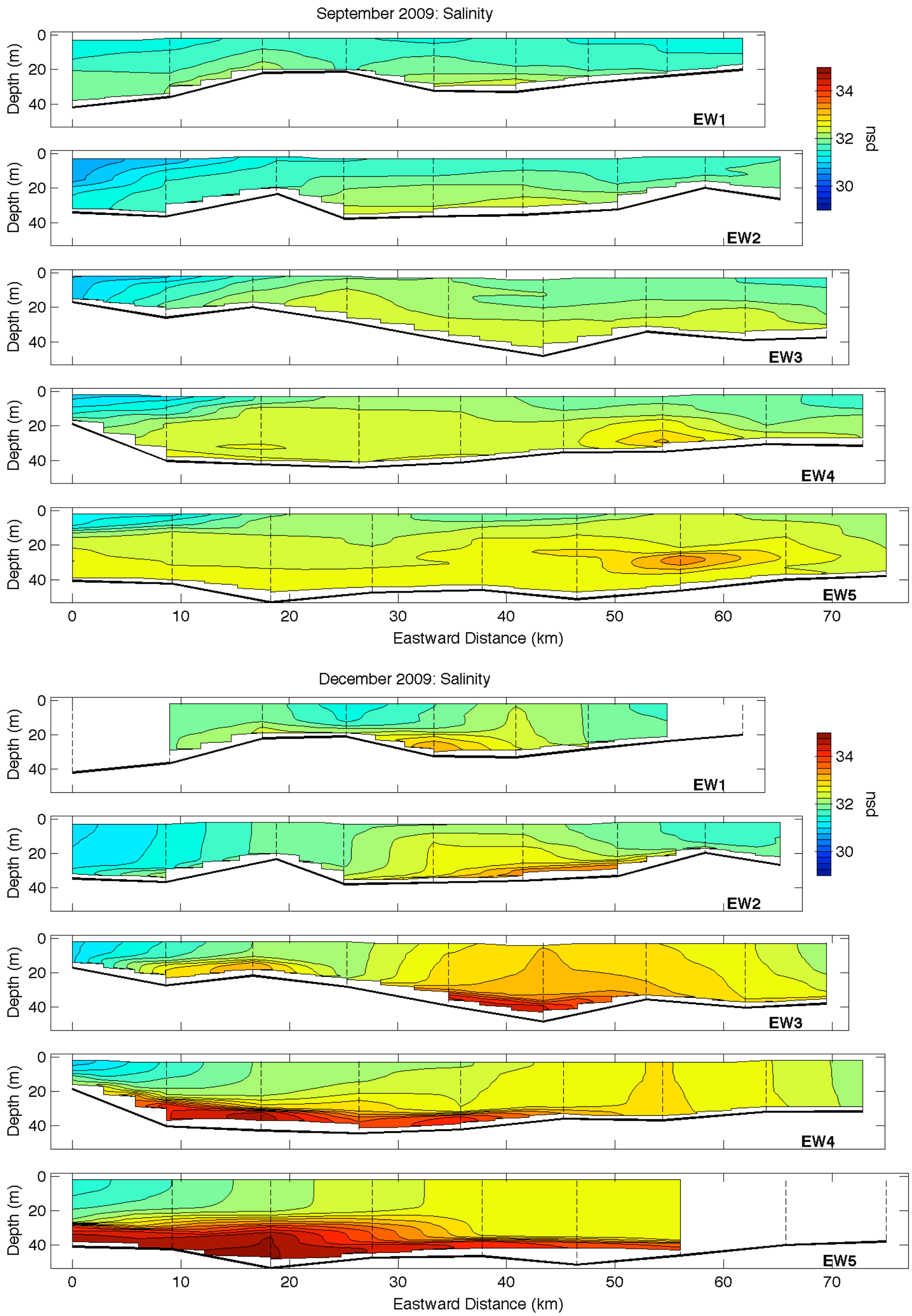

Figure 11. Surveys, Salinity, EW sections: September (upper); December (lower). The section numbers are referenced to the map in Figure 1. The dashed lines denote the locations of the CTD casts.

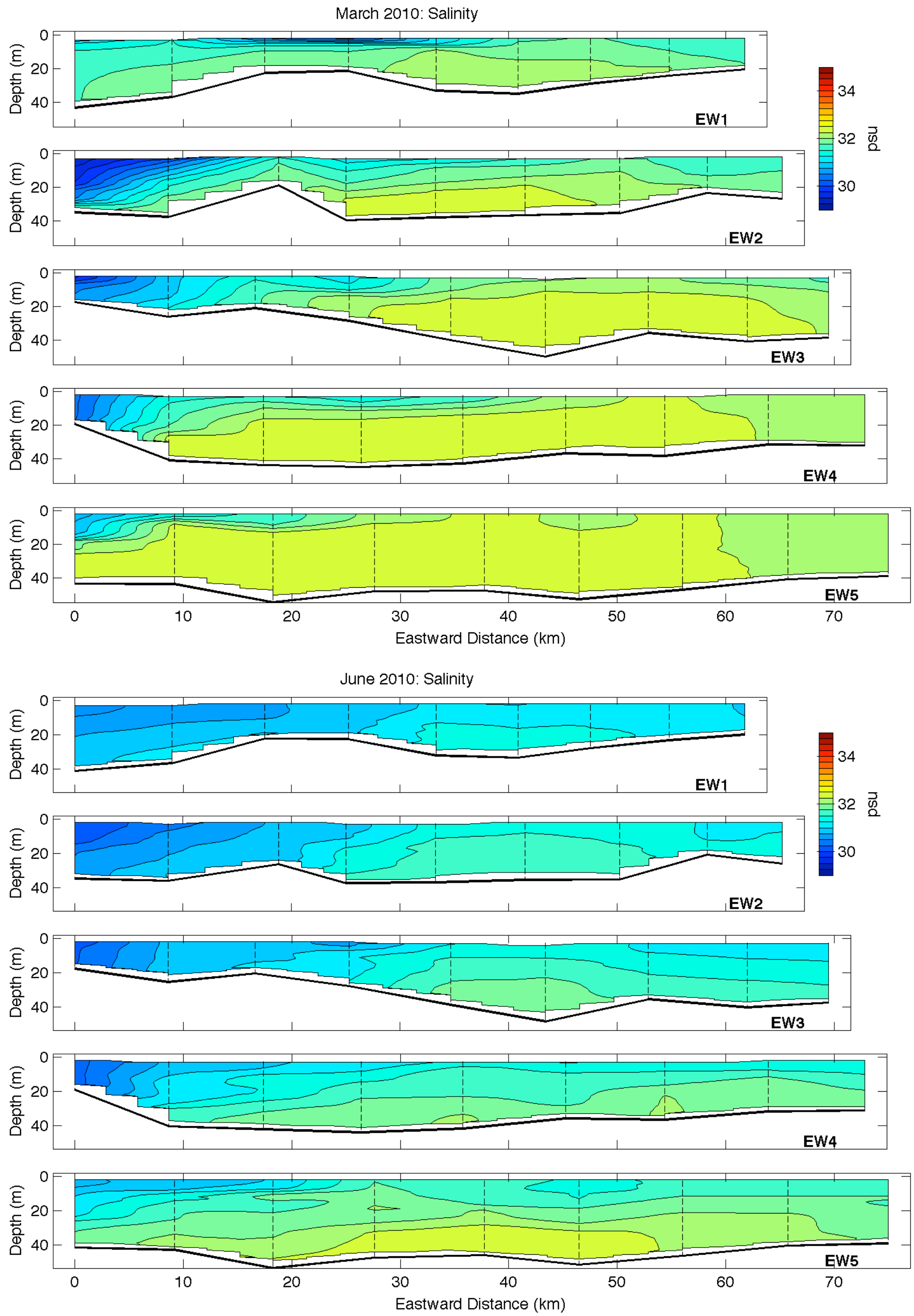

Figure 12. Surveys, Salinity, EW sections: March (upper); June (lower).
The section numbers are referenced to the map in Figure 1. The dashed lines denote the locations of the CTD casts.

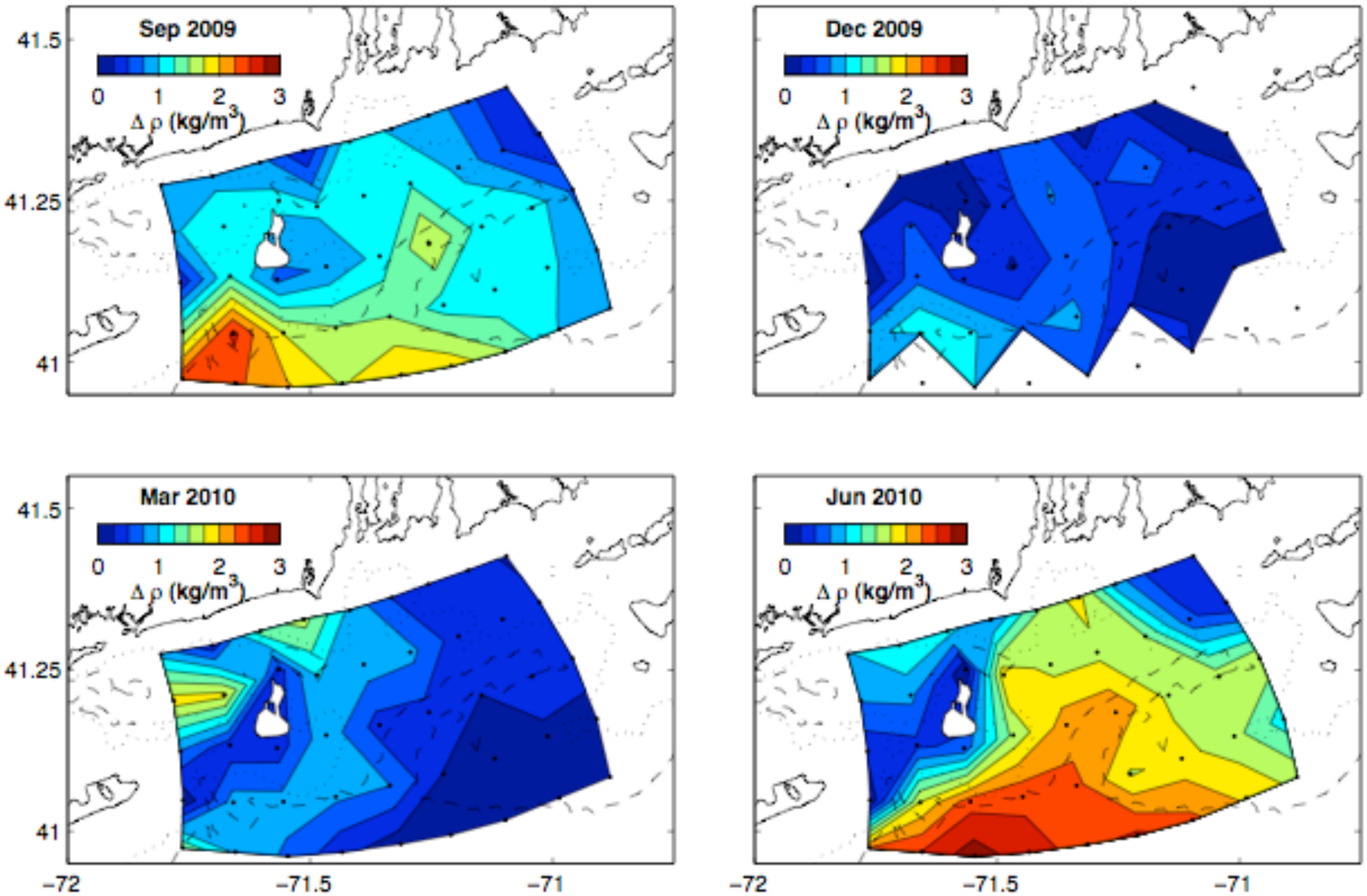

Figure 13. Surveys, Stratification (top-bottom density difference), all seasons.
Stratification is computed as the difference between the near-bottom (typically 2-3 meters above bottom) and near-surface (1m depth) water densities.

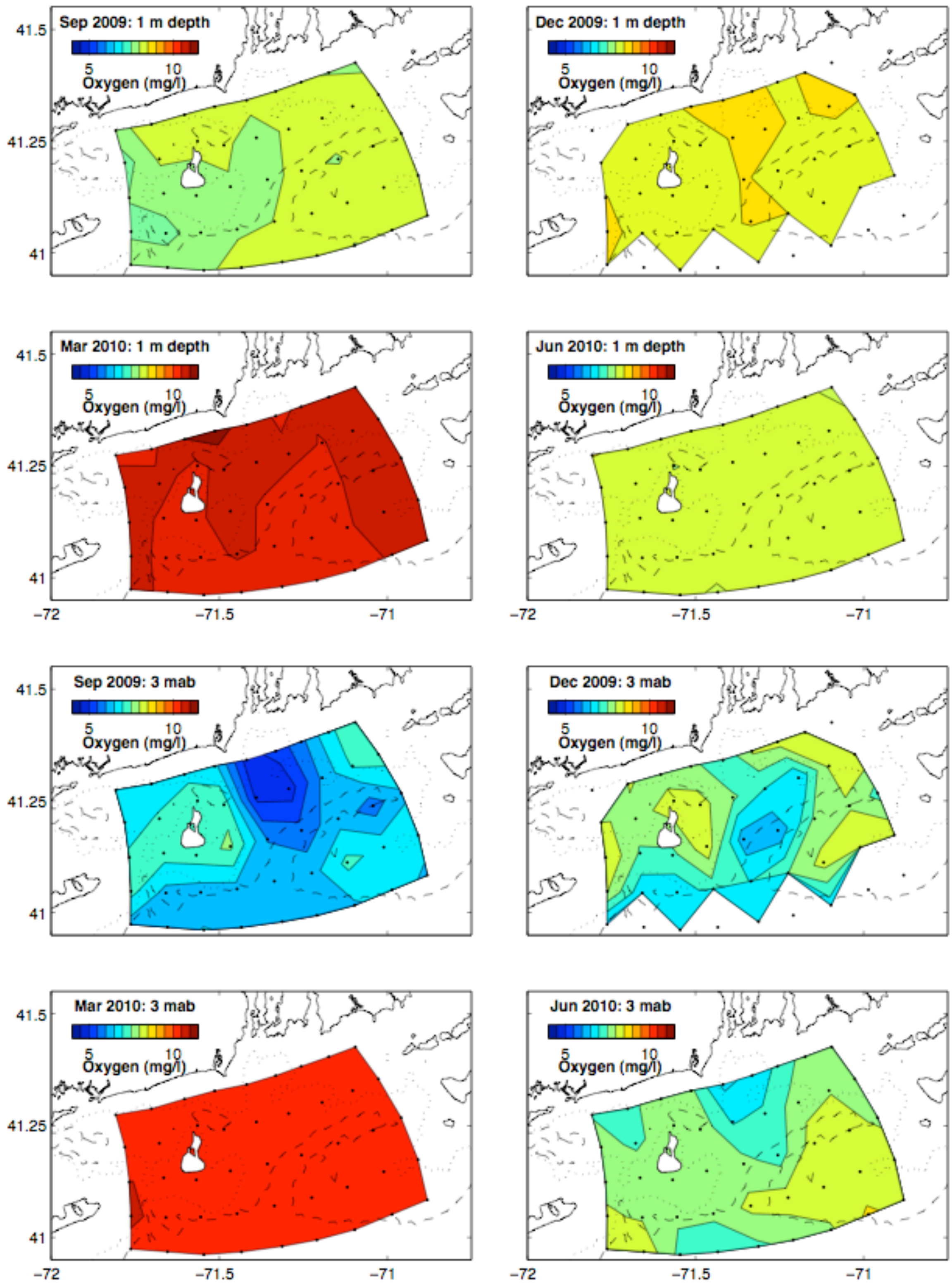

Figure 14. Surveys, Oxygen, all seasons: 1 m deep (upper); 3 m above seafloor (lower). The CTD cast locations are denoted by the black dots. The dotted and dashed lines are the 30 m and 40 m isobaths, respectively.

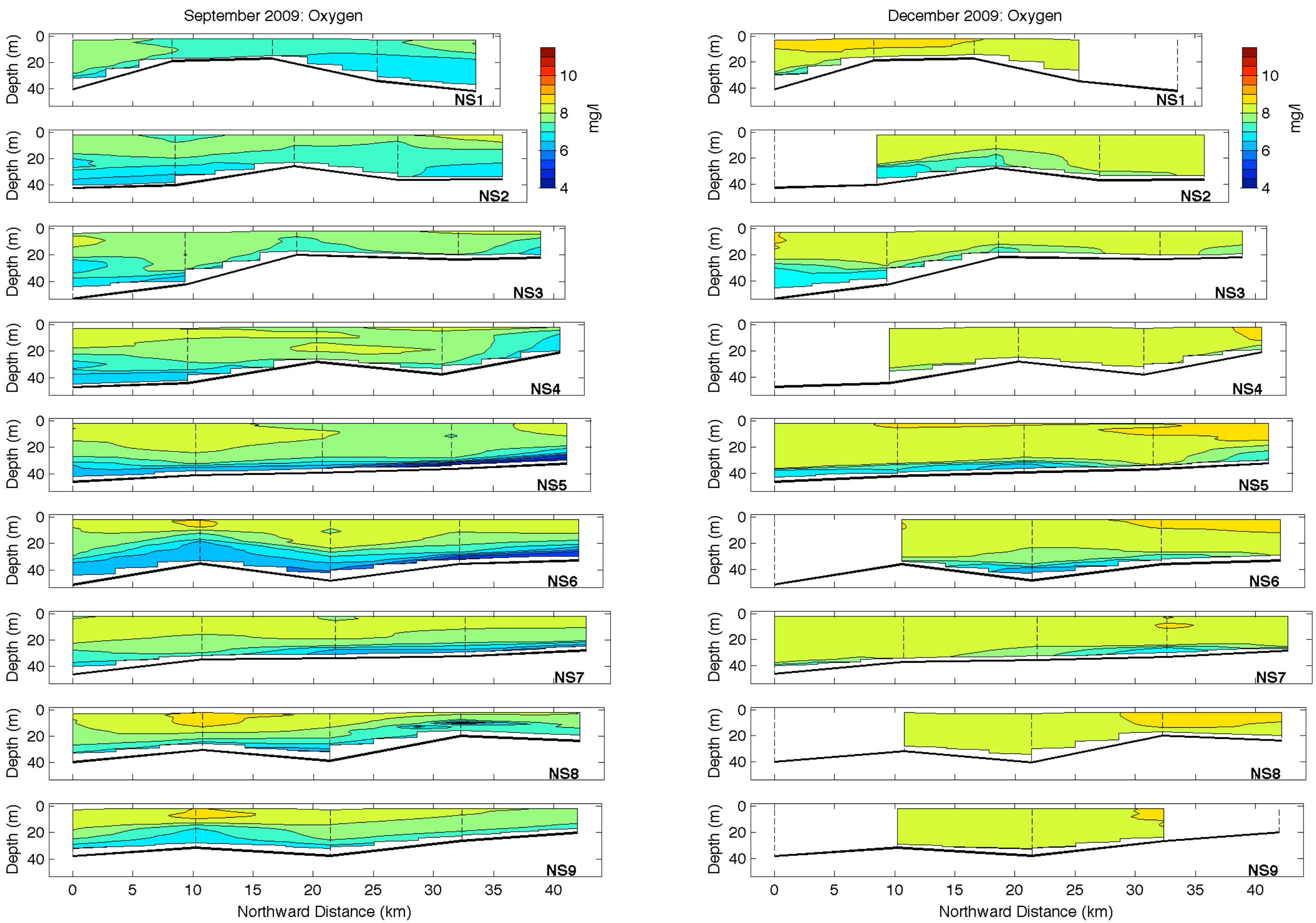

Figure 15. Surveys, Oxygen, NS sections: September (left); December (right).
The section numbers are referenced to the map in Figure 1. The dashed lines denote the locations of the CTD casts.

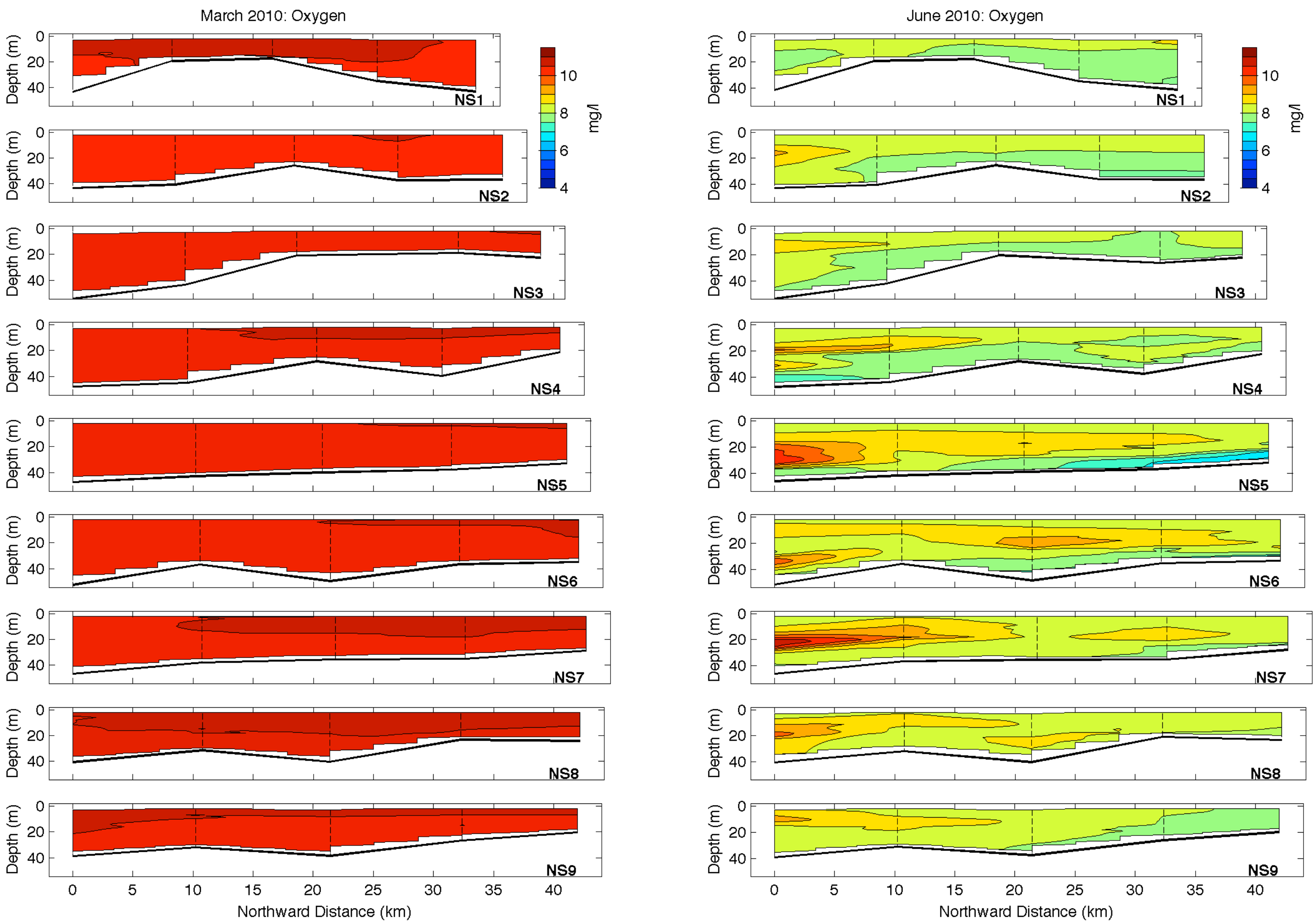

Figure 16. Surveys, Oxygen, NS sections: March (left); June (right).
The section numbers are referenced to the map in Figure 1. The dashed lines denote the locations of the CTD casts.

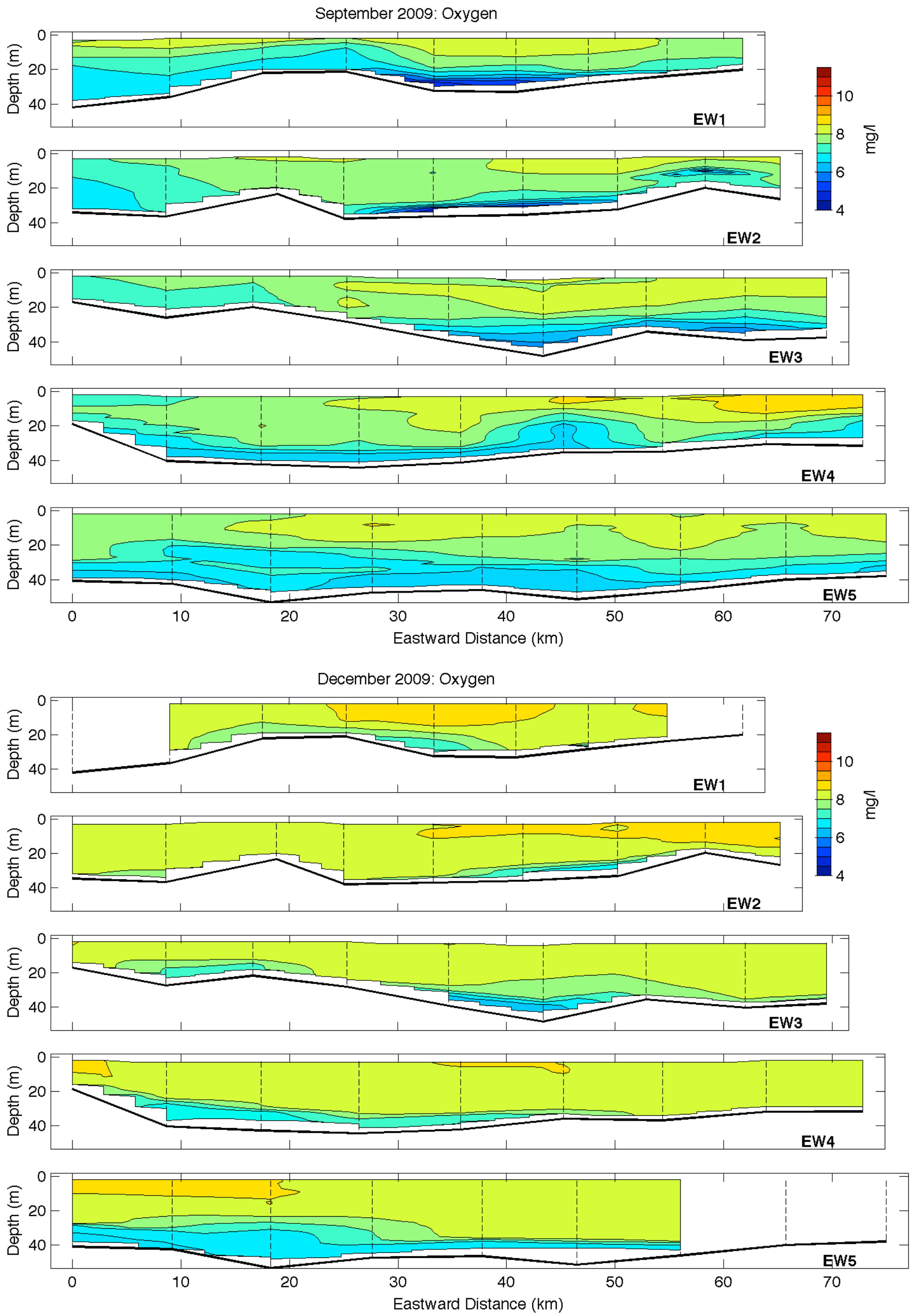

Figure 17. Surveys, Oxygen, EW sections: September (upper); December (lower).
The section numbers are referenced to the map in Figure 1. The dashed lines denote the locations of the CTD casts.

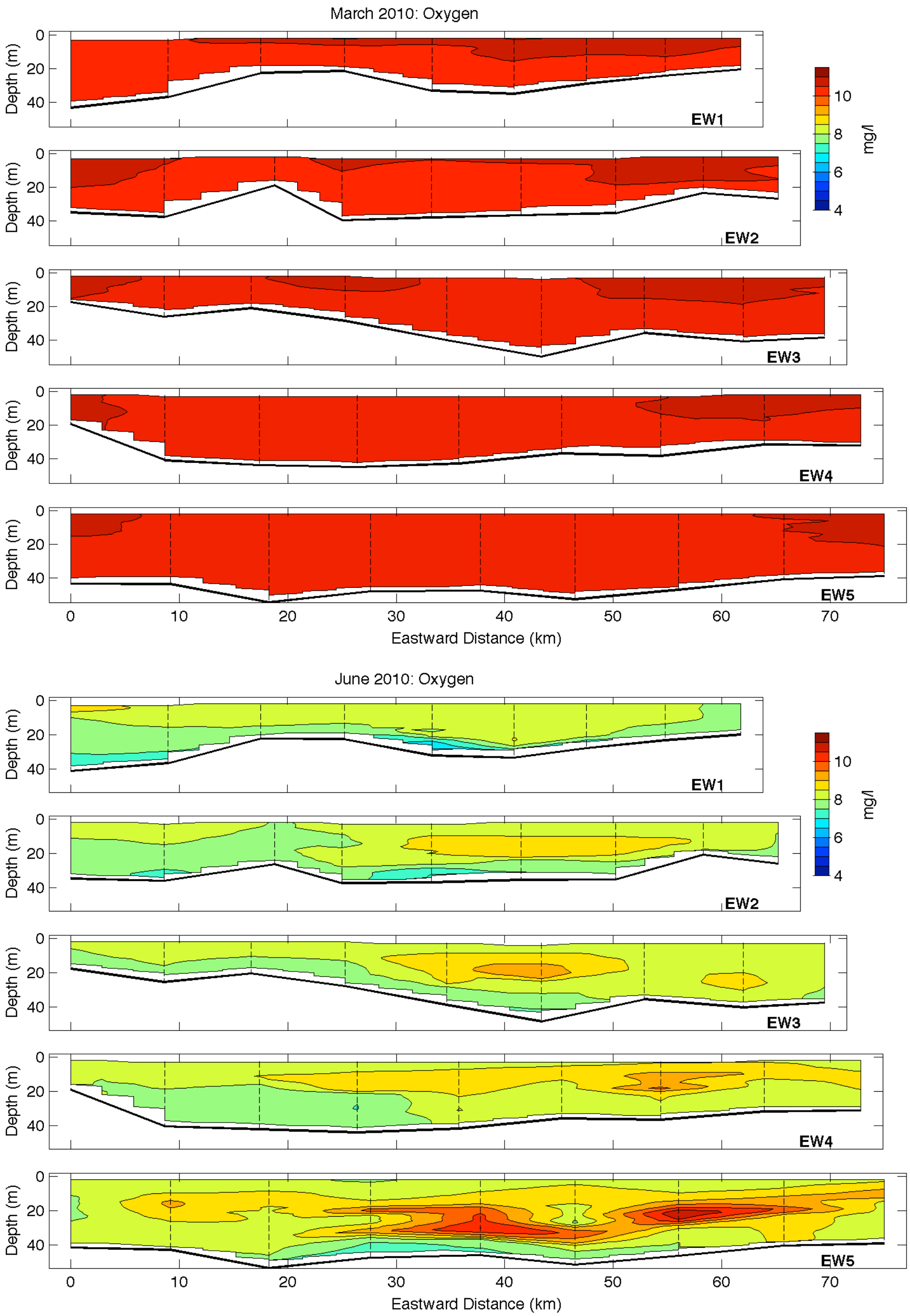

Figure 18. Surveys, Oxygen, EW sections: March (upper); June (lower).
The section numbers are referenced to the map in Figure 1. The dashed lines denote the locations of the CTD casts.

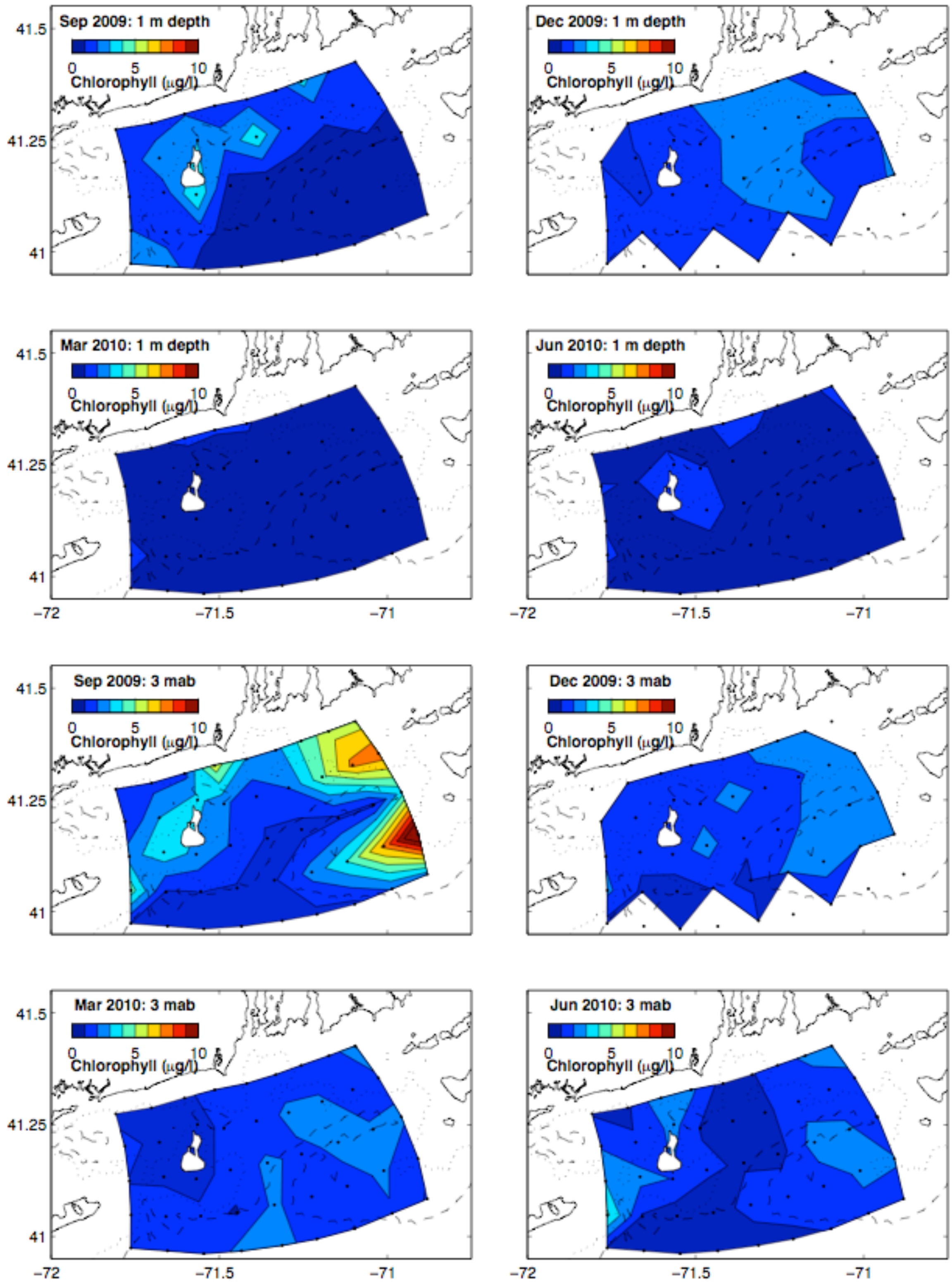

Figure 19. Surveys, Chlorophyll, all seasons: 1 m deep (upper); 3 m above seafloor (lower). The CTD cast locations are denoted by the black dots. The dotted and dashed lines are the 30 m and 40 m isobaths, respectively.

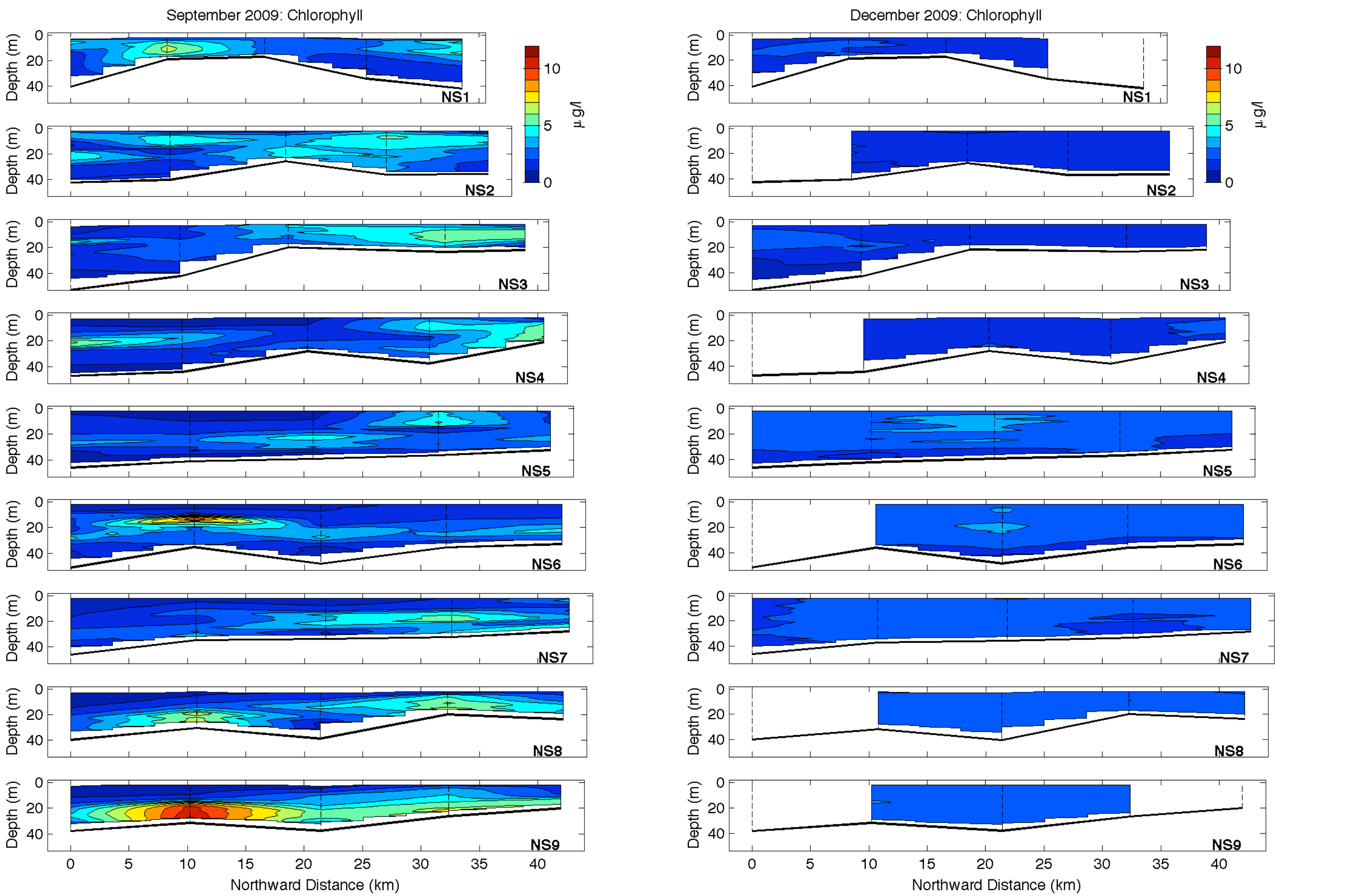

Figure 20. Surveys, Chlorophyll, NS sections: September (left); December (right).
The section numbers are referenced to the map in Figure 1. The dashed lines denote the locations of the CTD casts.

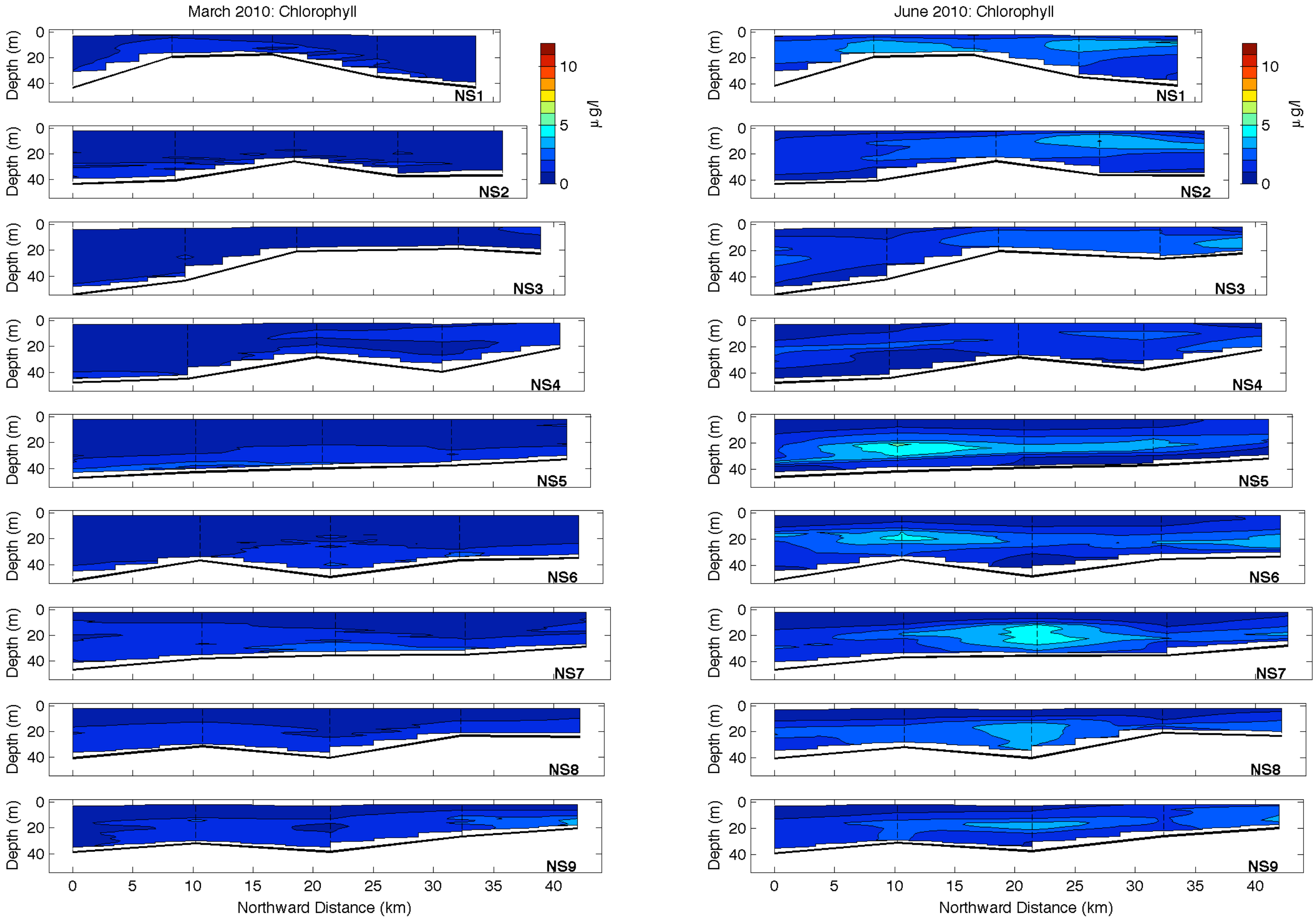

Figure 21. Surveys, Chlorophyll, NS sections: March (left); June (right).
The section numbers are referenced to the map in **Figure 1**. The dashed lines denote the locations of the CTD casts.

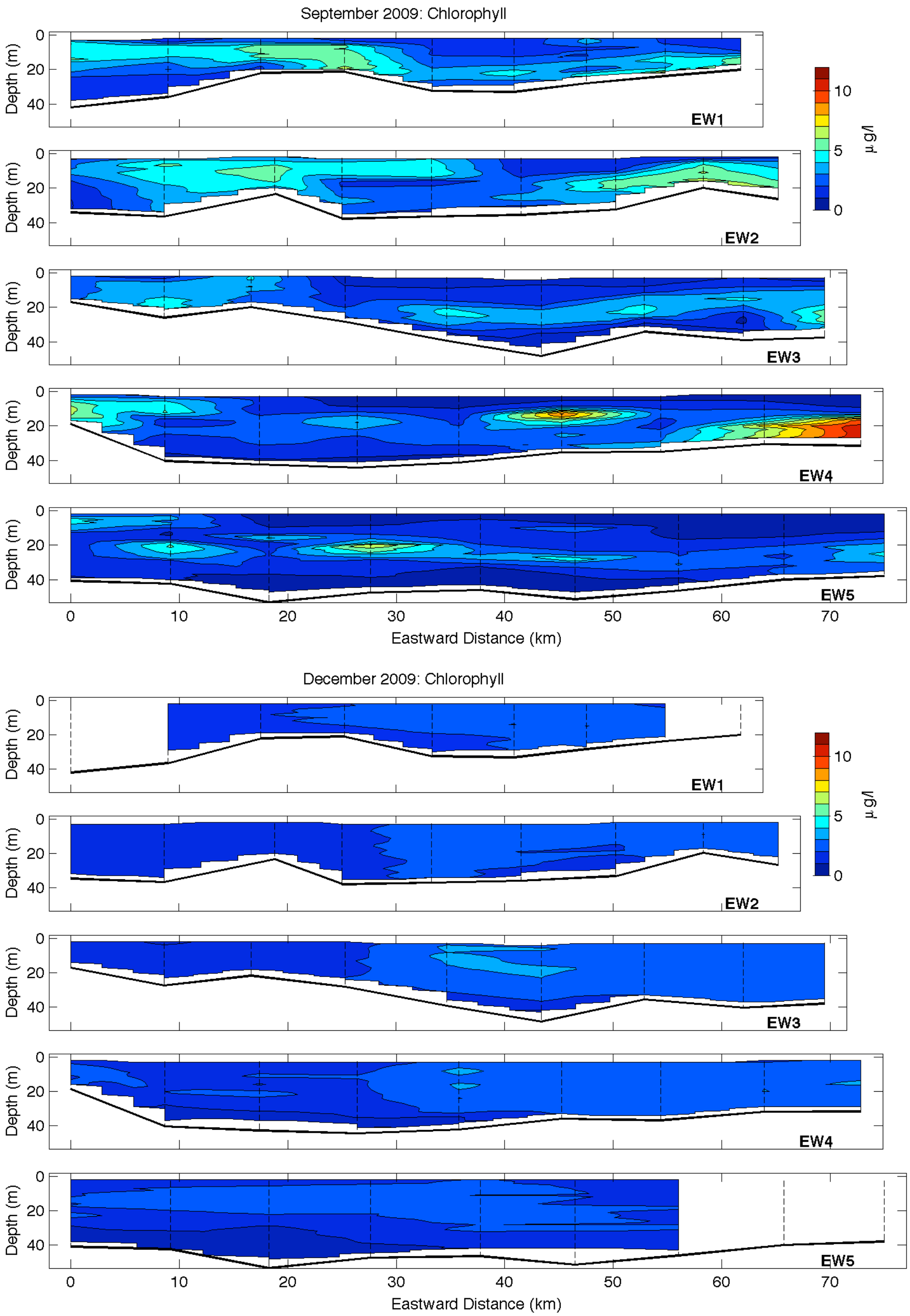

Figure 22. Surveys, Chlorophyll, EW sections: September (upper); December (lower). The section numbers are referenced to the map in Figure 1. The dashed lines denote the locations of the CTD casts.

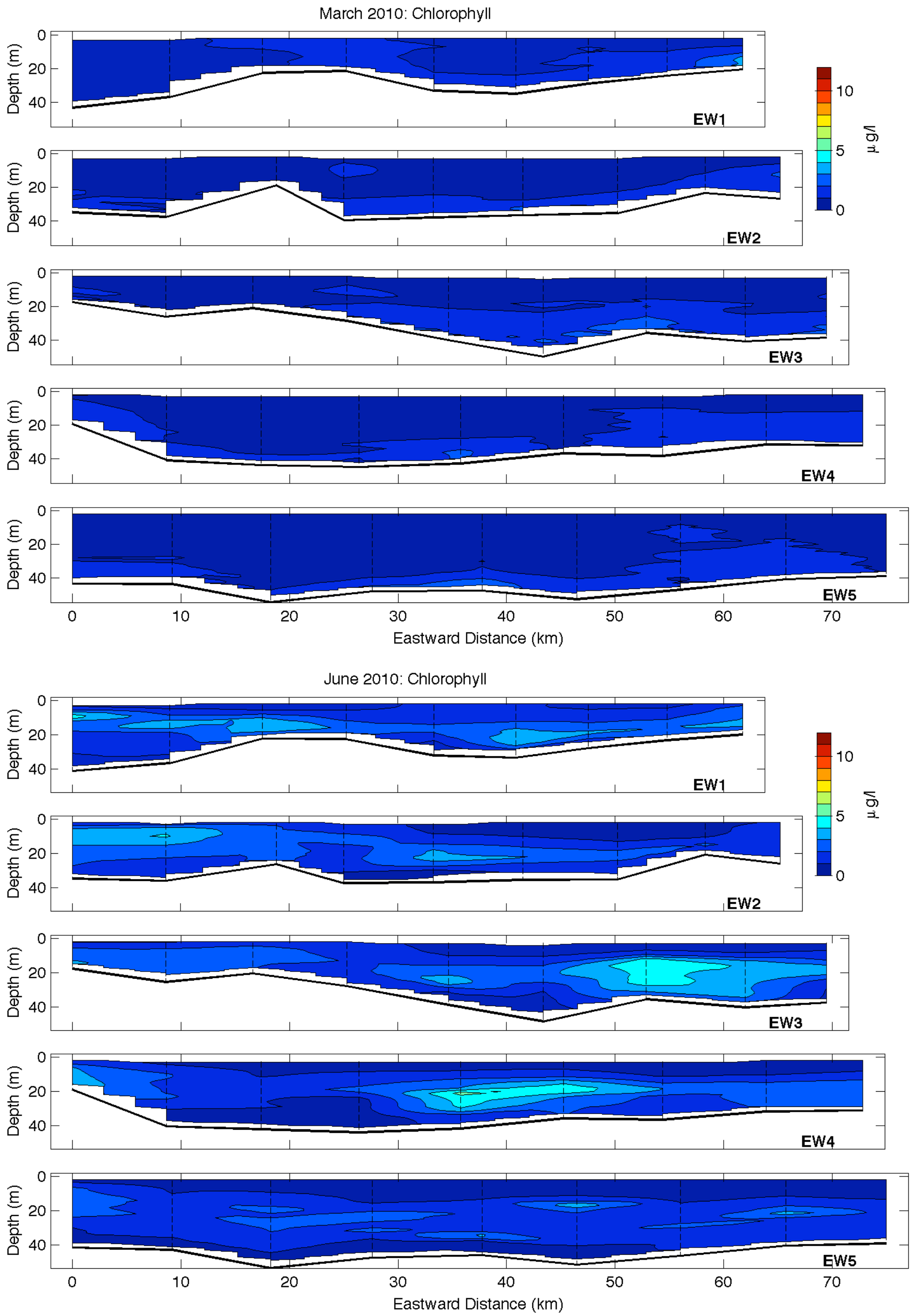

Figure 23. Surveys, Chlorophyll, EW sections: March (upper); June (lower).
The section numbers are referenced to the map in Figure 1. The dashed lines denote the locations of the CTD casts.

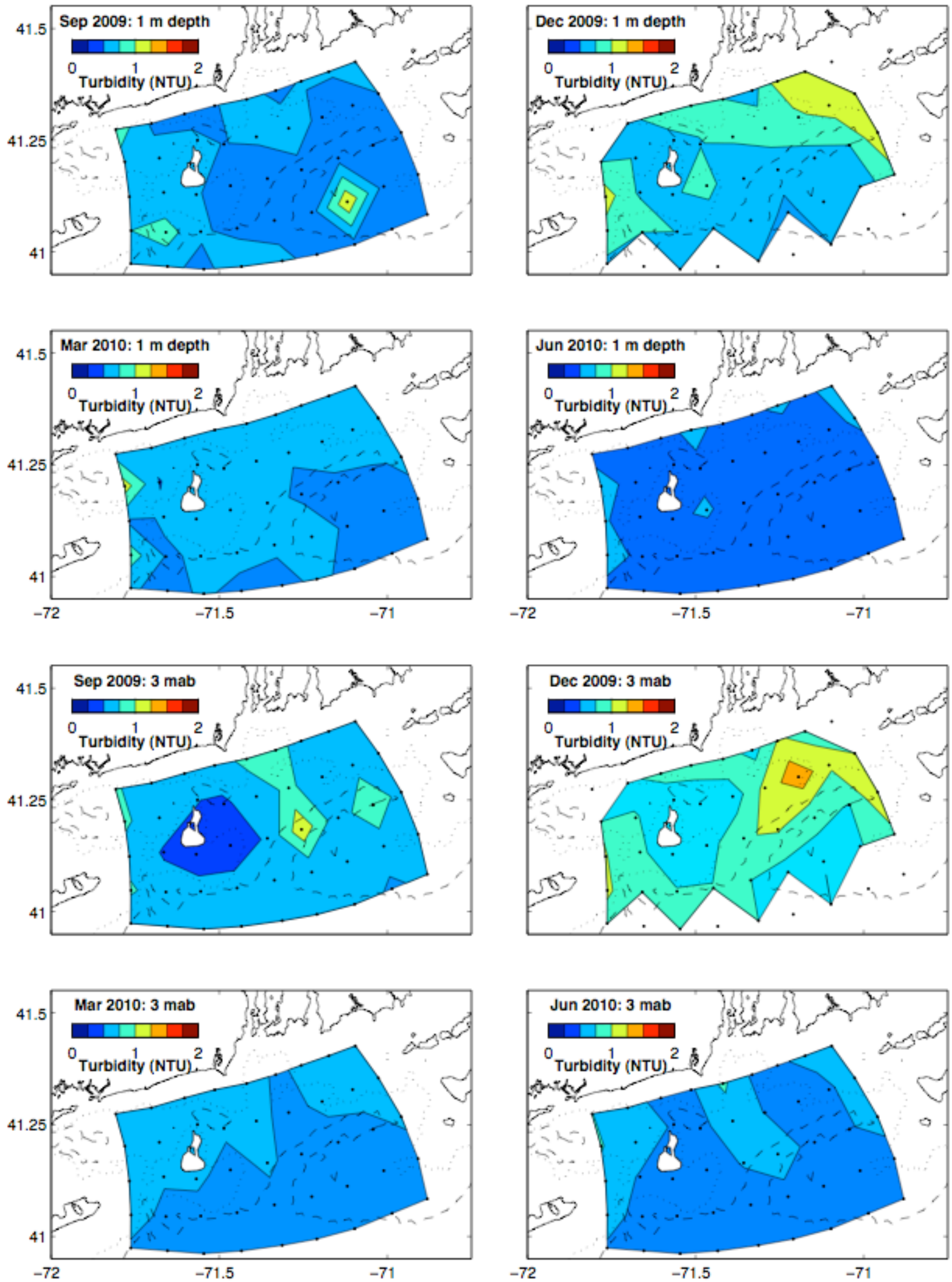

Figure 24. Surveys, Turbidity, all seasons: 1 m deep (upper); 3 m above seafloor (lower). The CTD cast locations are denoted by the black dots. The dotted and dashed lines are the 30 m and 40 m isobaths, respectively.

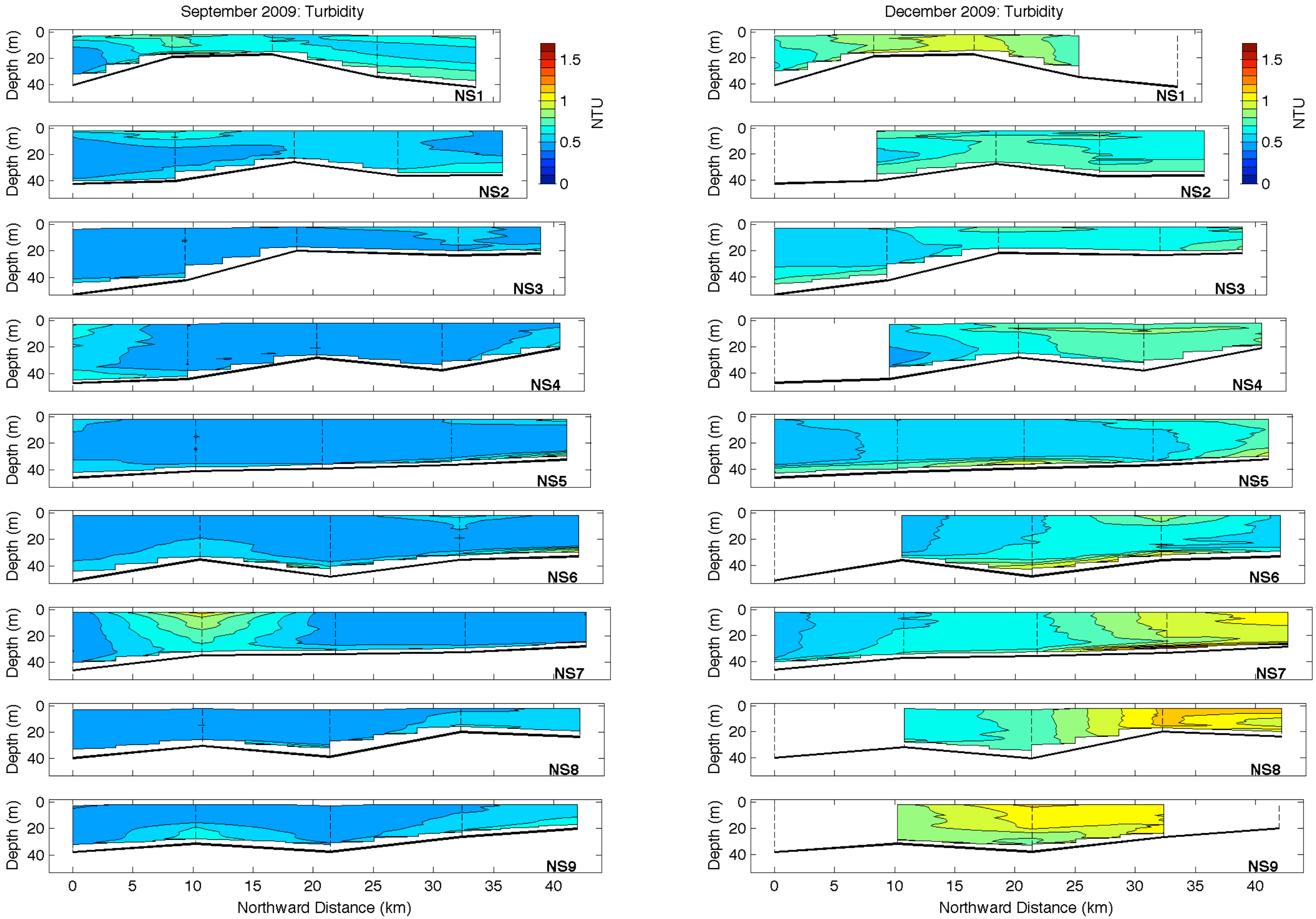

Figure 25. Surveys, Turbidity, NS sections: September (left); December (right).
The section numbers are referenced to the map in Figure 1. The dashed lines denote the locations of the CTD casts.

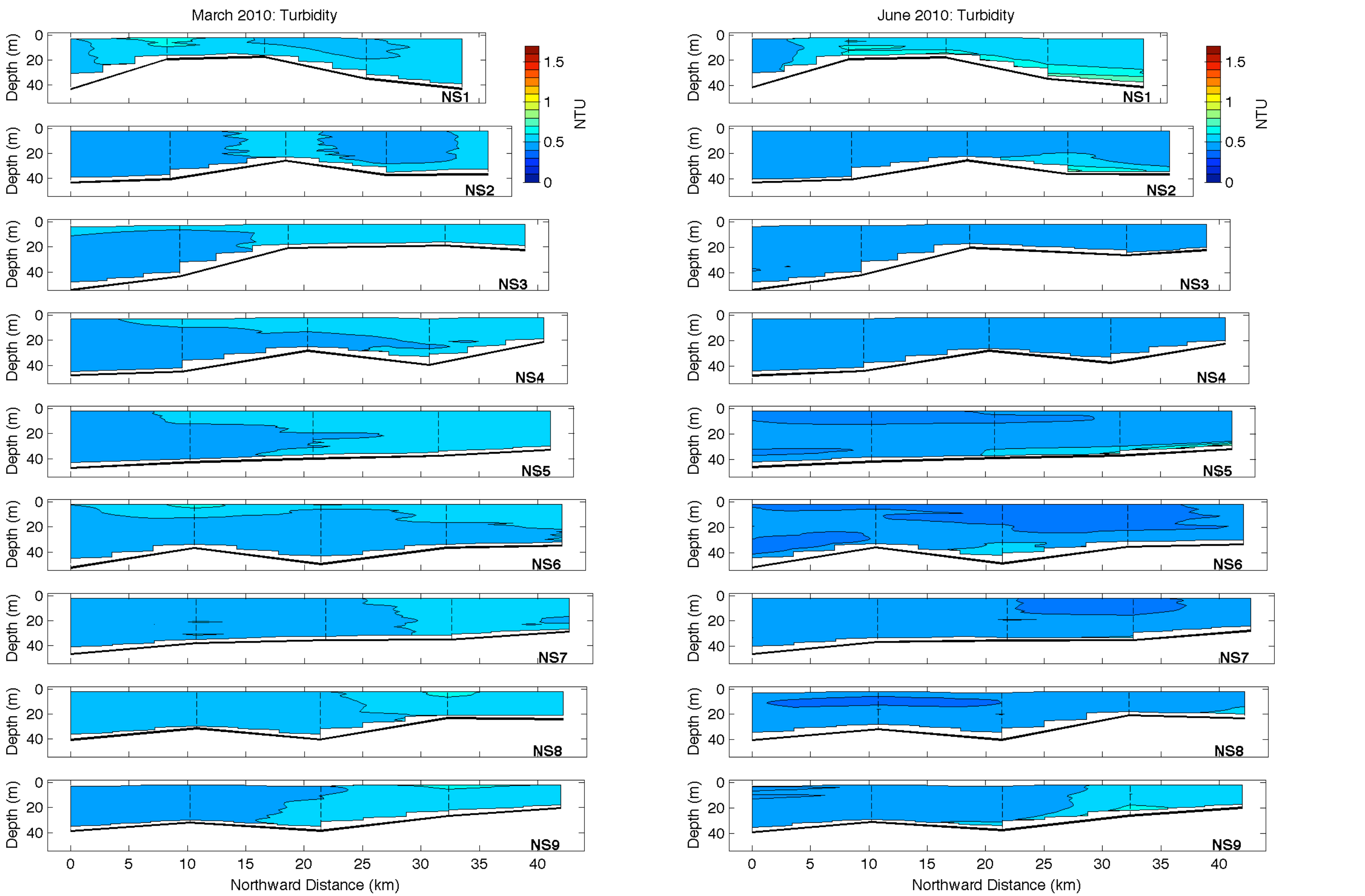

Figure 26. Surveys, Turbidity, NS sections: March (left); June (right).
The section numbers are referenced to the map in Figure 1. The dashed lines denote the locations of the CTD casts.

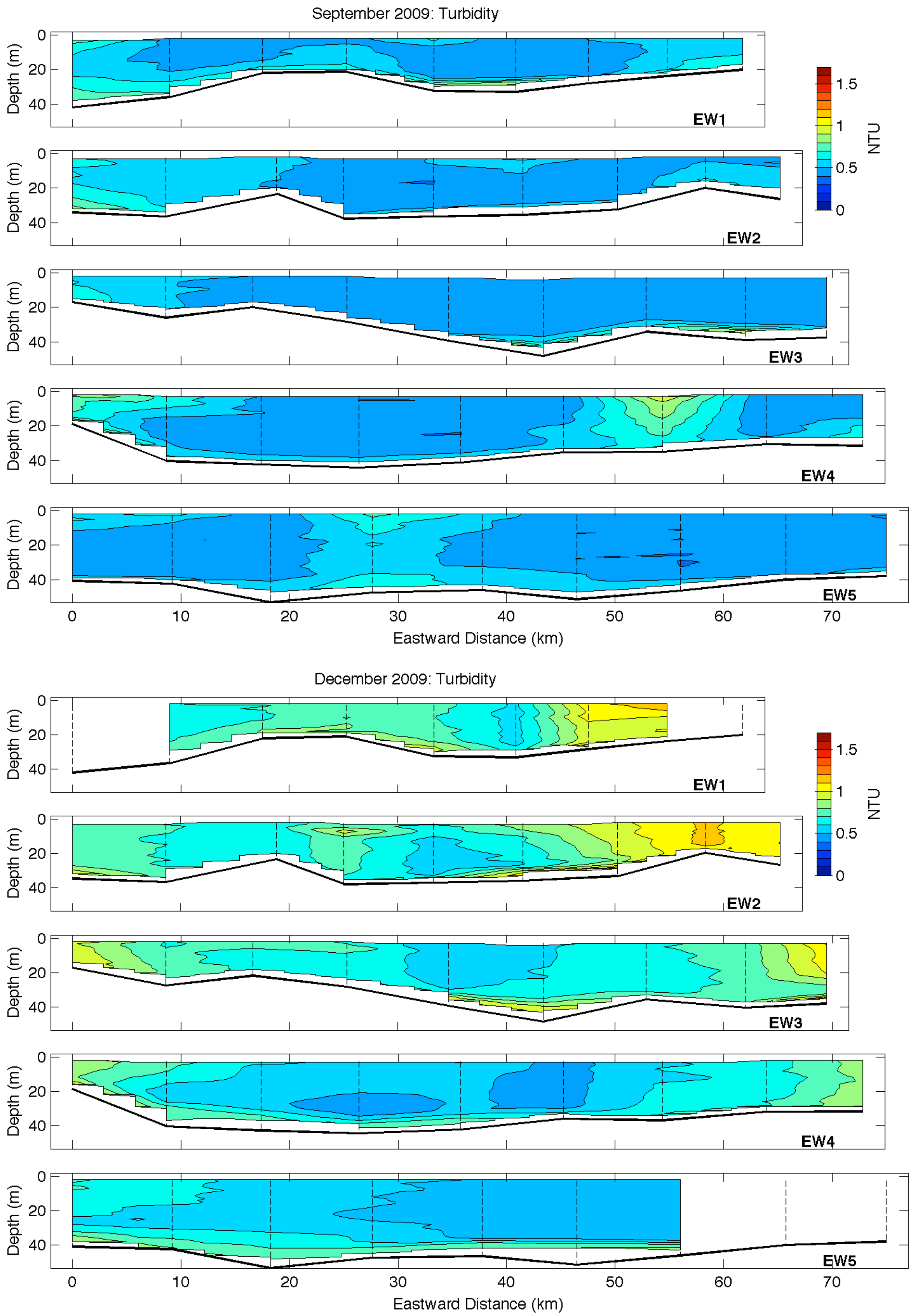

Figure 27. Surveys, Turbidity, EW sections: September (upper); December (lower). The section numbers are referenced to the map in Figure 1. The dashed lines denote the locations of the CTD casts.

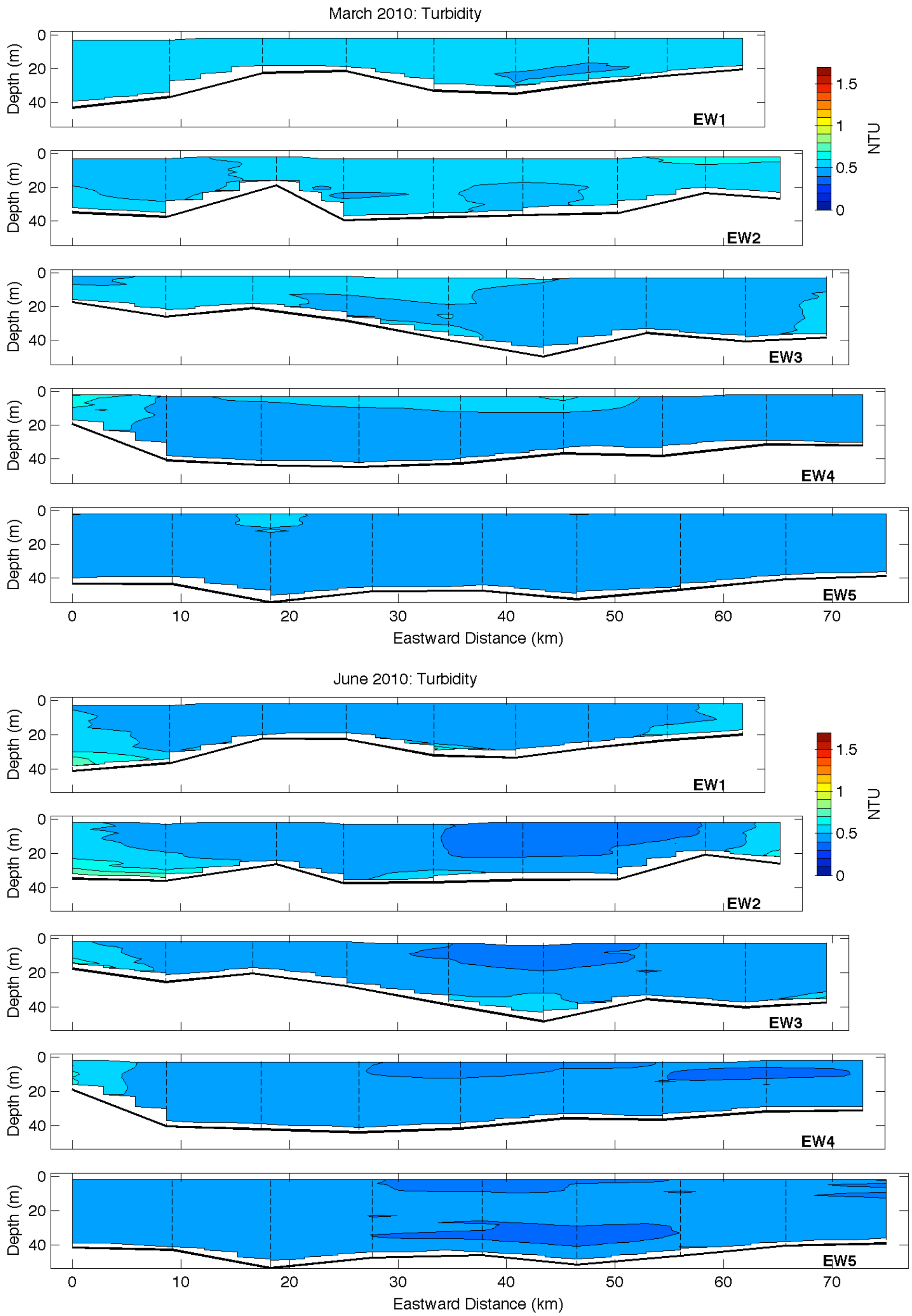

Figure 28. Surveys, Turbidity, EW sections: March (upper); June (lower).
The section numbers are referenced to the map in Figure 1. The dashed lines denote the locations of the CTD casts.

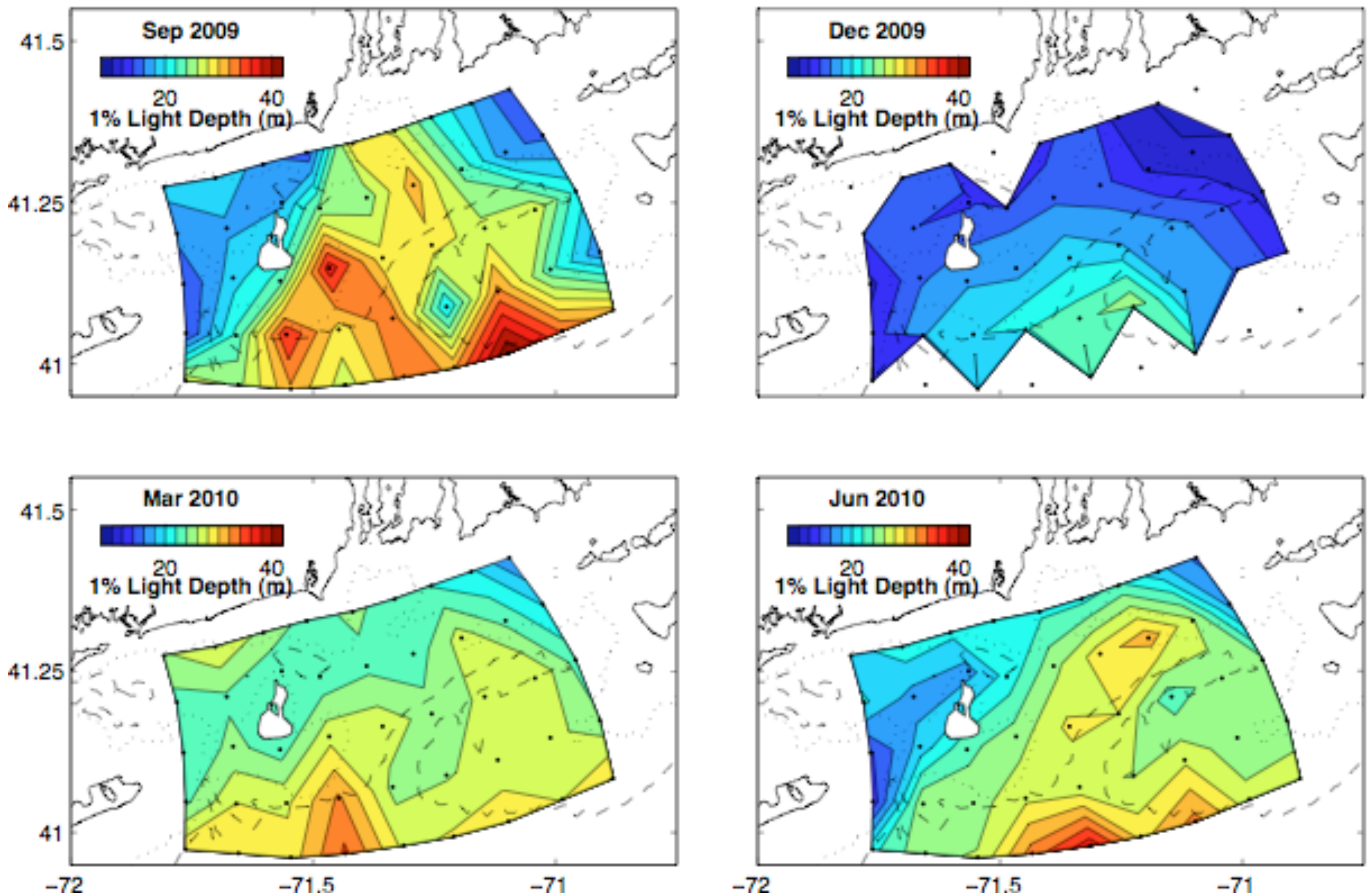

Figure 29. Surveys, Euphotic zone depth, all seasons.

The CTD cast locations are denoted by the black dots. The dotted and dashed lines are the 30 m and 40 m isobaths, respectively.

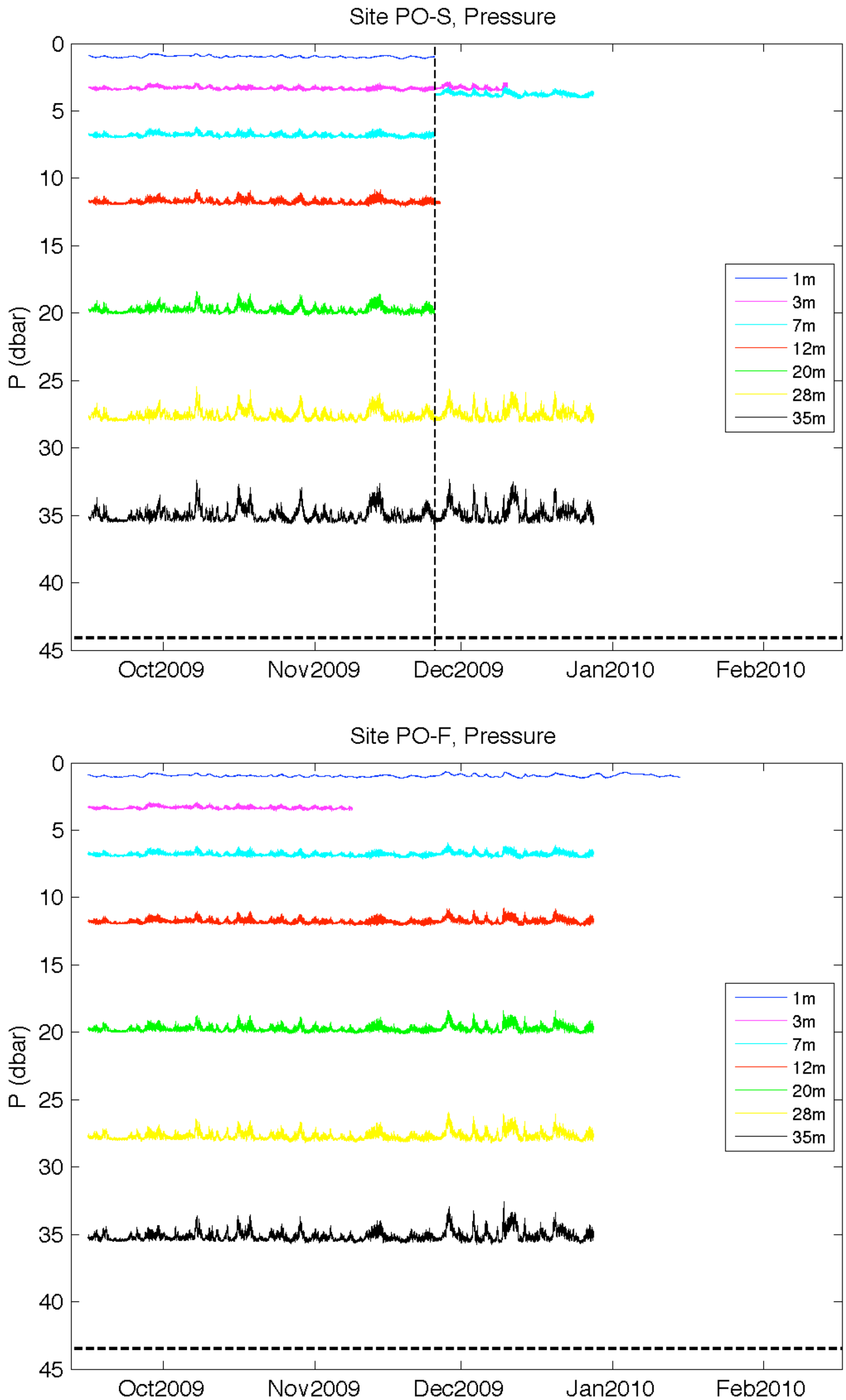

Figure 30. CTD Moorings, Fall/Winter: PO-S and PO-F pressure records.
The legend lists the nominal depths of each instrument. The vertical dashed line in the bottom plot shows the time at which the mooring was dragged.

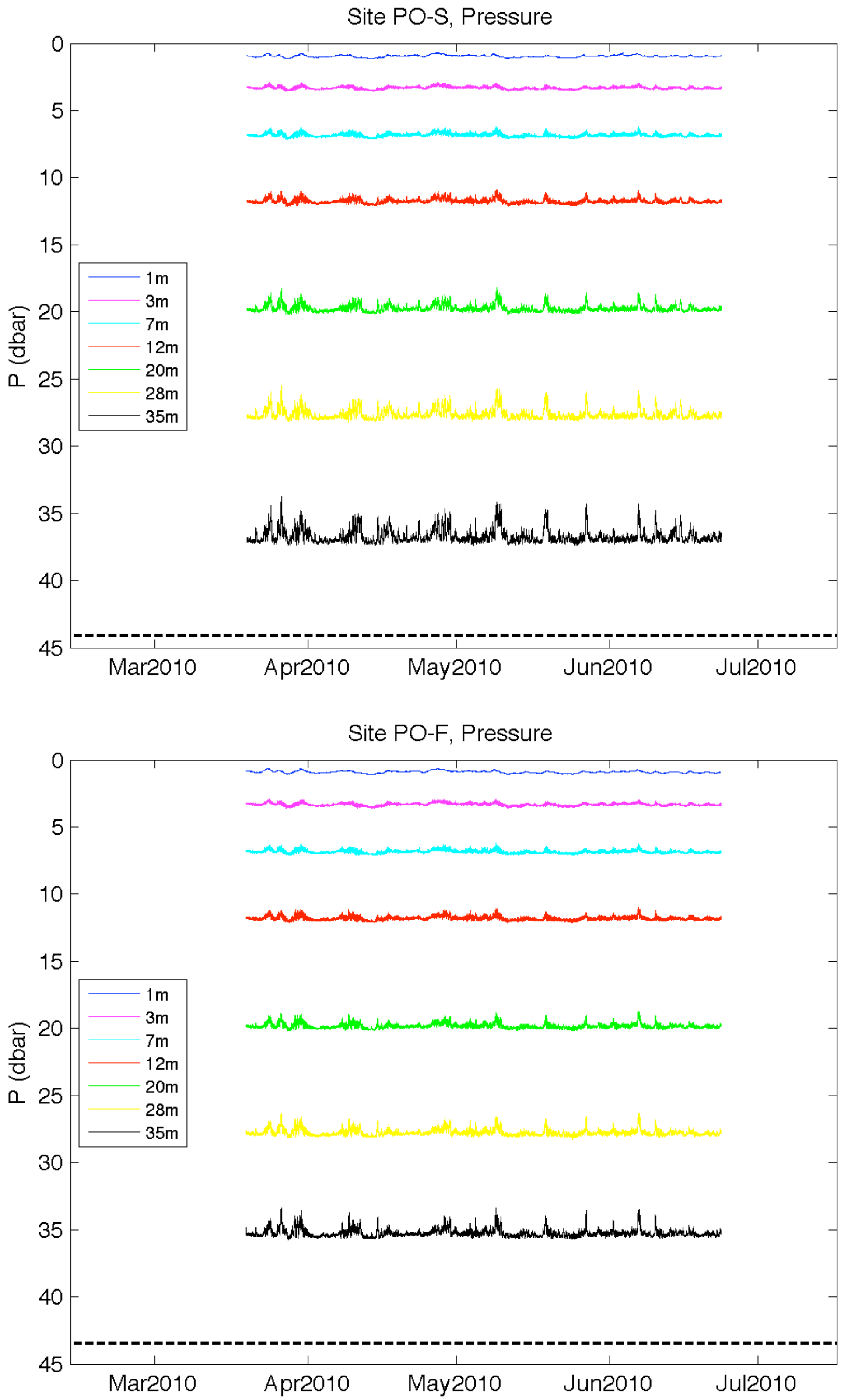

Figure 31. CTD Moorings, Spring/Summer: PO-S and PO-F pressure records. The legend lists the nominal depths of each instrument.

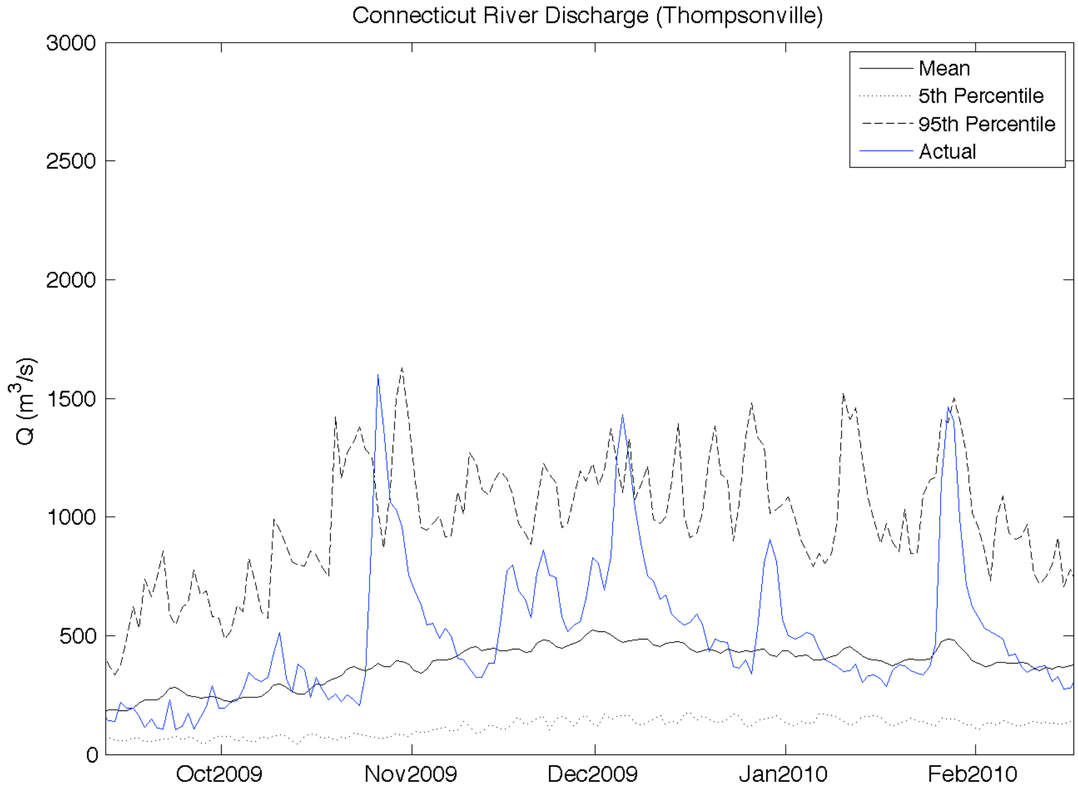

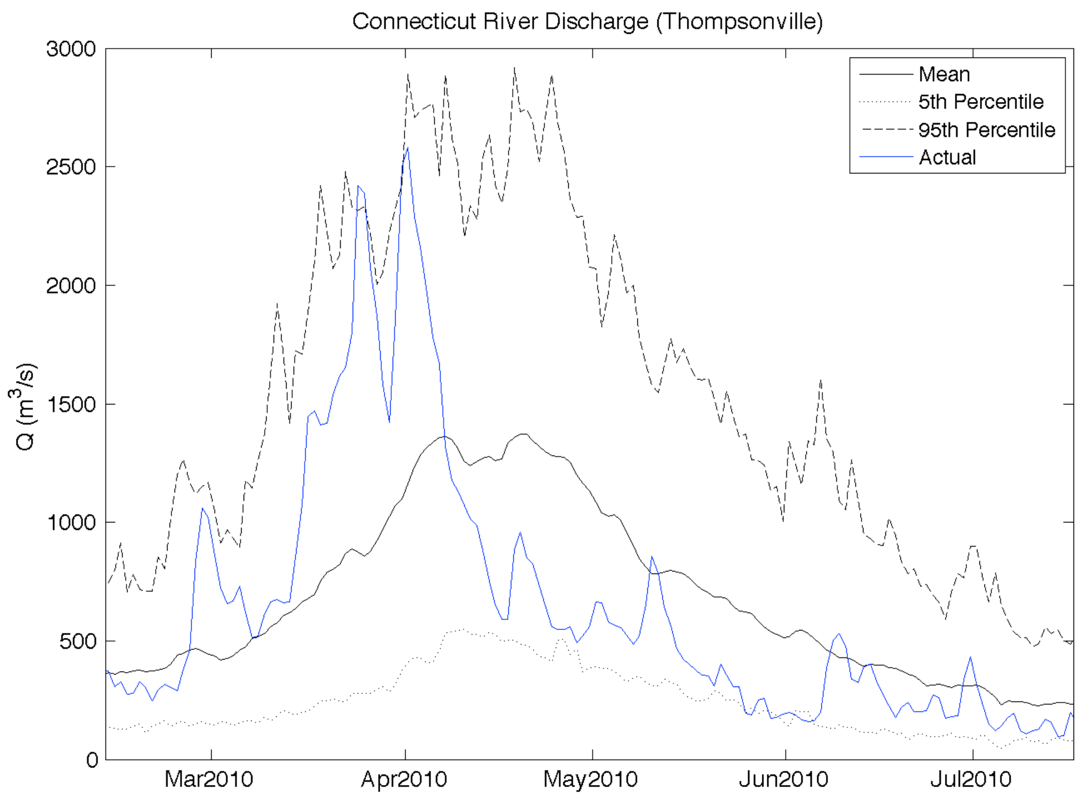

Figure 32. Connecticut River Discharge: Fall/Winter (upper), Spring/Summer (lower). Actual is 2009/2010. Mean and percentiles are based on previous 80-year period.

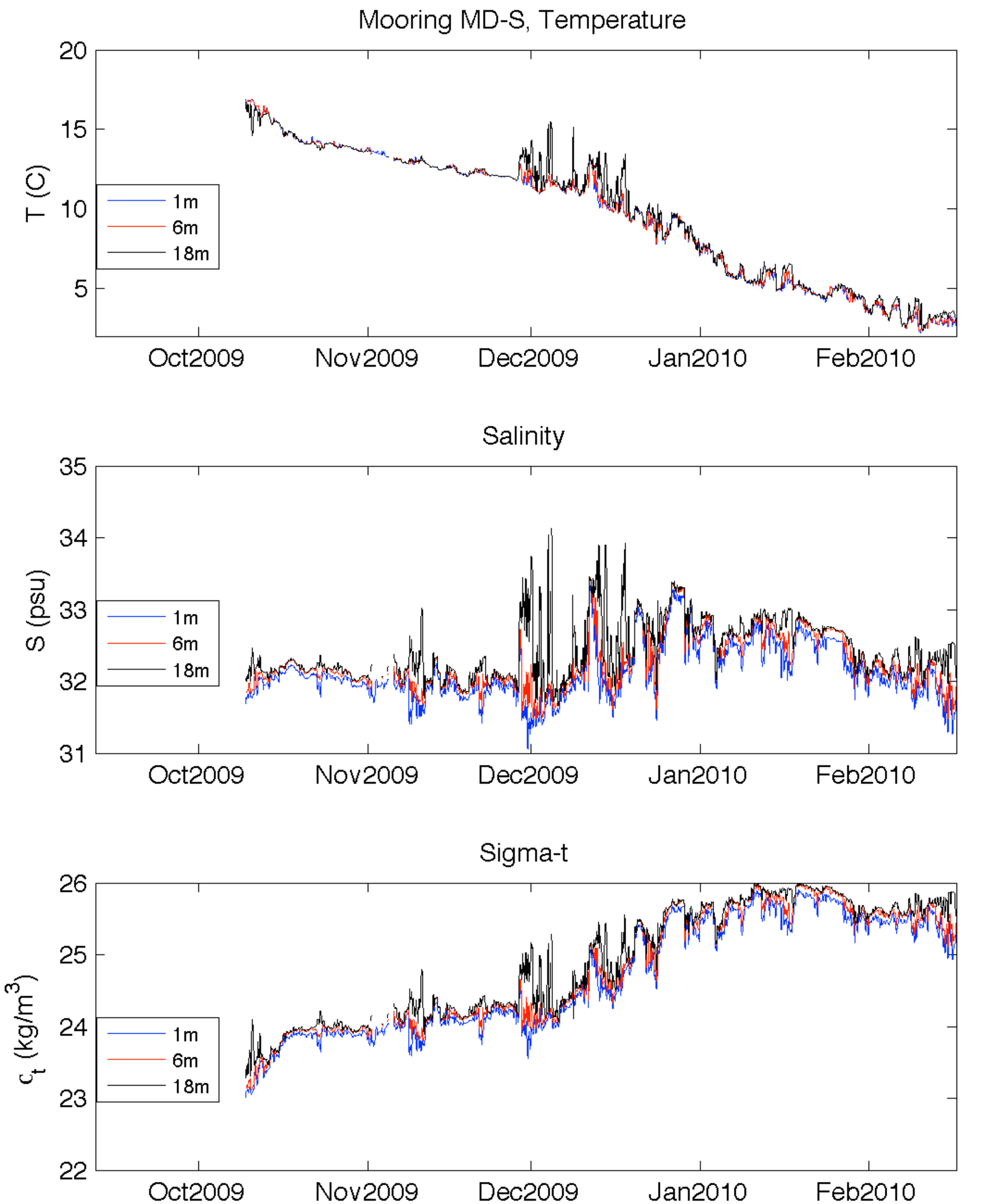

Figure 33. CTD Moorings, Fall/Winter, MD-S: temp. (top), sal. (middle), sigma-t (bottom). The legend gives the nominal depth of each CTD.

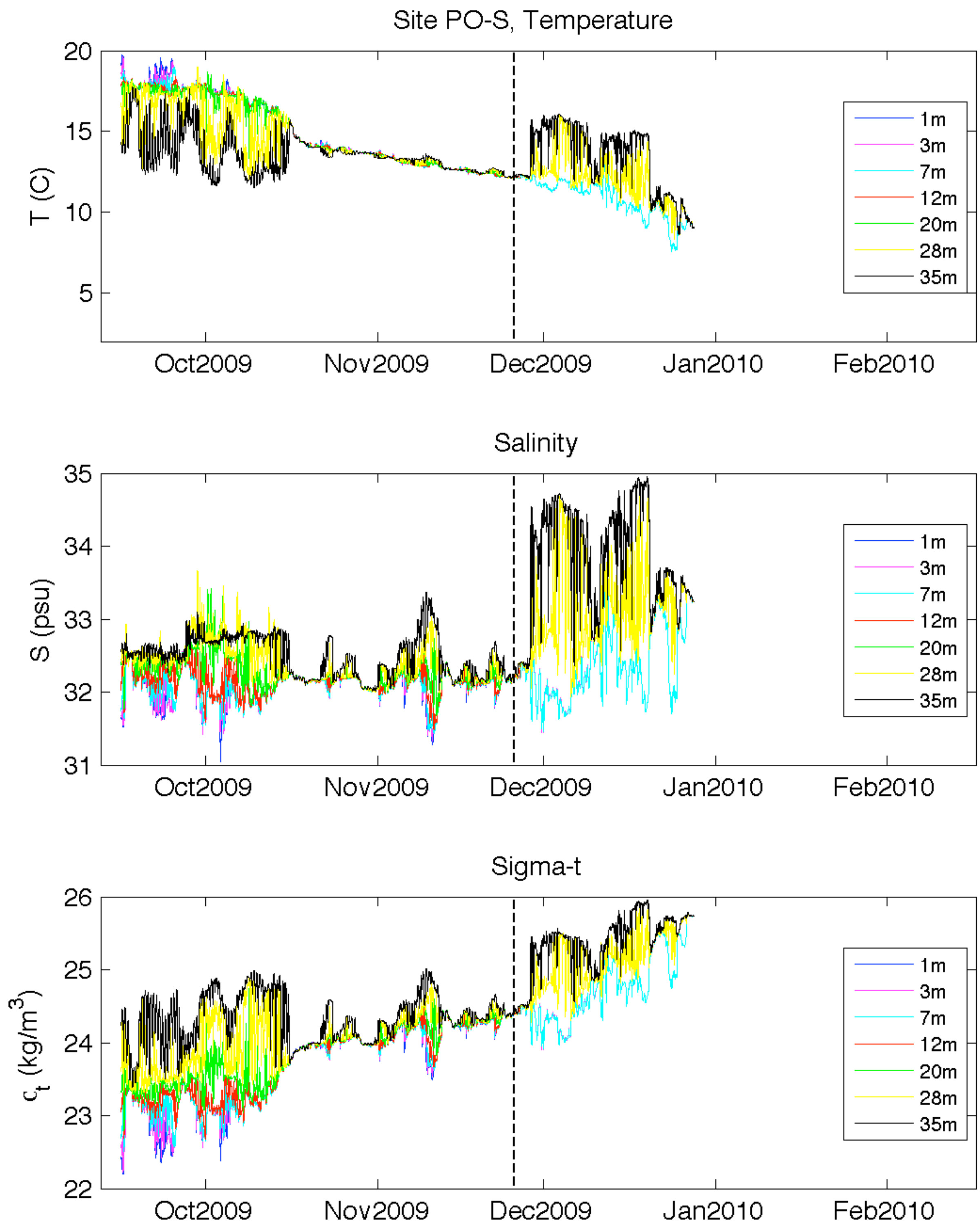

Figure 34. CTD Moorings, Fall/Winter, PO-S: temp. (top), sal. (middle), sigma-t (bottom). The legend gives the nominal depths of each CTD. The dashed vertical line is the time at which the mooring was dragged.

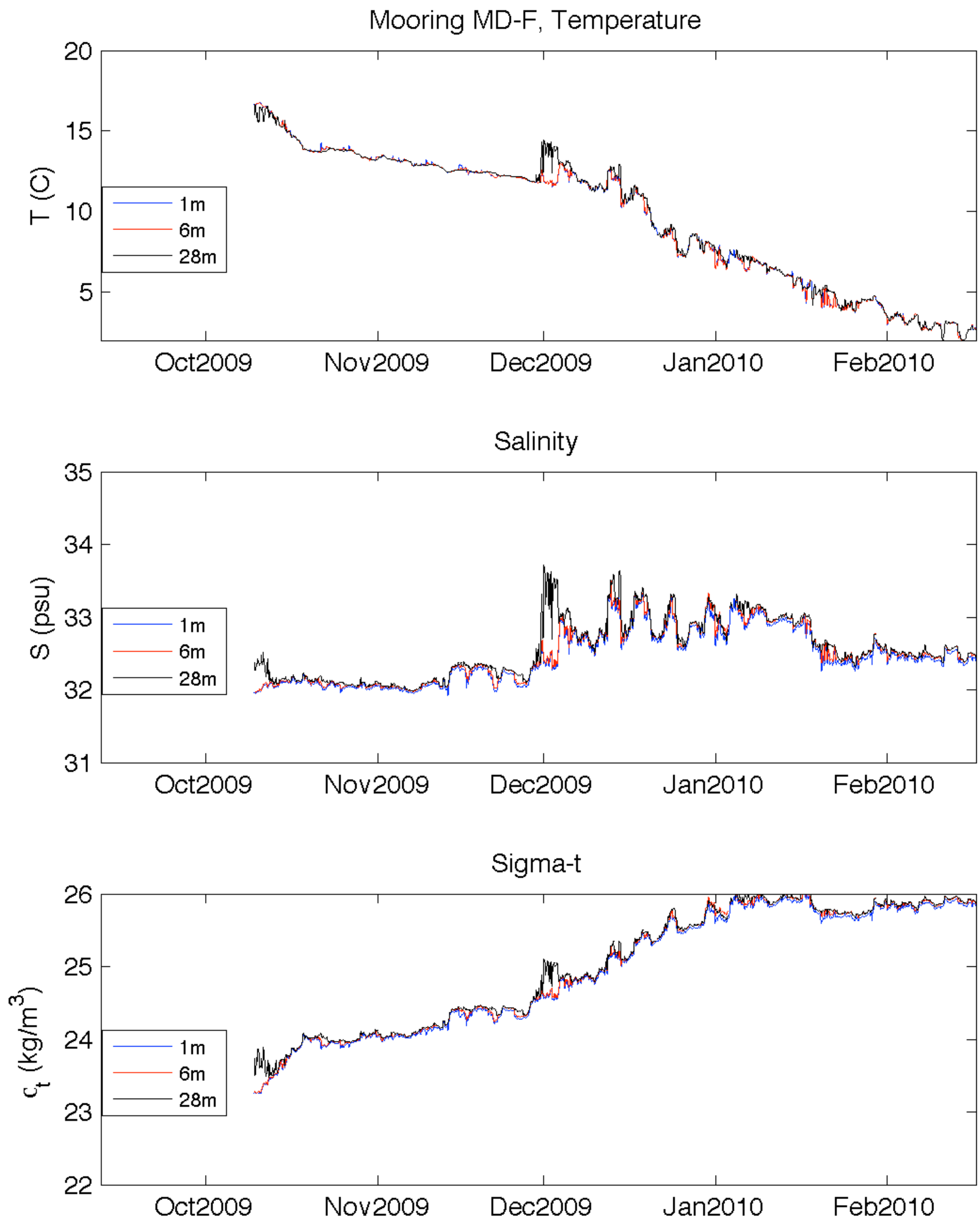

Figure 35. CTD Moorings, Fall/Winter, MD-F: temp. (top), sal. (middle), sigma-t (bottom). The legend gives the nominal depth of each CTD.

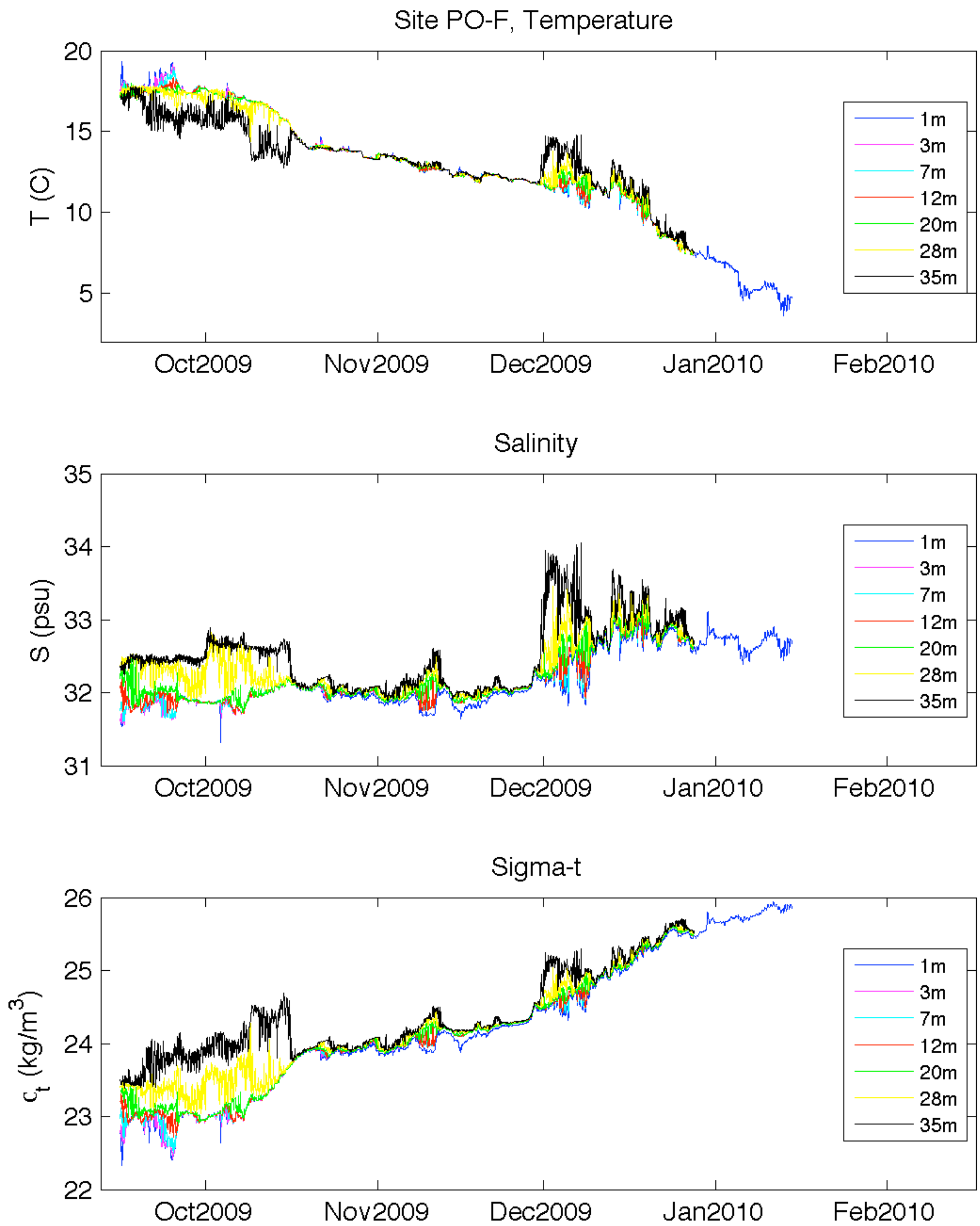

Figure 36. CTD Moorings, Fall/Winter, PO-F: temp. (top), sal. (middle), sigma-t (bottom). The legend gives the nominal depths of each CTD.

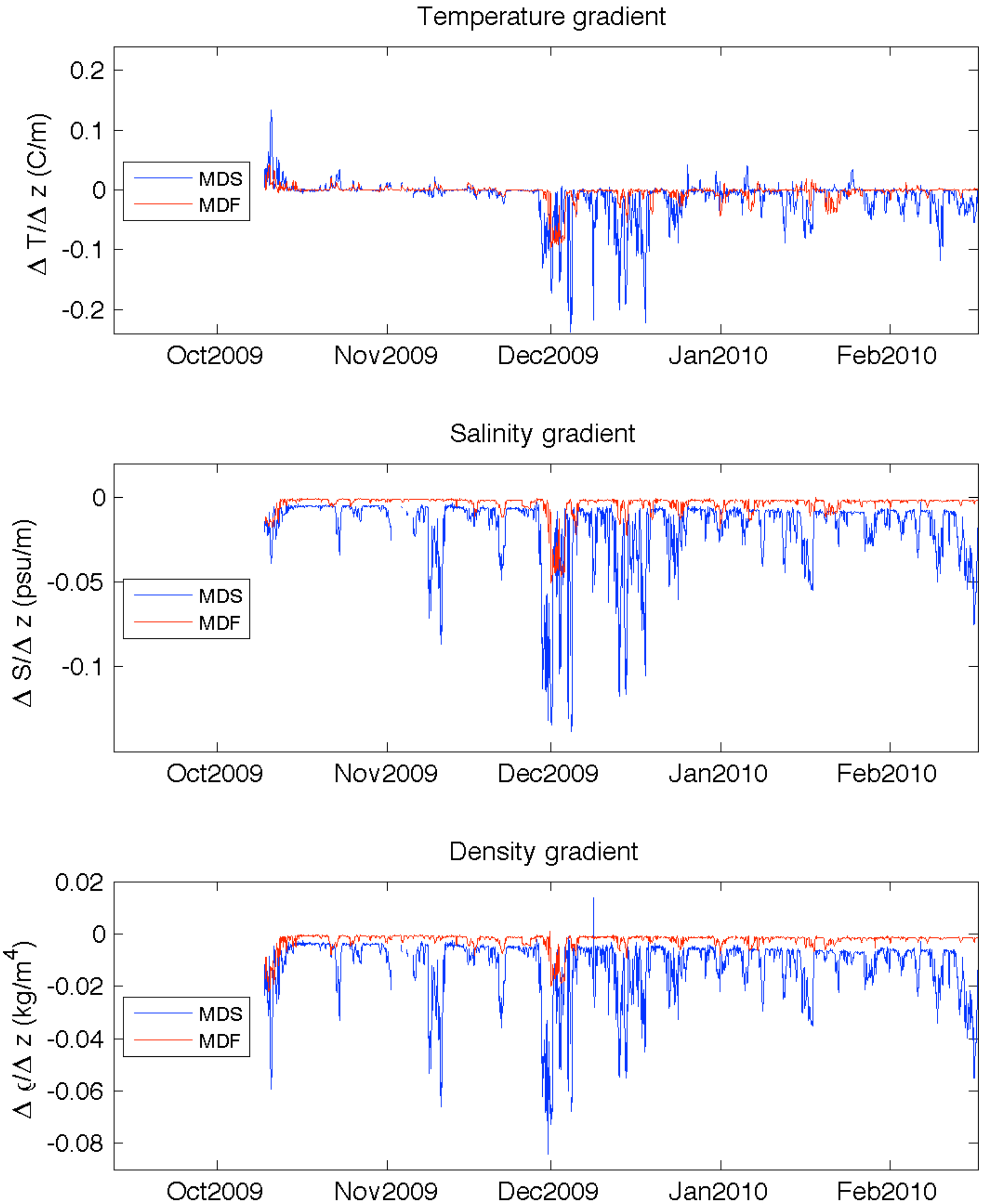

Figure 37. CTD Moorings, Fall/Winter, MD-S and MD-F : Vertical gradients. Differences are computed as the value at 1 m minus the value at 28 m (MD-F) or 18 m (MD-S).

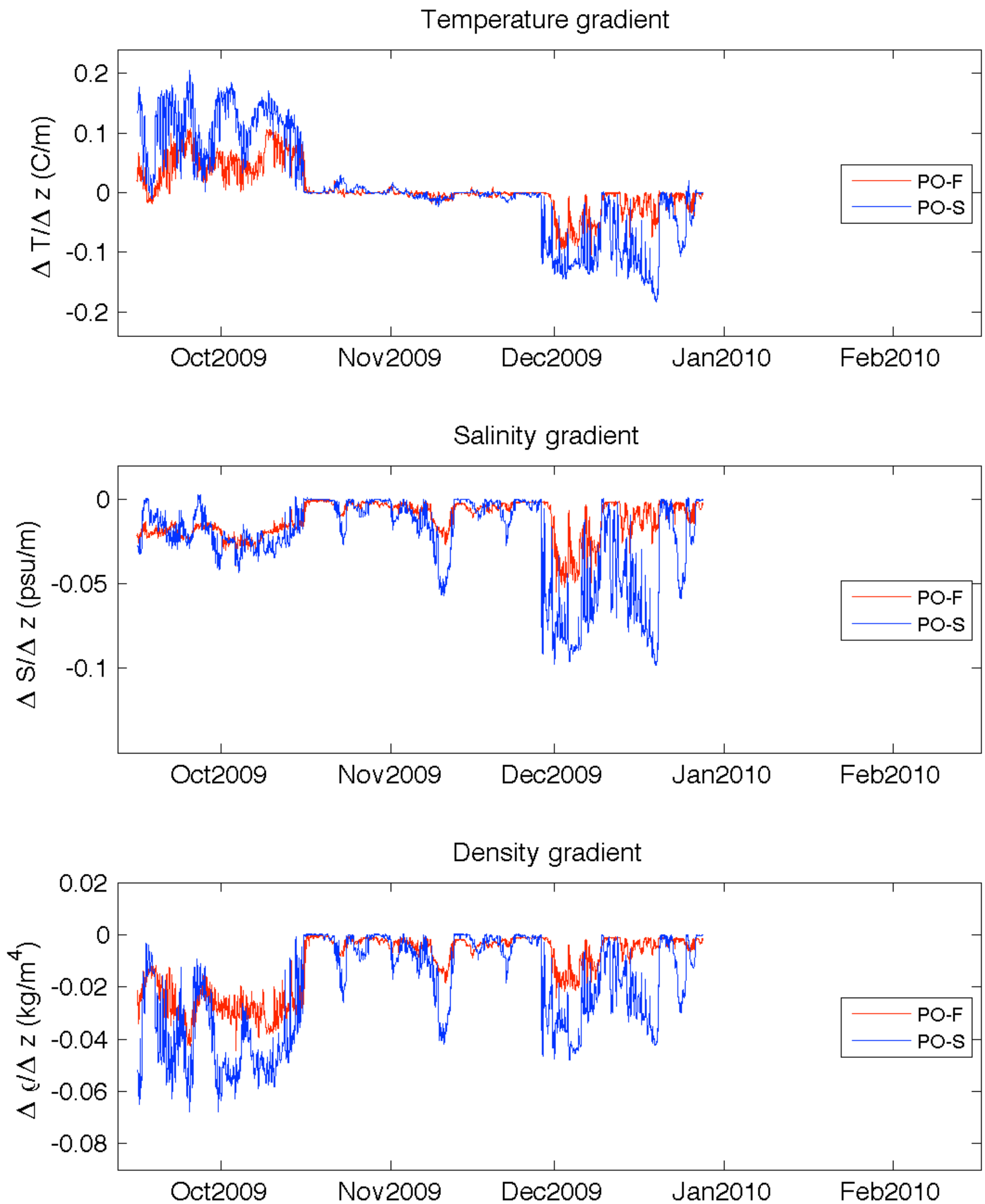

Figure 38. CTD Moorings, Fall/Winter, PO-S and PO-F: Vertical gradients.
Differences are computed as the value at 1 m (nominal) minus the value at 35 m (nominal).

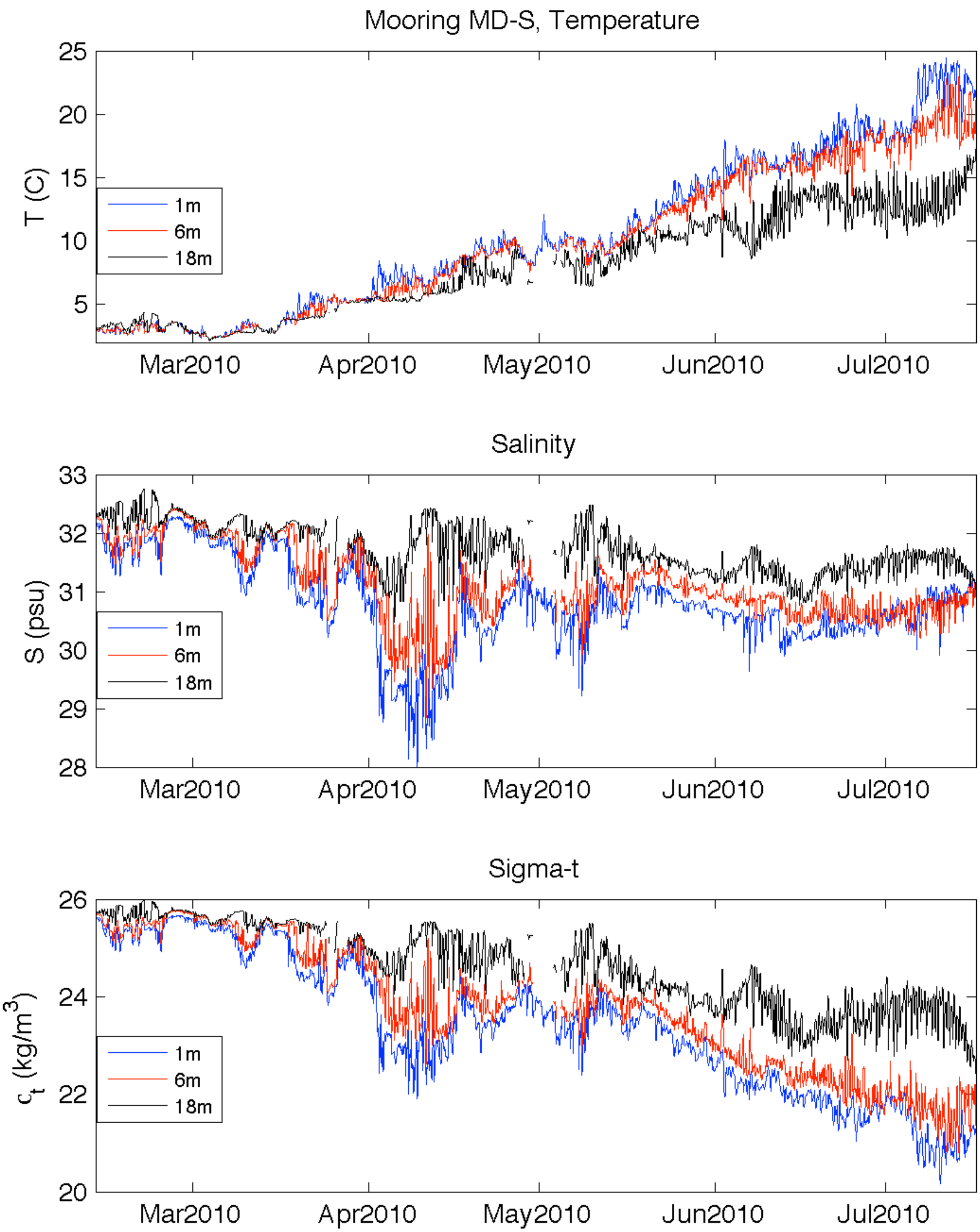

Figure 39. CTD Moorings, Spring/Summer, MD-S: temp. (top), sal. (middle), sigma-t (bottom).

.

The legend gives the nominal depth of each CTD.

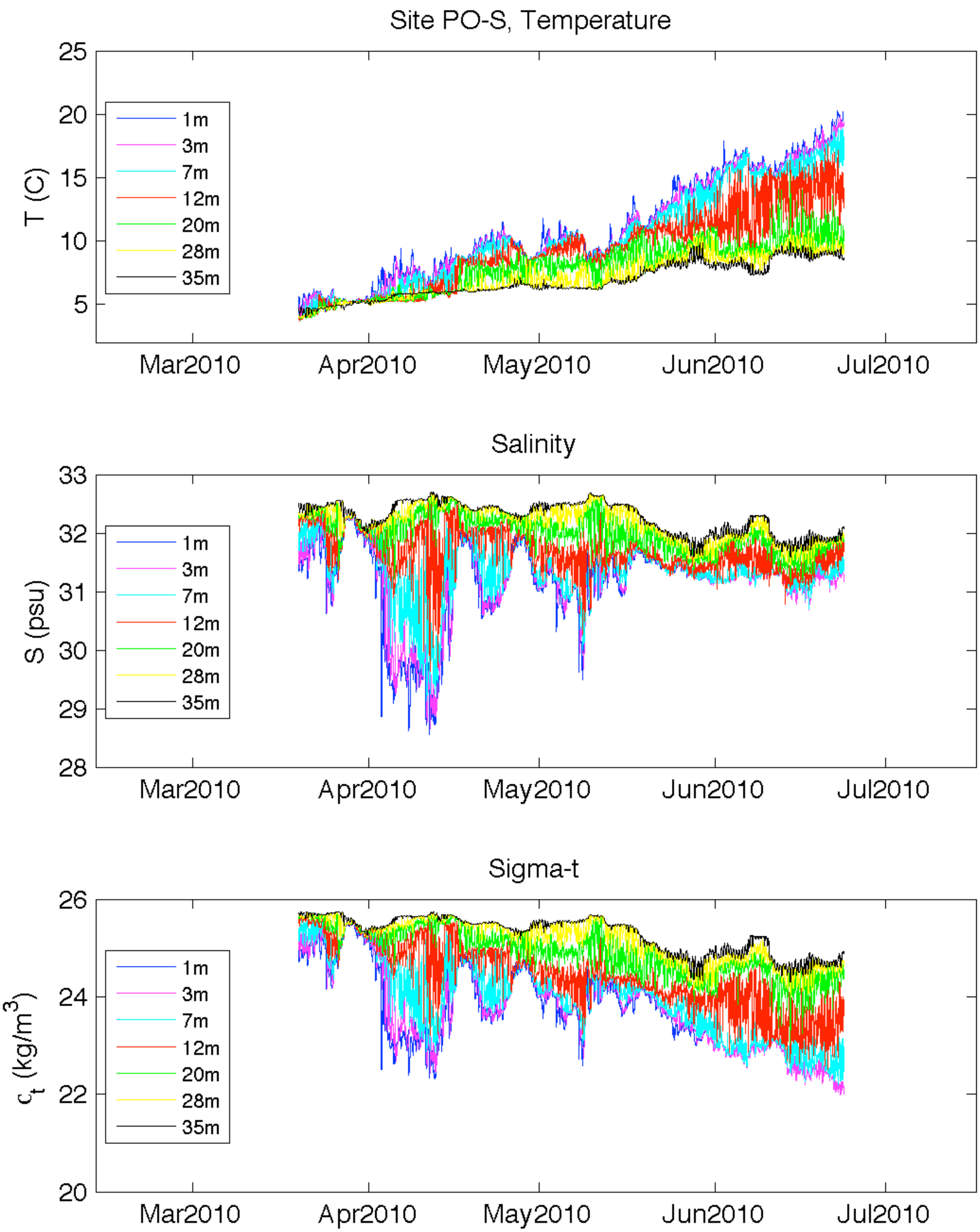

Figure 40. CTD Moorings, Spring/Summer, PO-S: temp. (top), sal. (middle), sigma-t (bottom).

The legend lists the nominal depths of each instrument.

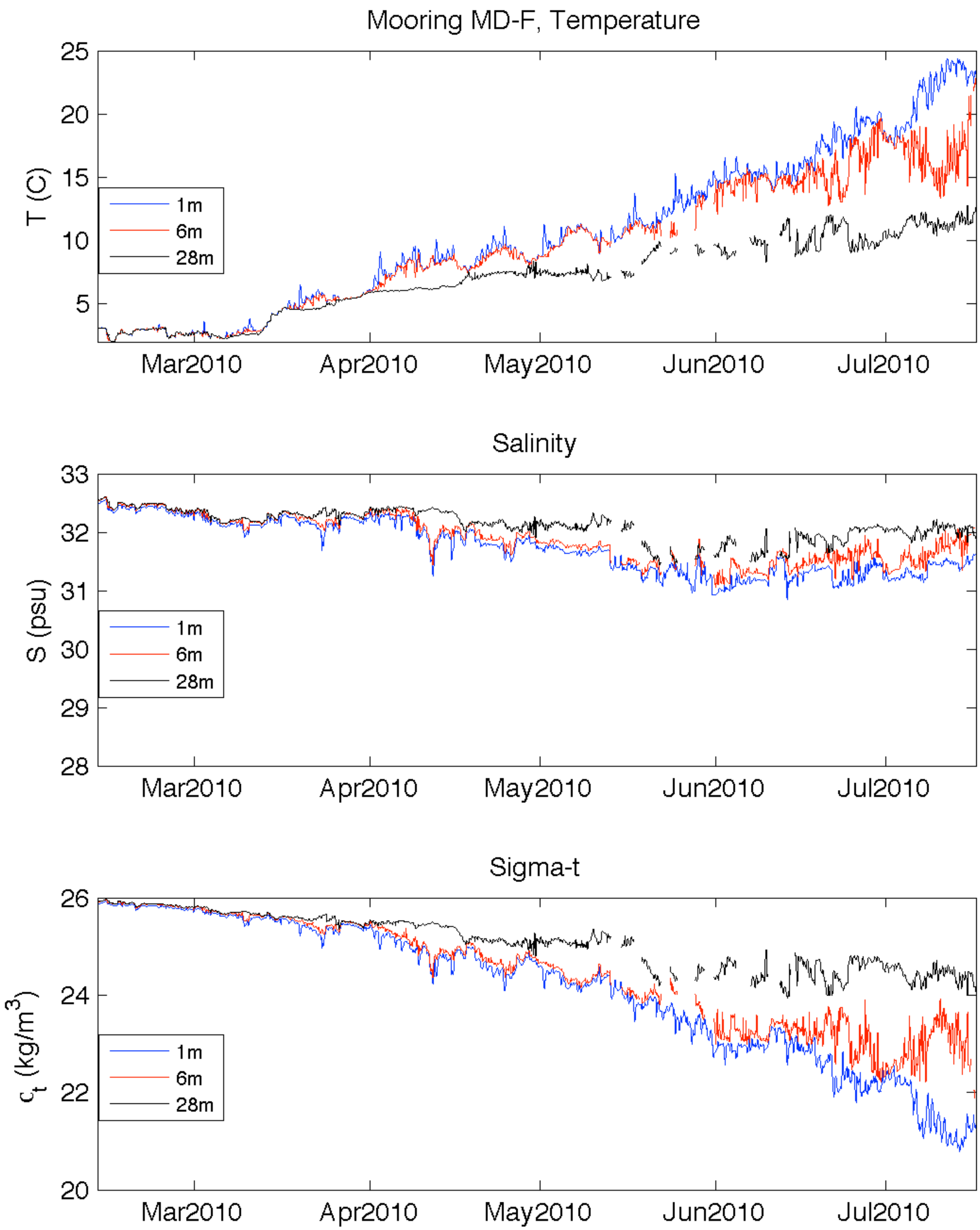

Figure 41. CTD Moorings, Spring/Summer, MD-F: temp. (top), sal. (middle), sigma-t (bottom).

The legend gives the nominal depth of each CTD.

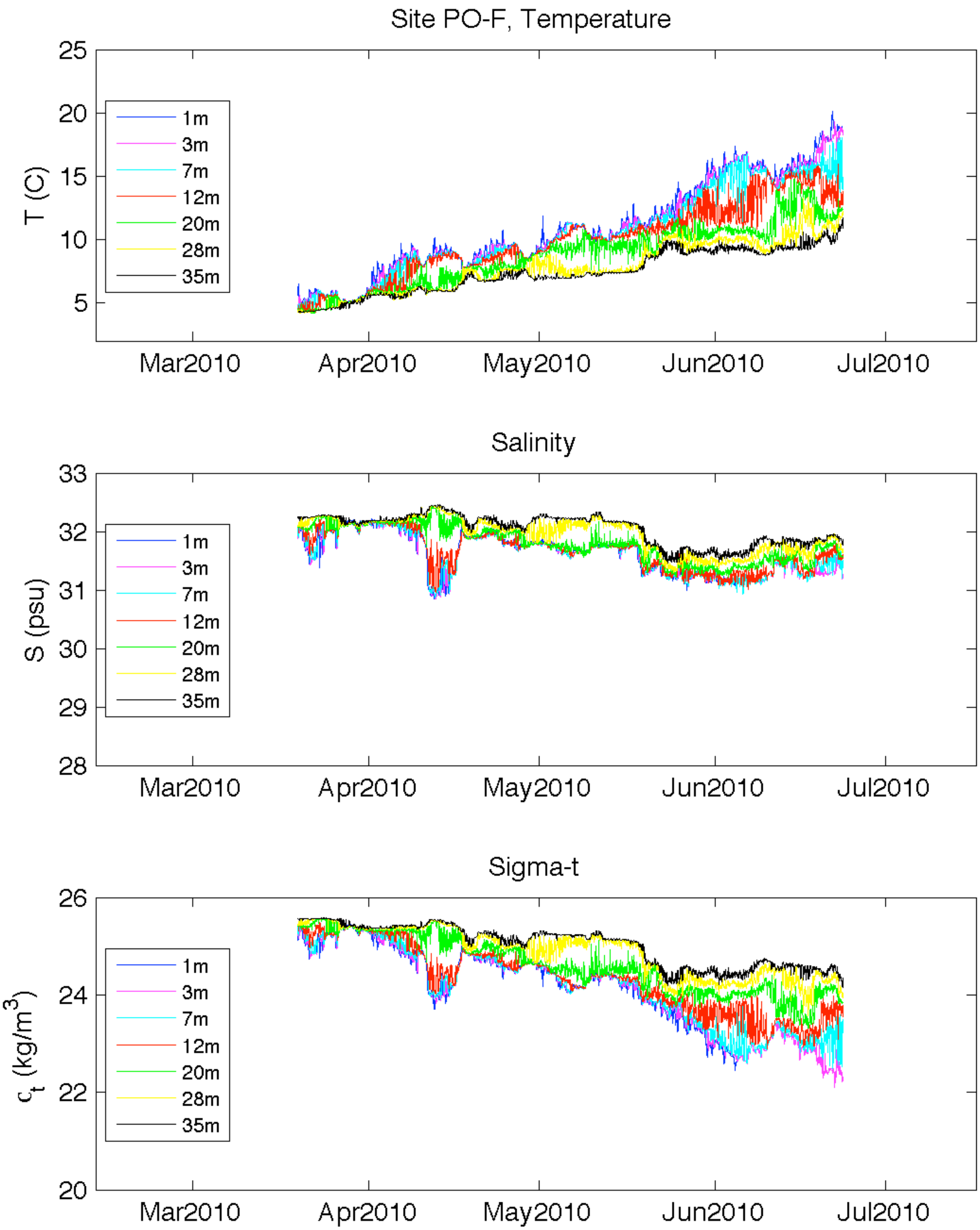

Figure 42. CTD Moorings, Spring/summer, PO-F: temp. (top), sal. (middle), sigma-t (bottom).
The legend lists the nominal depths of each instrument.

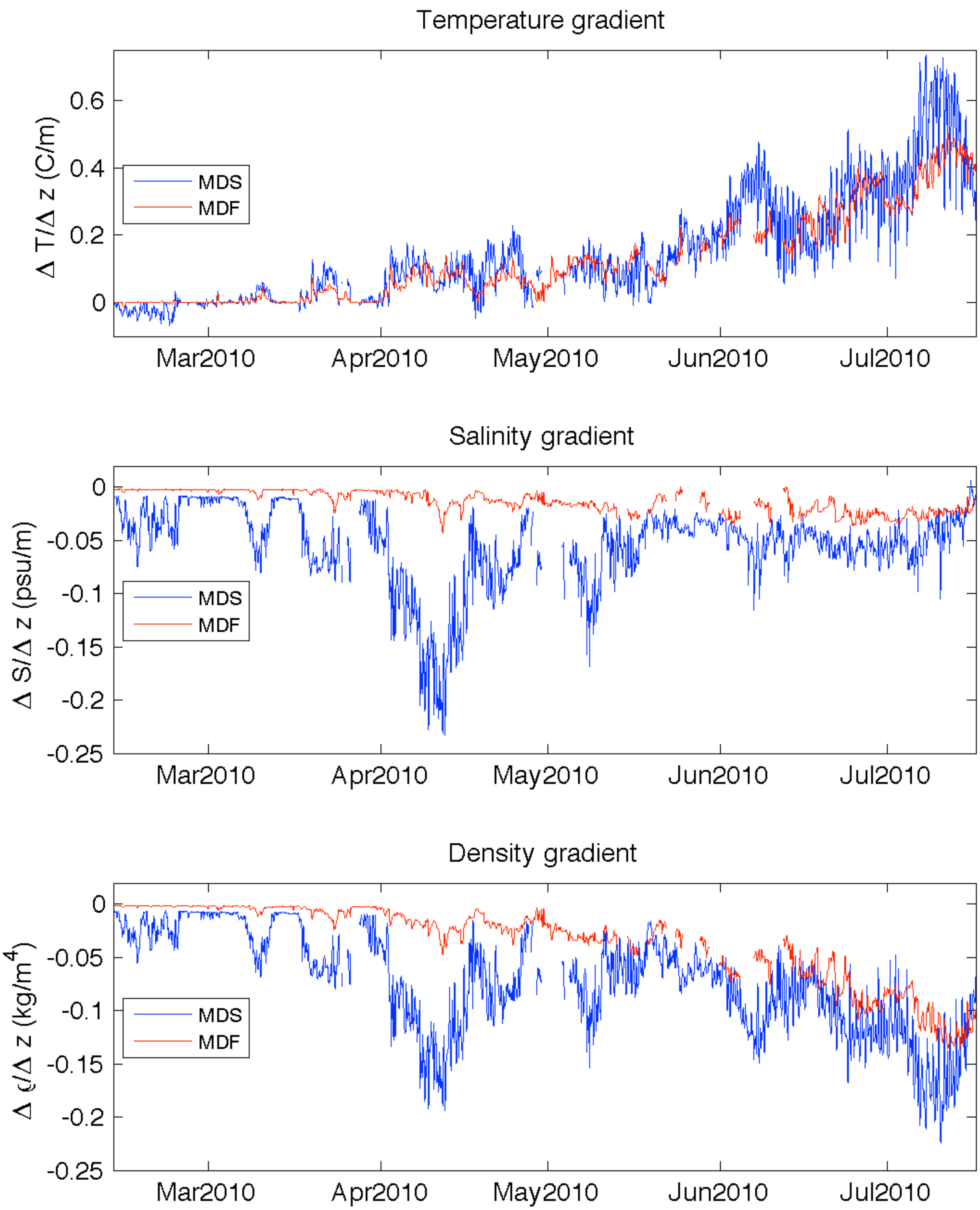

Figure 43. CTD Moorings, Spring/Summer, MD-S and MD-F : Vertical gradients. Differences are computed as the value at 1 m minus the value at 28 m (MD-F) or 18 m (MD-S).

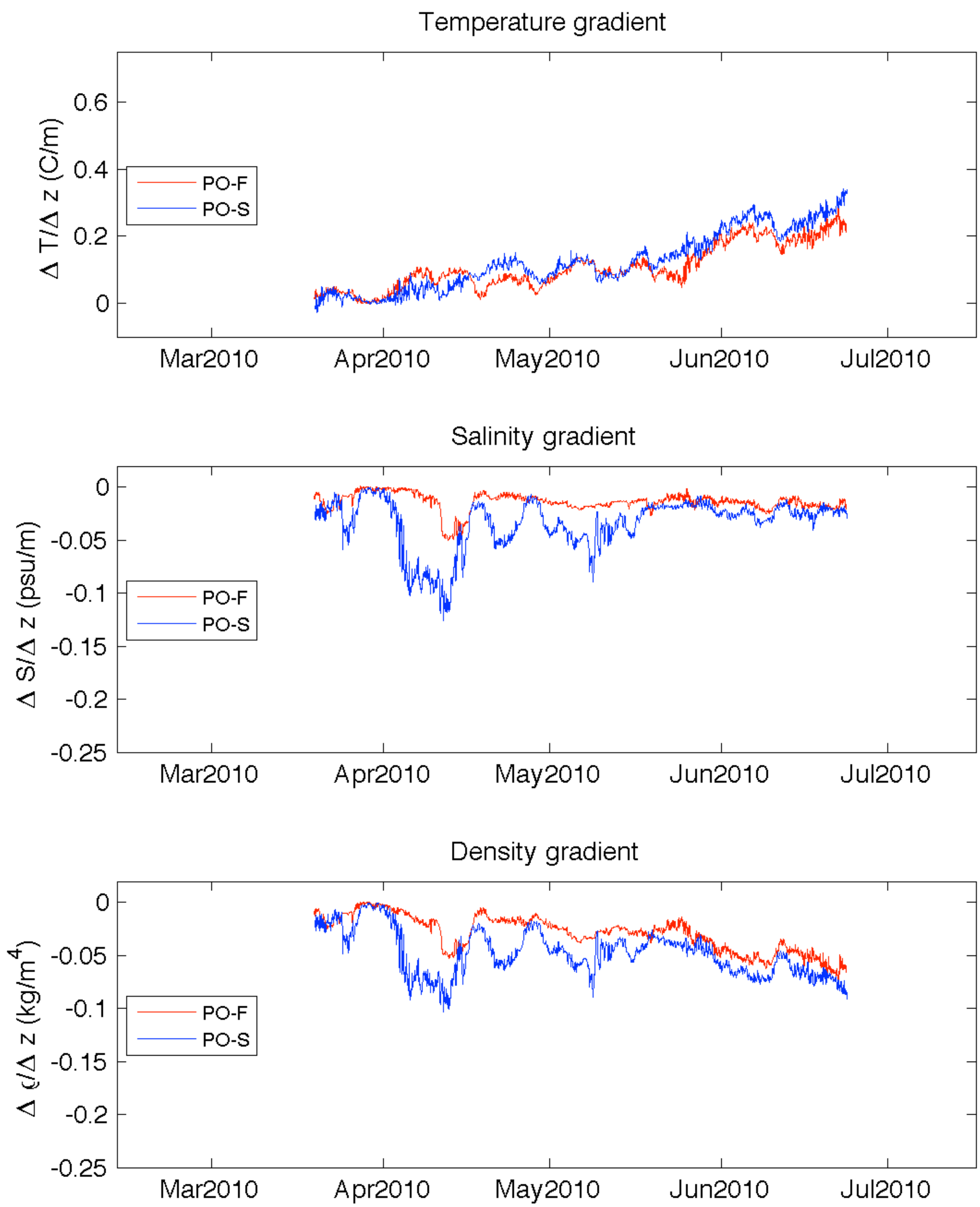

Figure 44. CTD Moorings, Spring/Summer, PO-S and PO-F : Vertical gradients. Differences are computed as the value at 1 m (nominal) minus the value at 35 m (nominal).

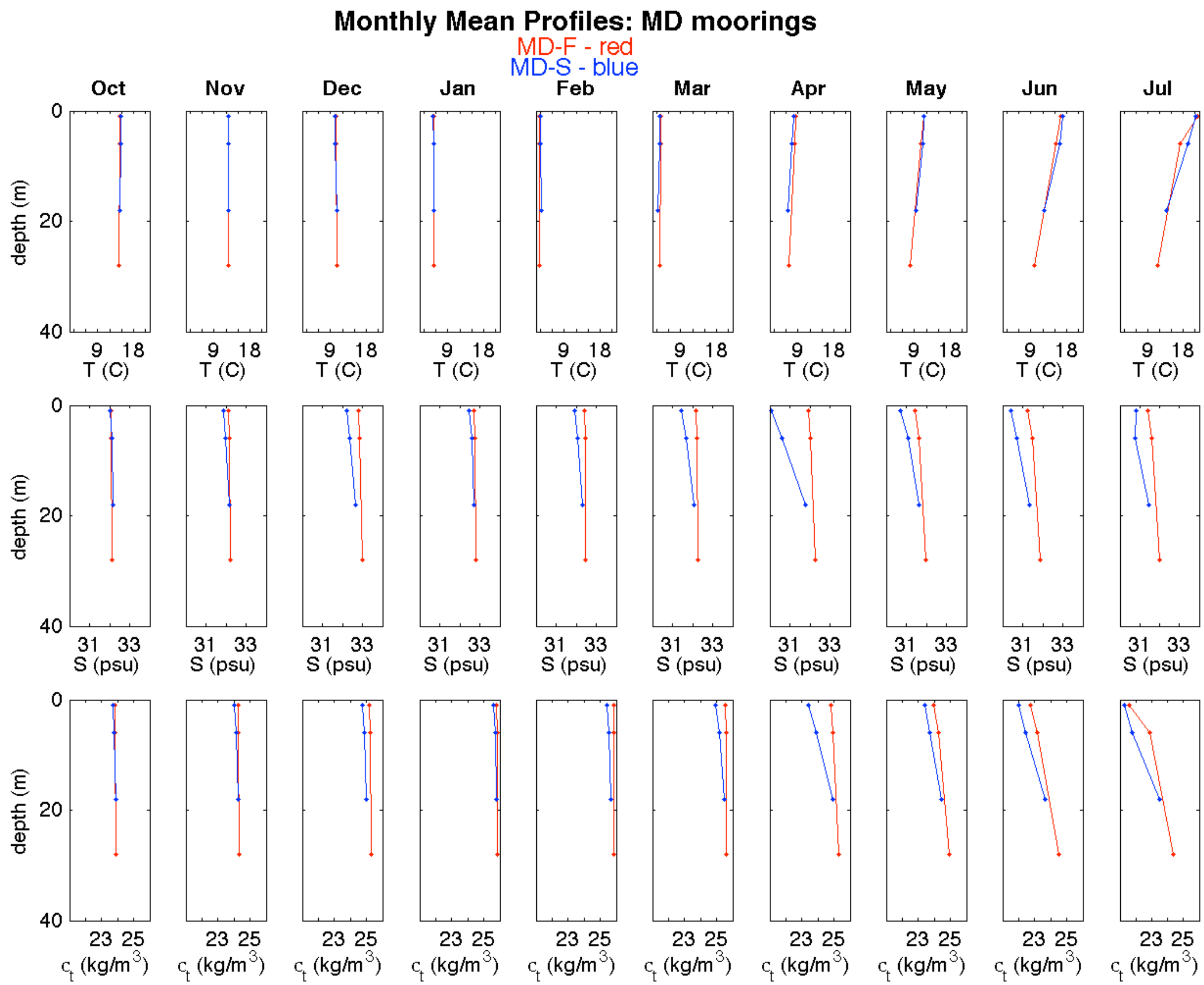

Figure 45. CTD Moorings, monthly-mean vertical profiles, MD-S and MD-F: temp., sal., sigma-t.

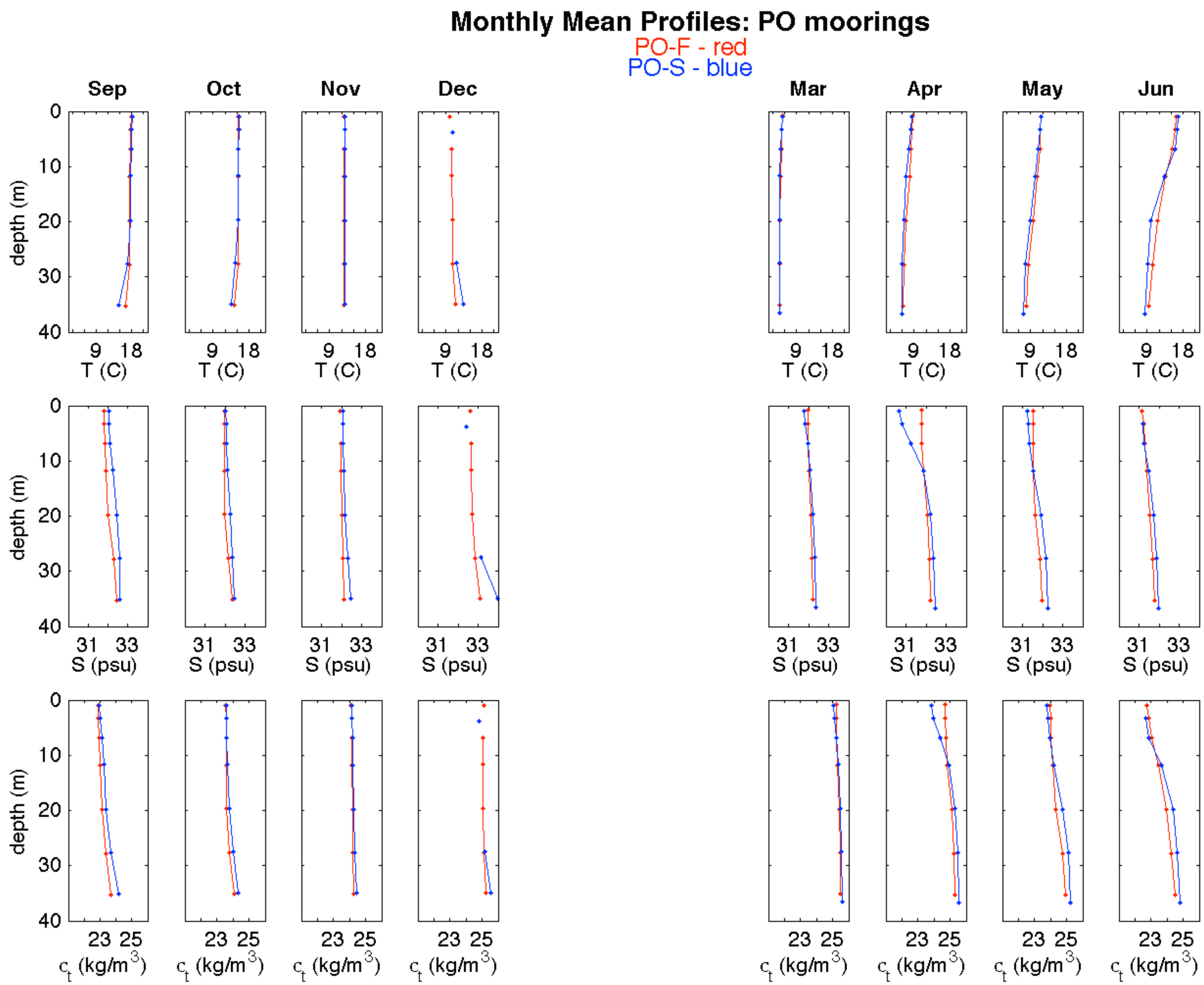

Figure 46. CTD Moorings, monthly-mean vertical profiles, PO-S and PO-F: temp., sal., sigma-t.

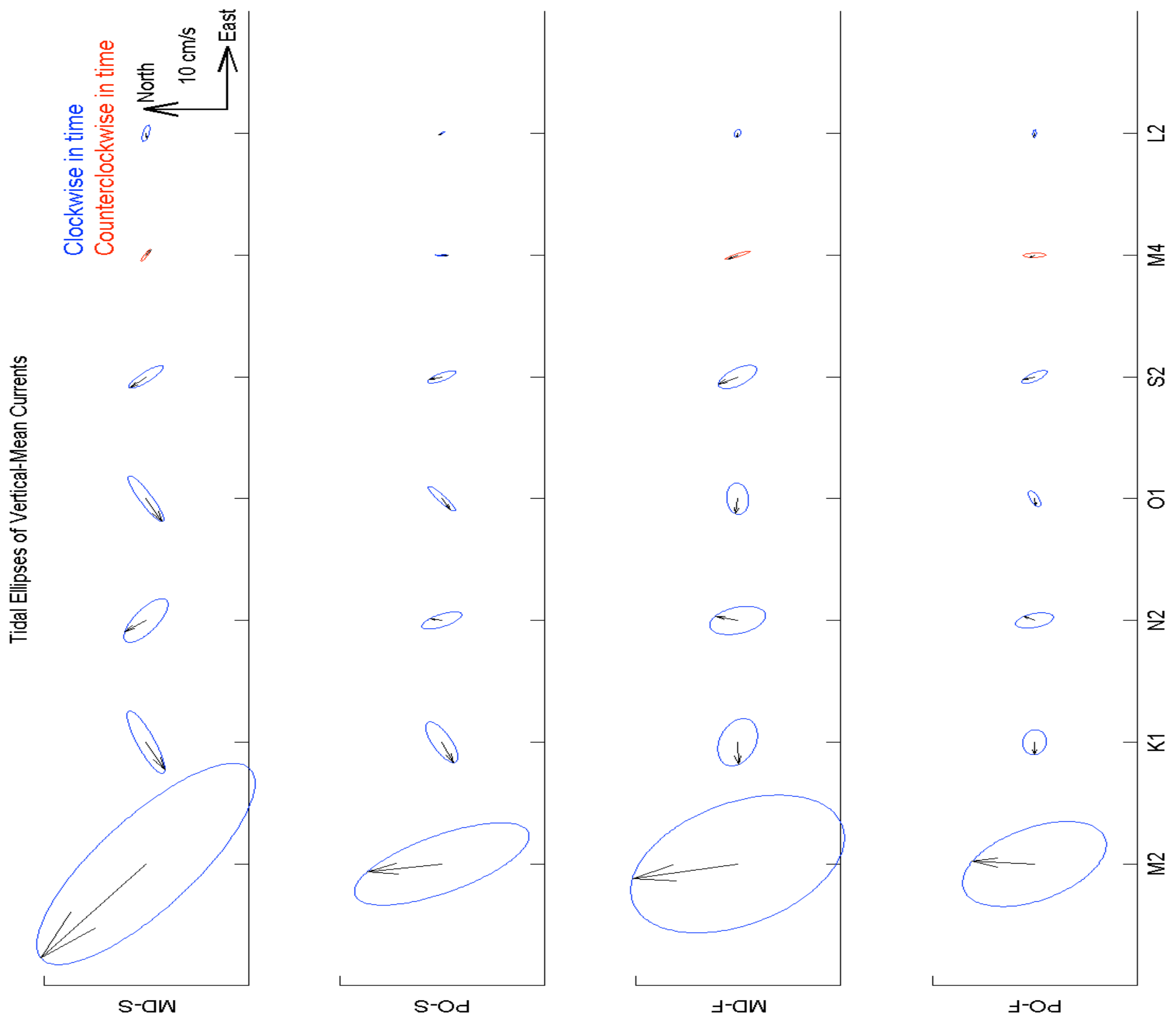

Figure 47. Tidal current ellipses, vertical-mean currents: seven dominant constituents, four sites. Greenwich phase lag is indicated by the instantaneous velocity vector within each ellipse.

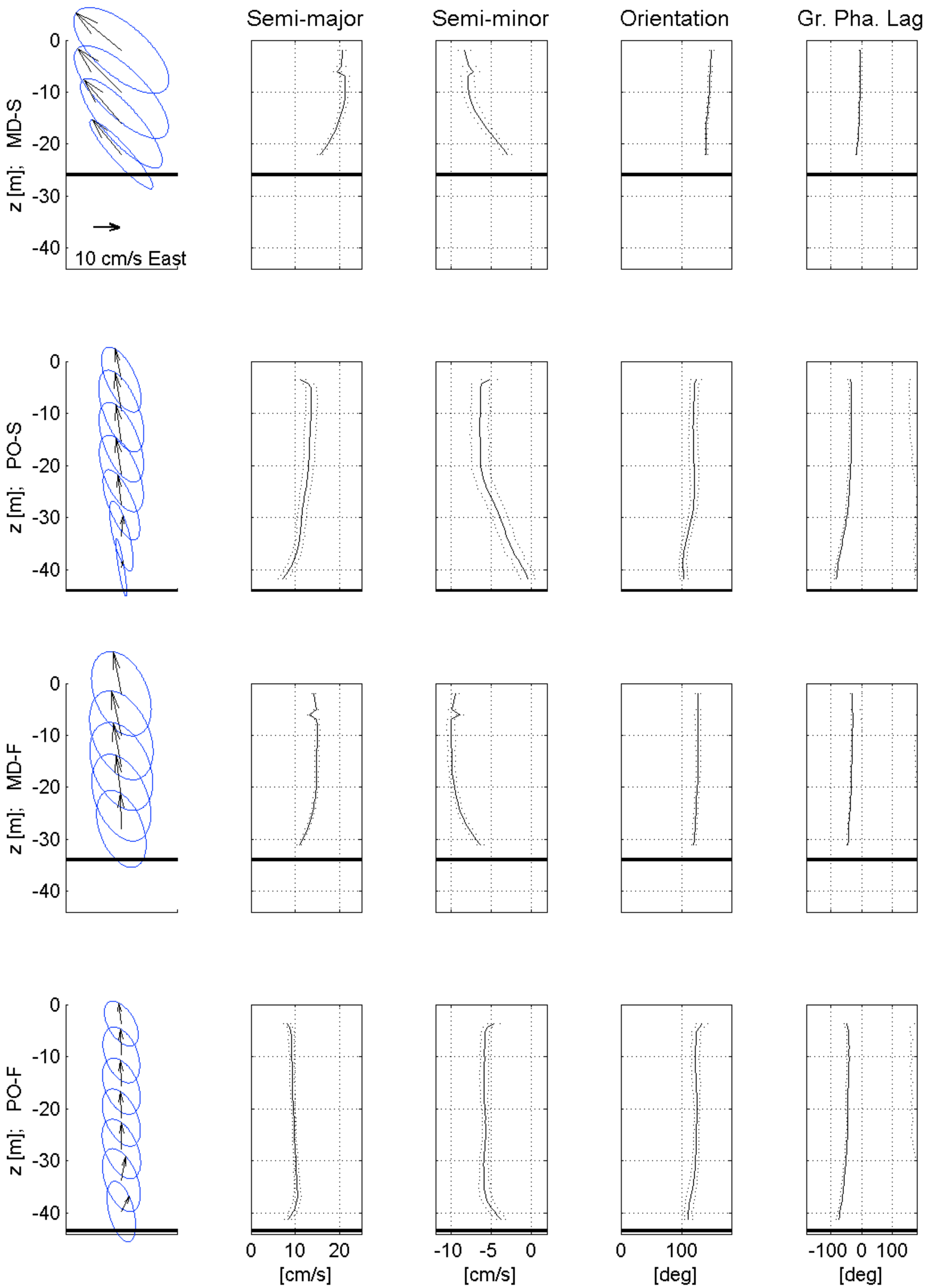

Figure 48. Tidal current ellipses, M_2 constituent, vertical profiles, four sites.

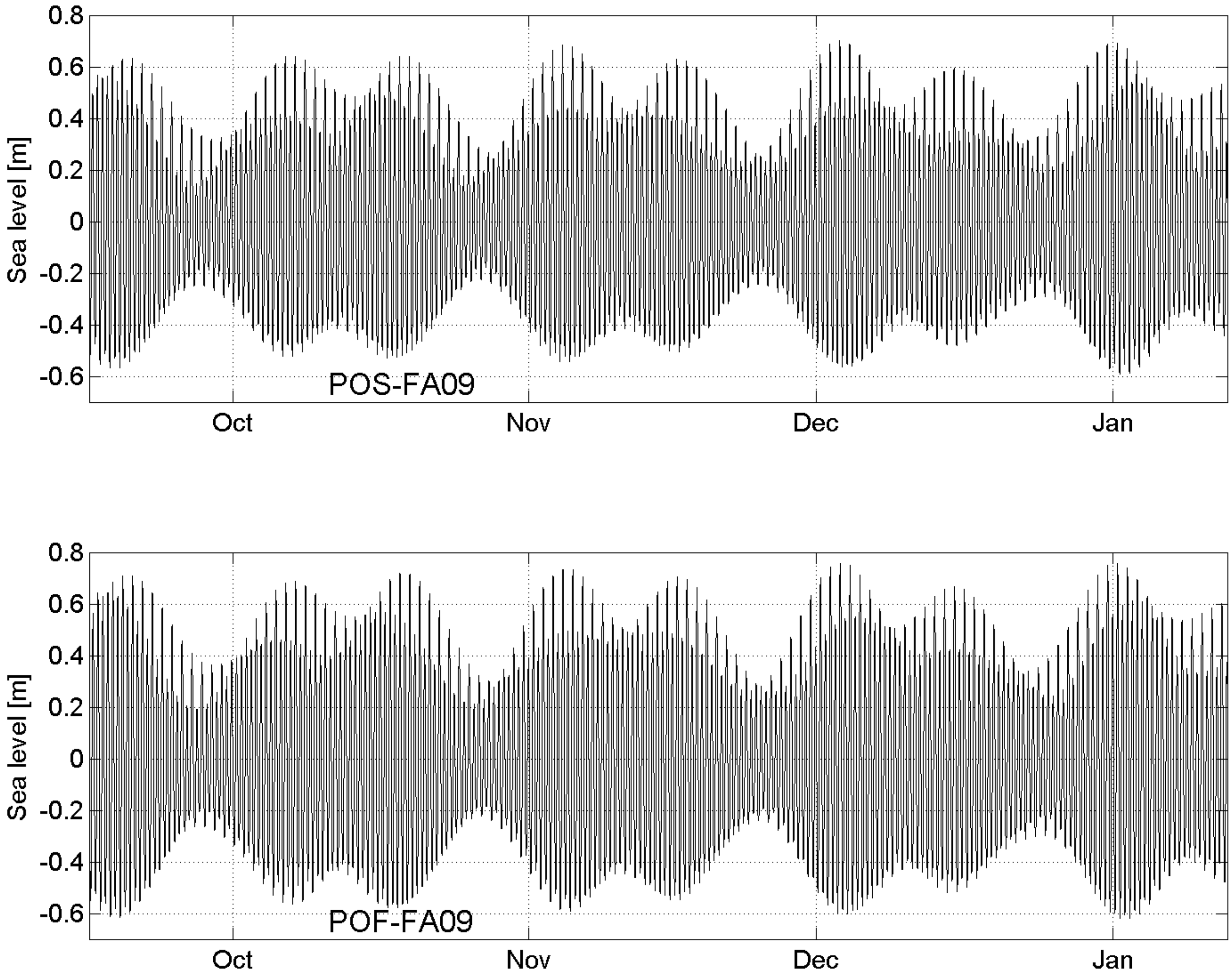

Figure 49. Tidal sea level variations: PO-S (upper) and PO-F (lower).

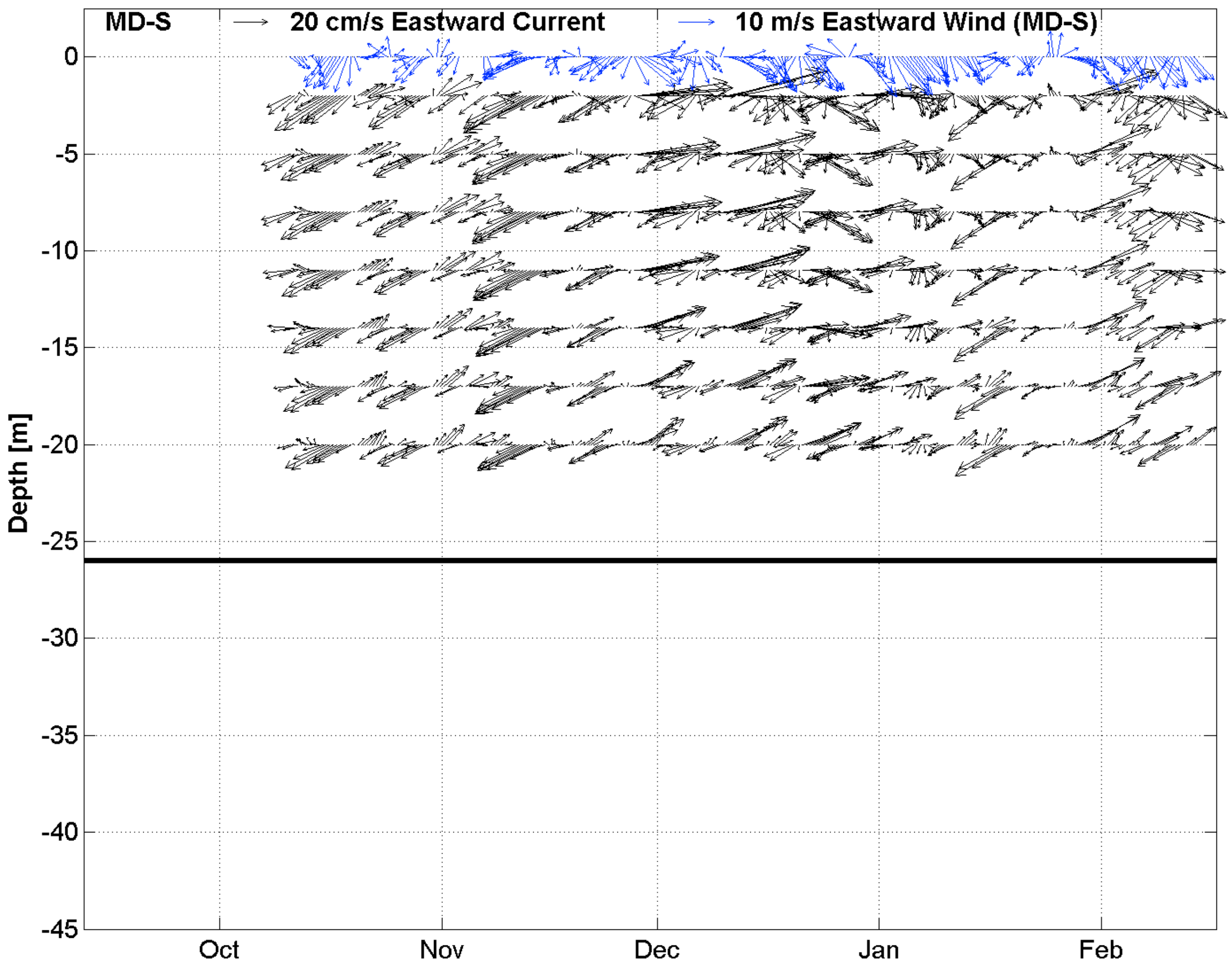

Figure 50. Subtidal currents and winds, MD-S, Fall/Winter.

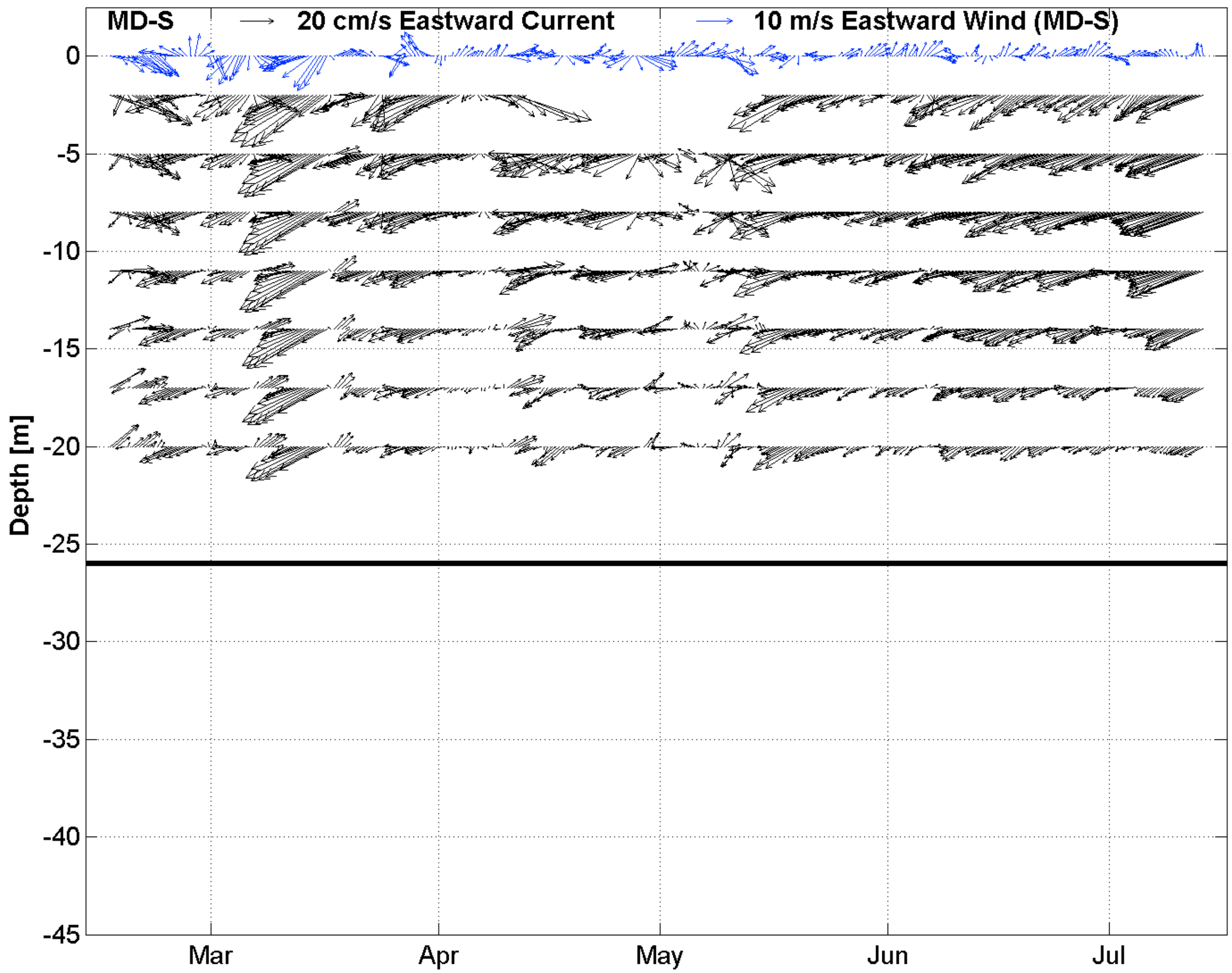

Figure 51. Subtidal currents and winds, MD-S, Spring/Summer.

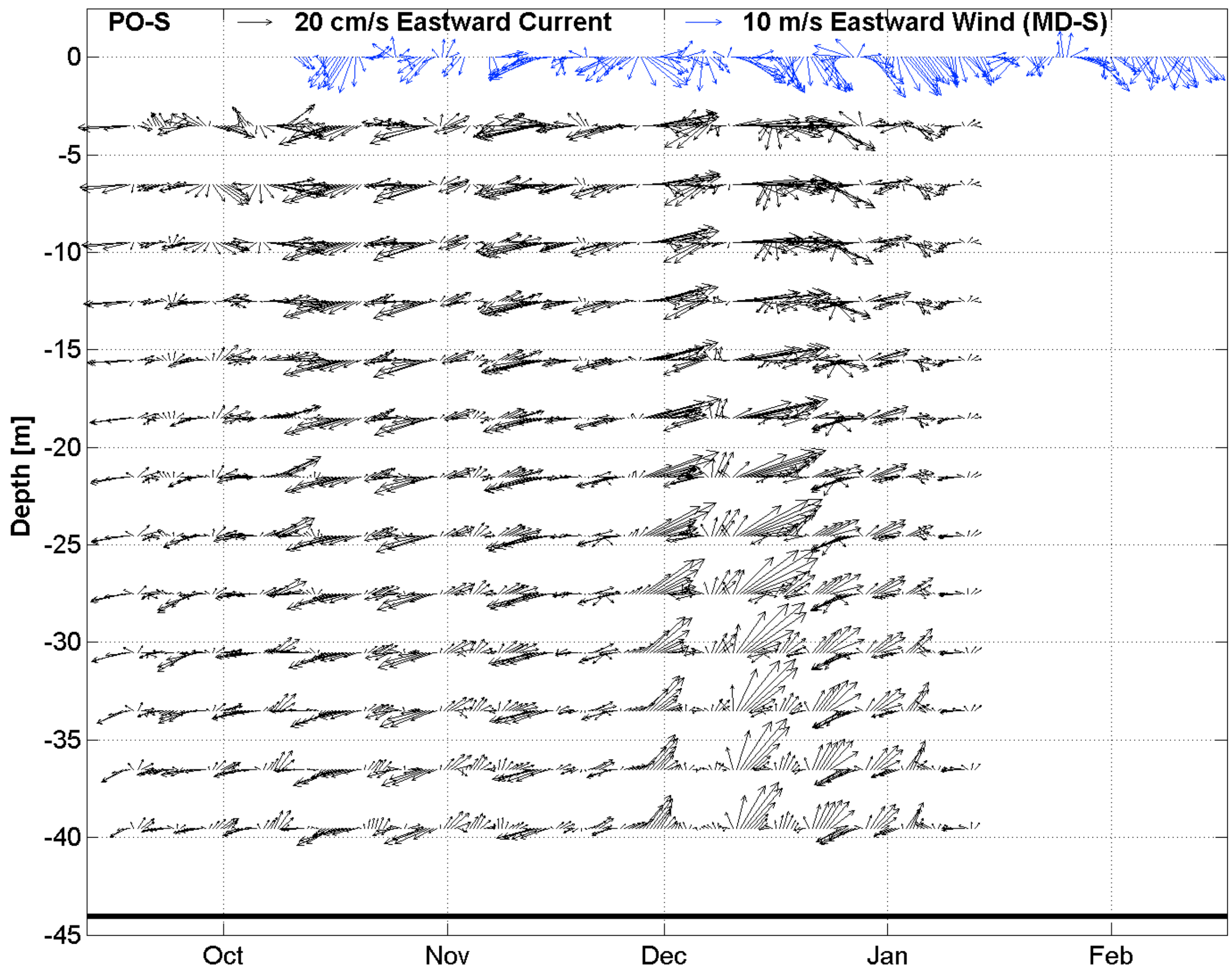

Figure 52. Subtidal currents and winds, PO-S, Fall/Winter.

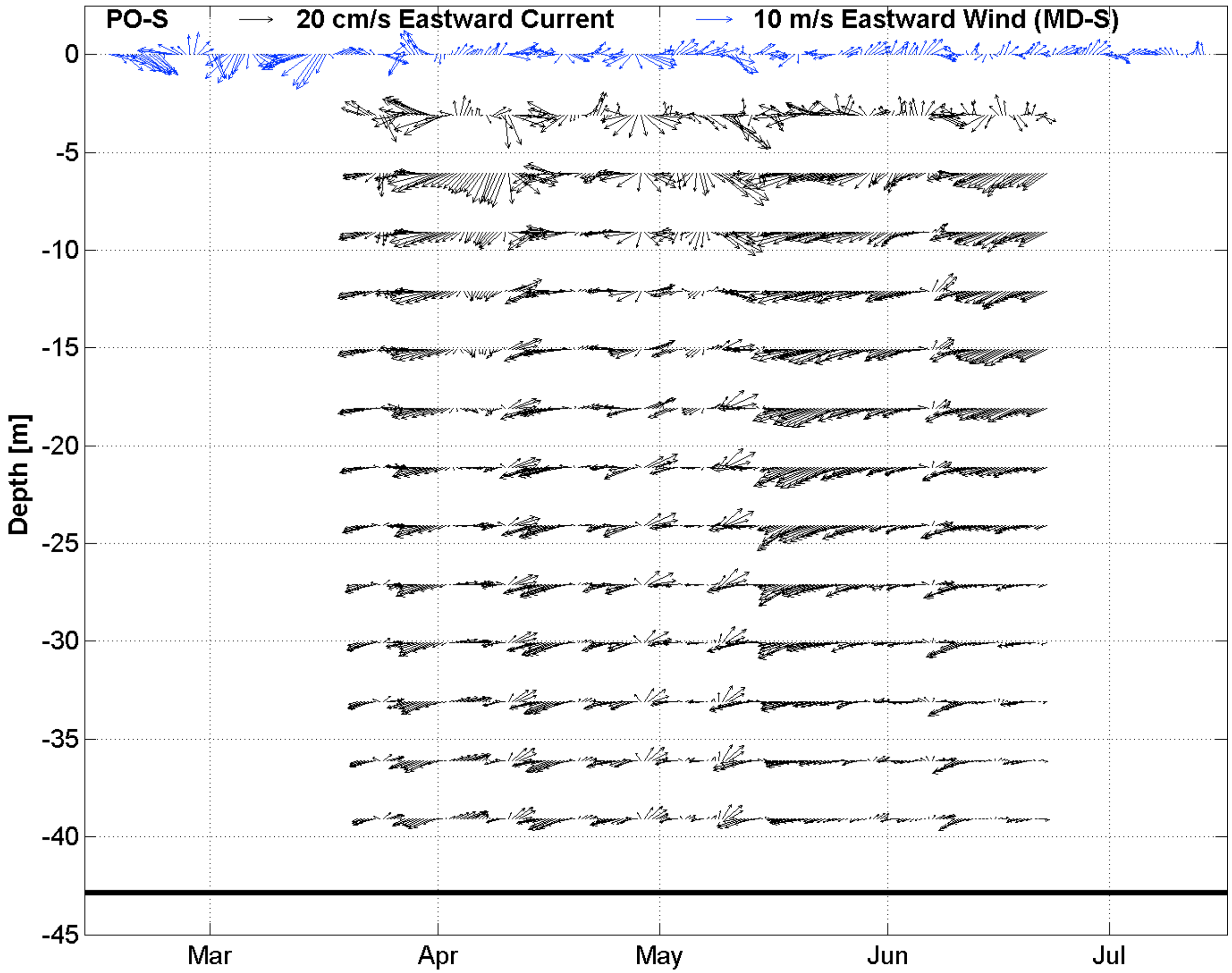

Figure 53. Subtidal currents and winds, PO-S, Spring/Summer.

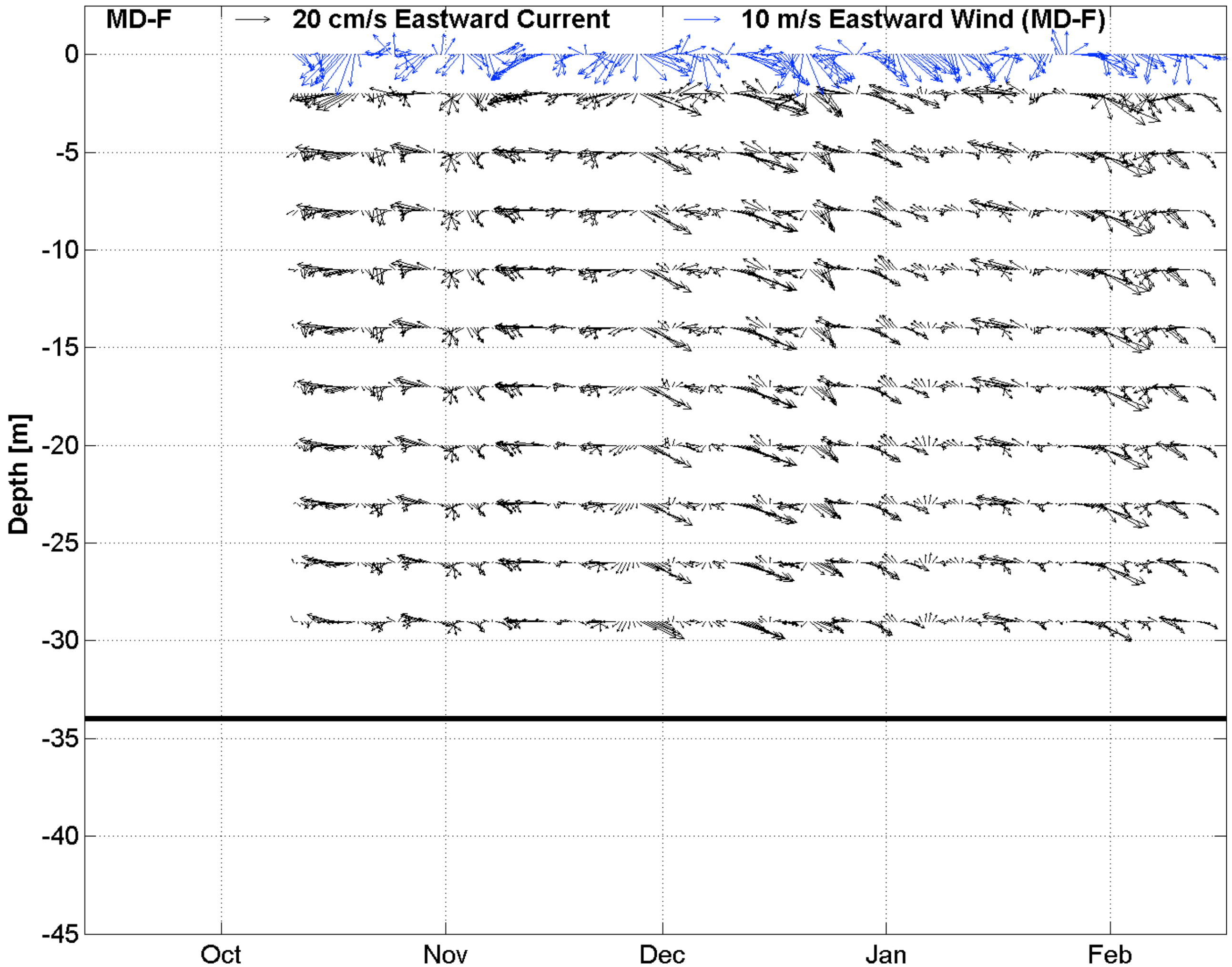

Figure 54. Subtidal currents and winds, MD-F, Fall/Winter.

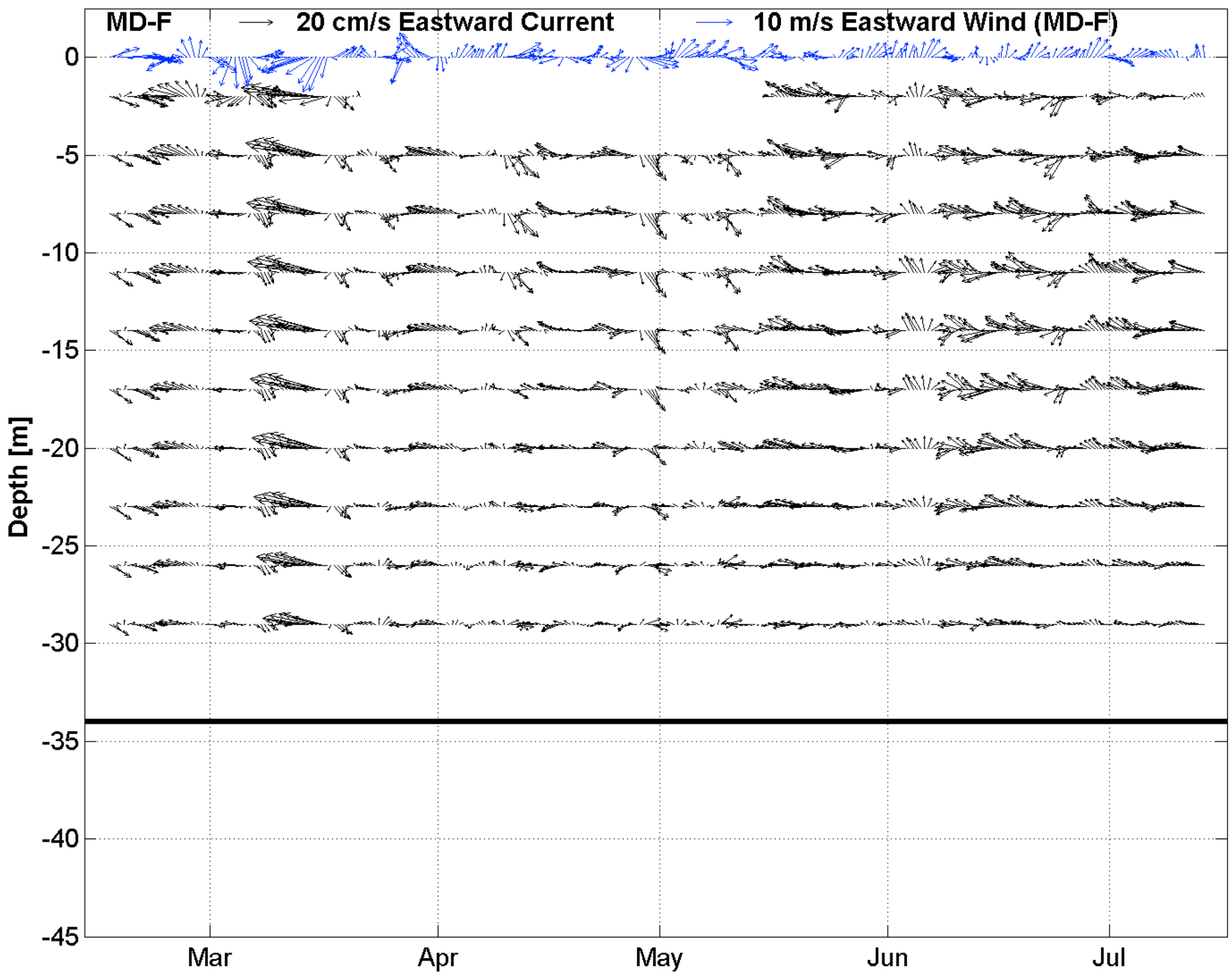

Figure 55. Subtidal currents and winds, MD-F, Spring/Summer.

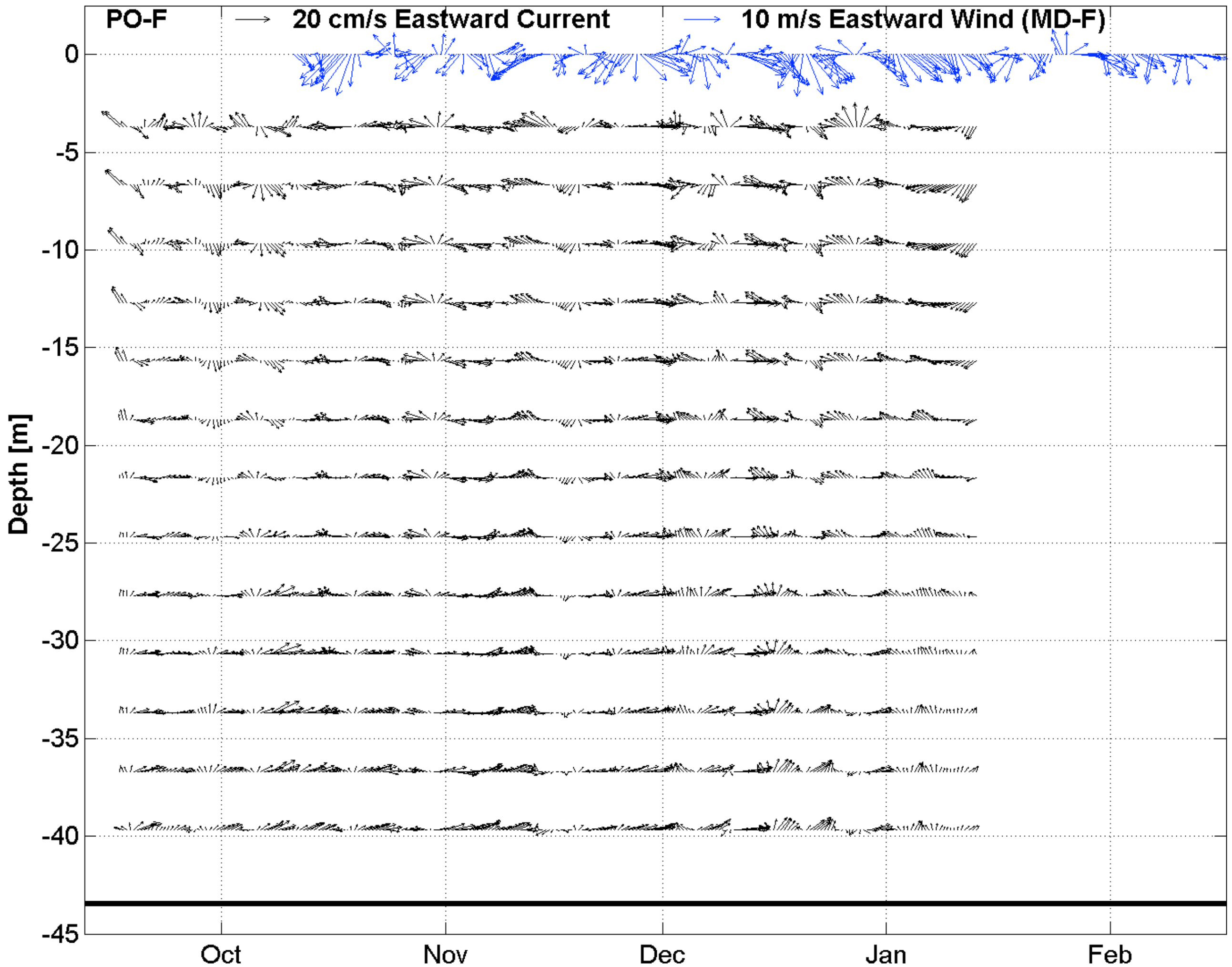

Figure 56. Subtidal currents and winds, PO-F, Fall/Winter.

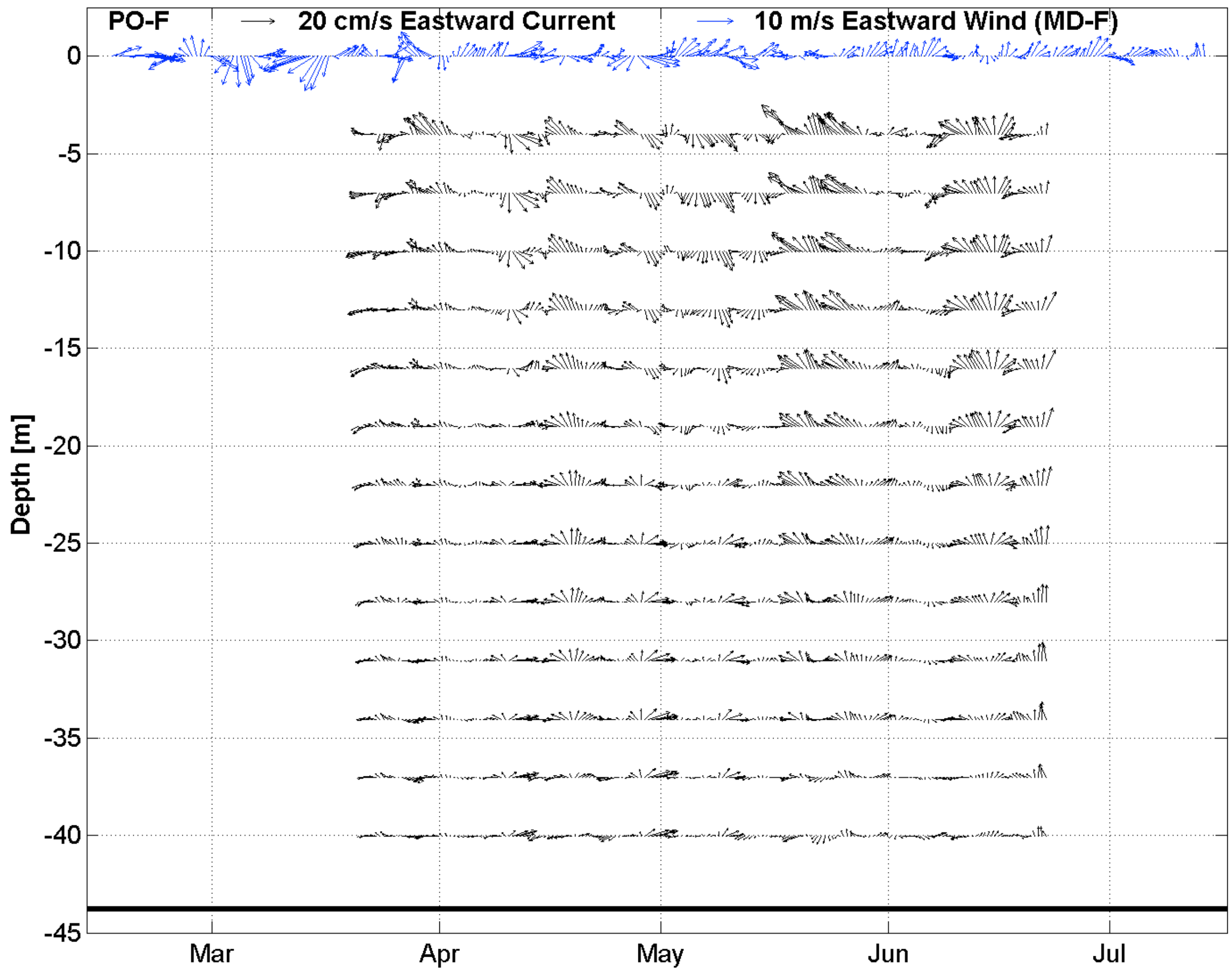

Figure 57. Subtidal currents and winds, PO-F, Spring/Summer.

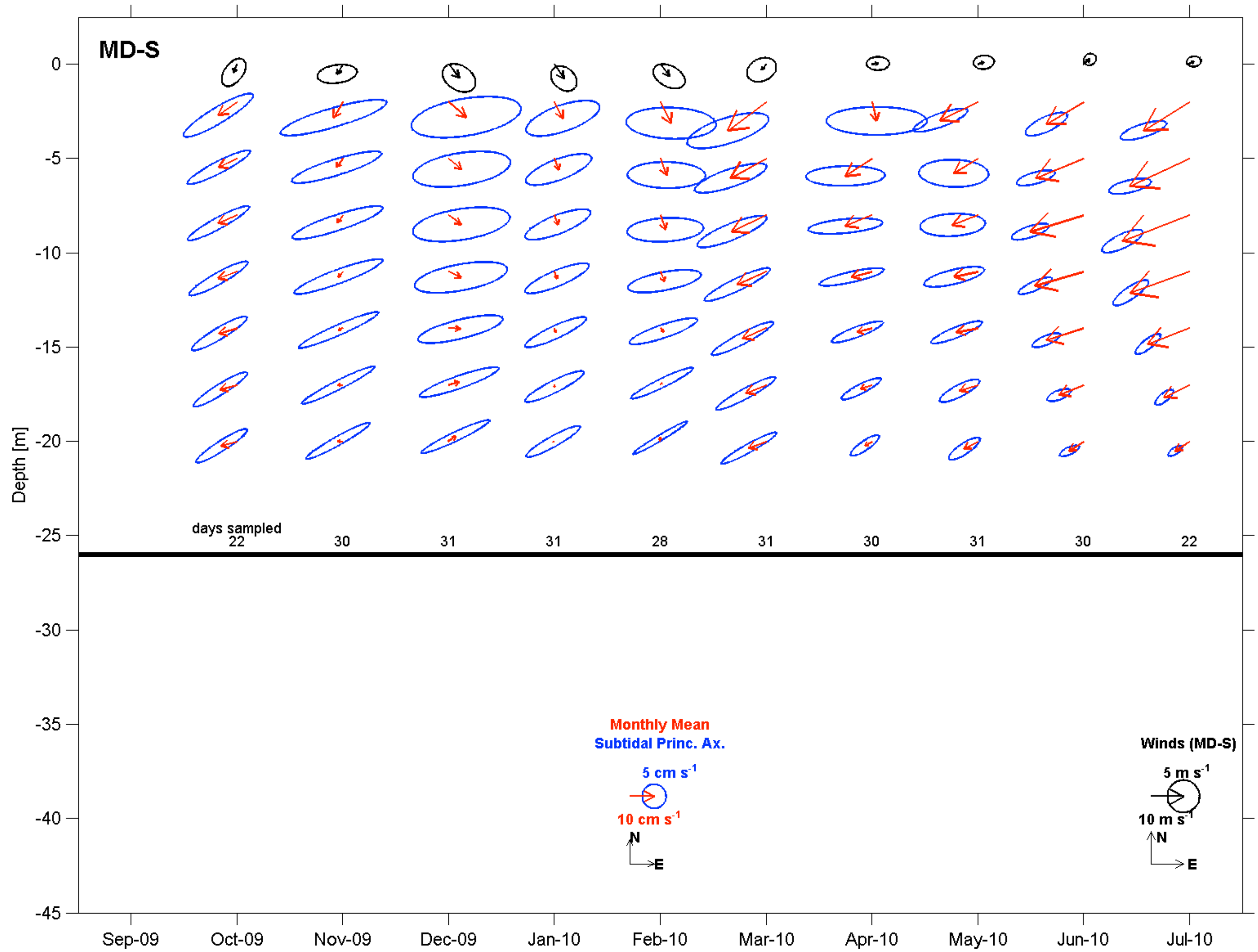

Figure 58. Monthly-mean currents and subtidal principal axes , MD-S, all seasons.

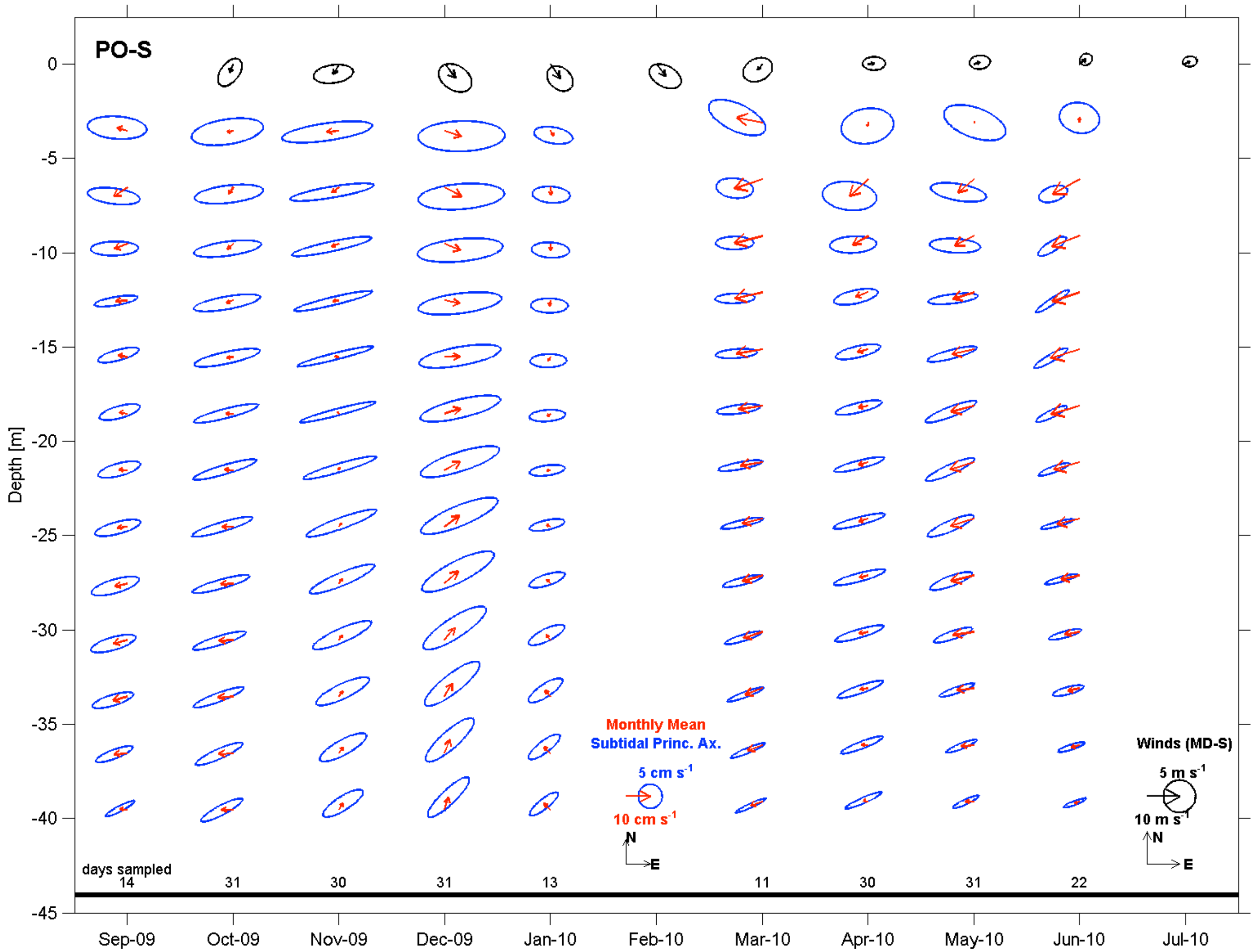

Figure 59. Monthly-mean currents and subtidal principal axes, PO-S, all seasons.

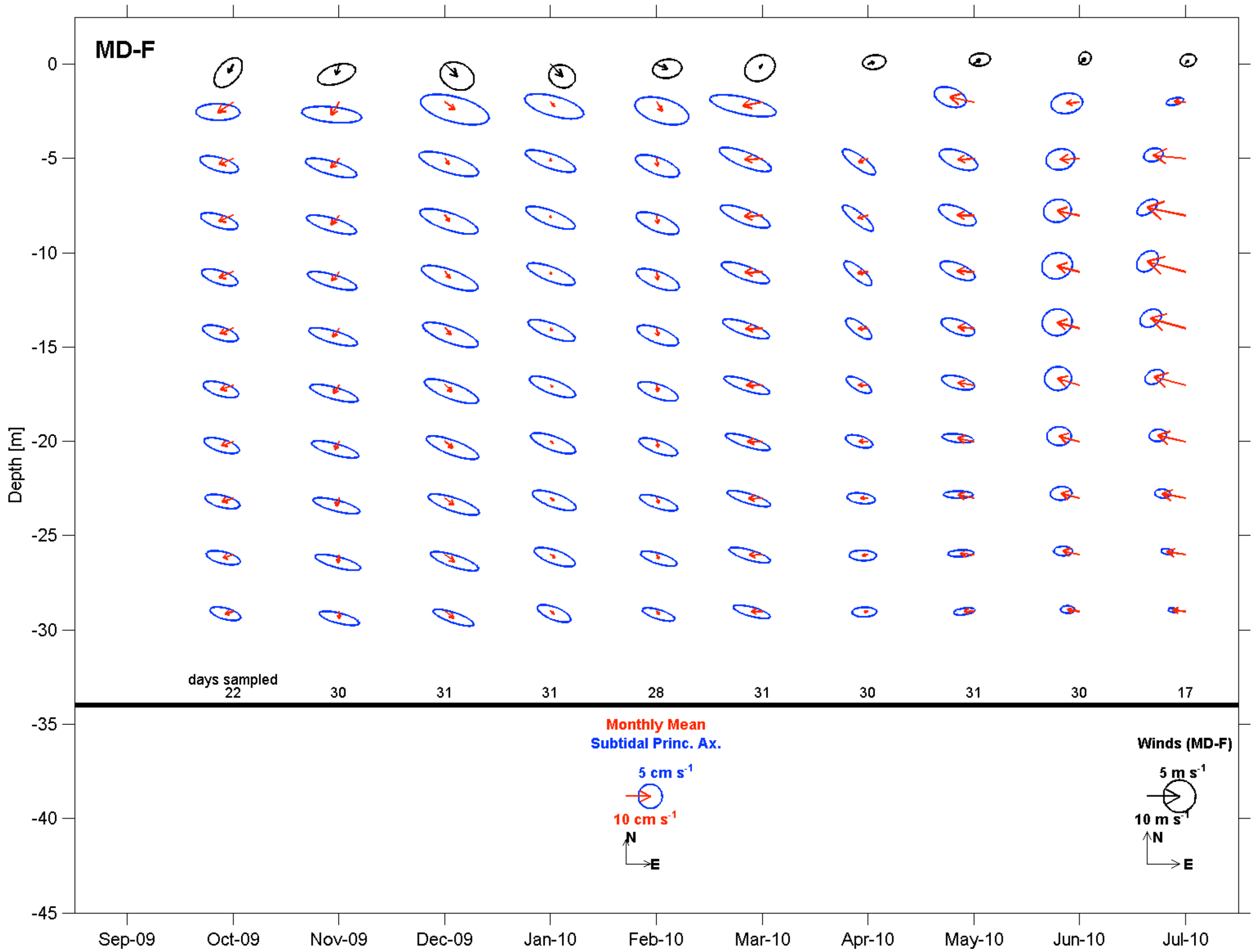

Figure 60. Monthly-mean currents and subtidal principal axes, MD-F, all seasons.

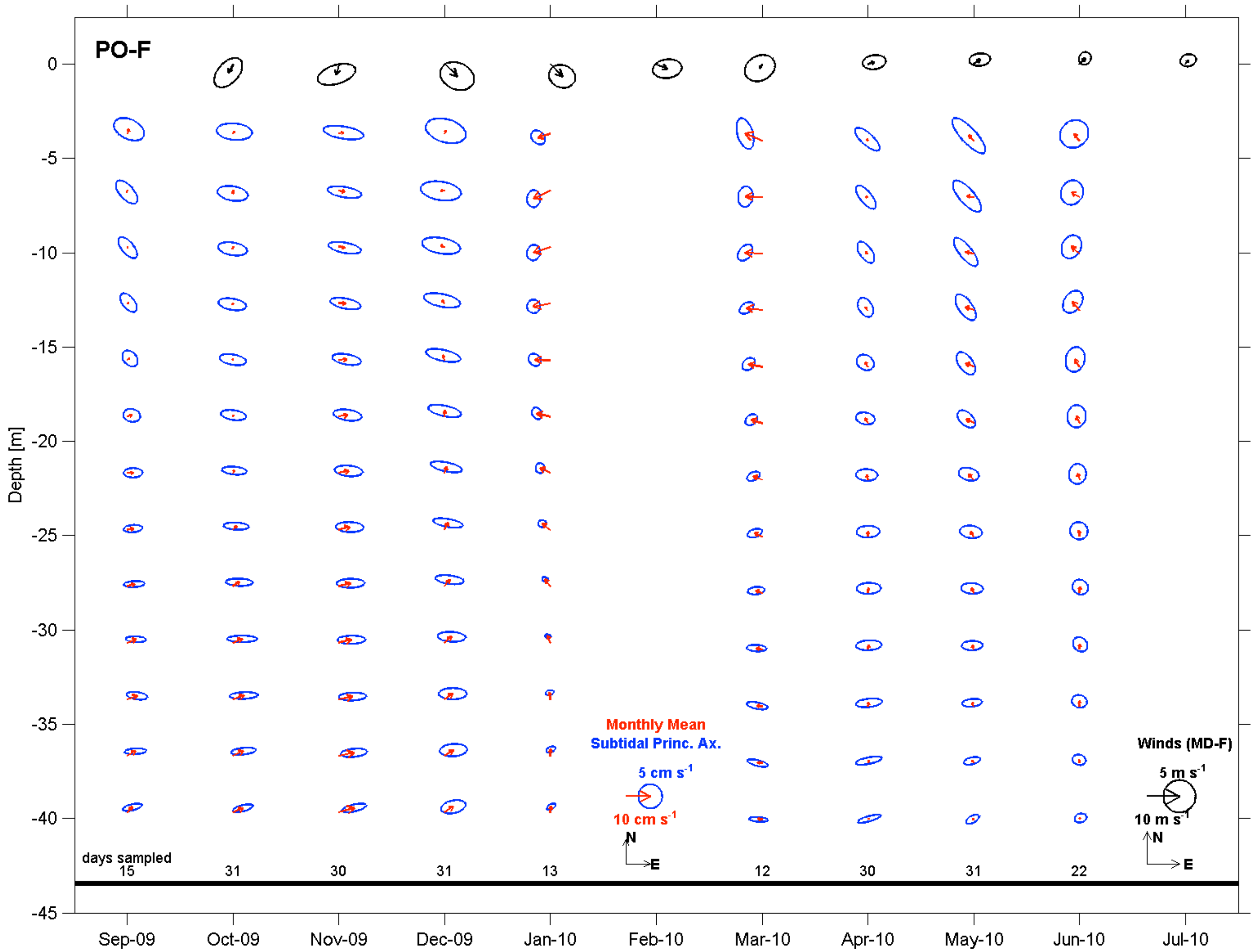

Figure 61. Monthly-mean currents and subtidal principal axes, PO-F, all seasons.

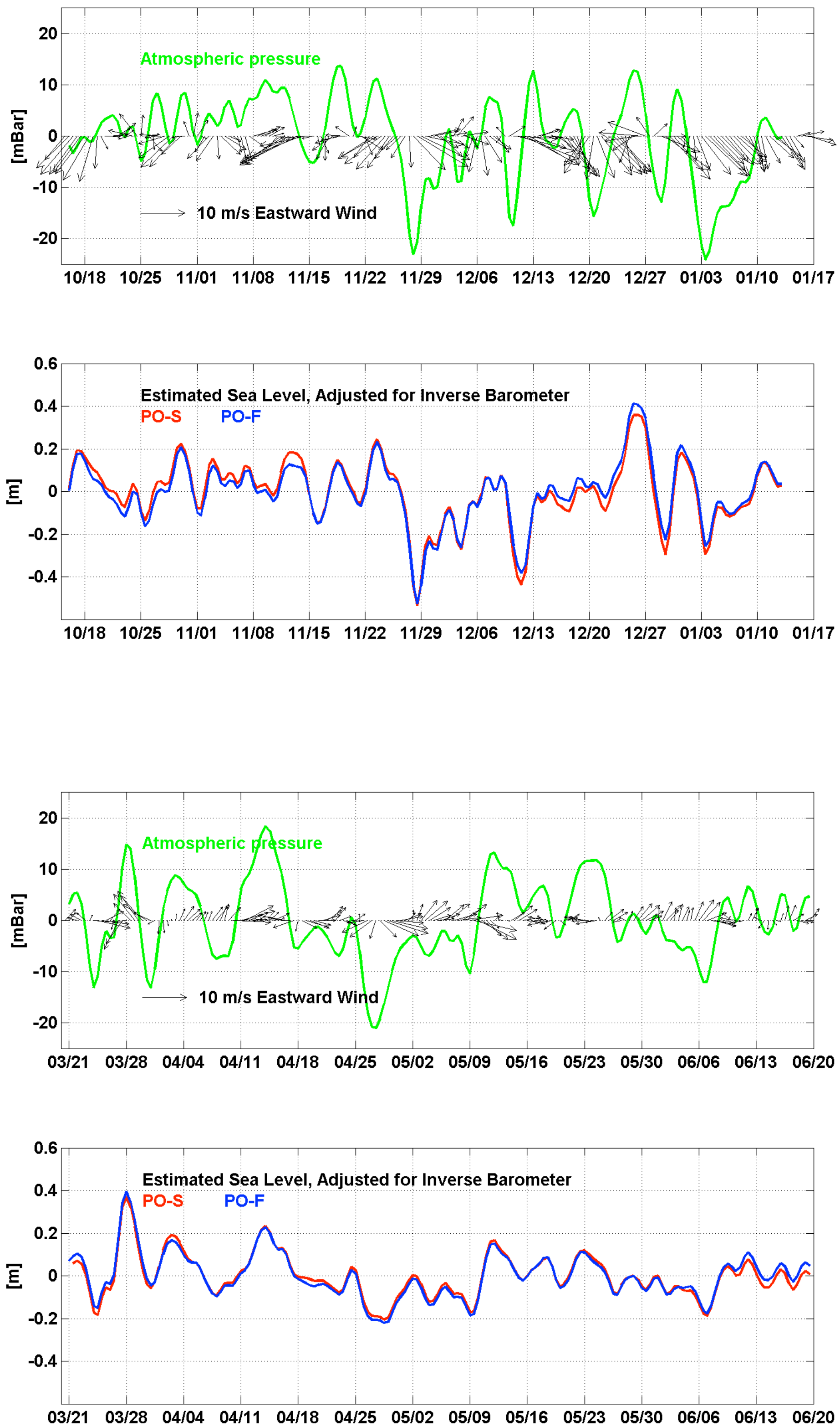

Figure 62. Subtidal Variability, Estimated Sea Level: FA09 (upper); SP10 (lower).

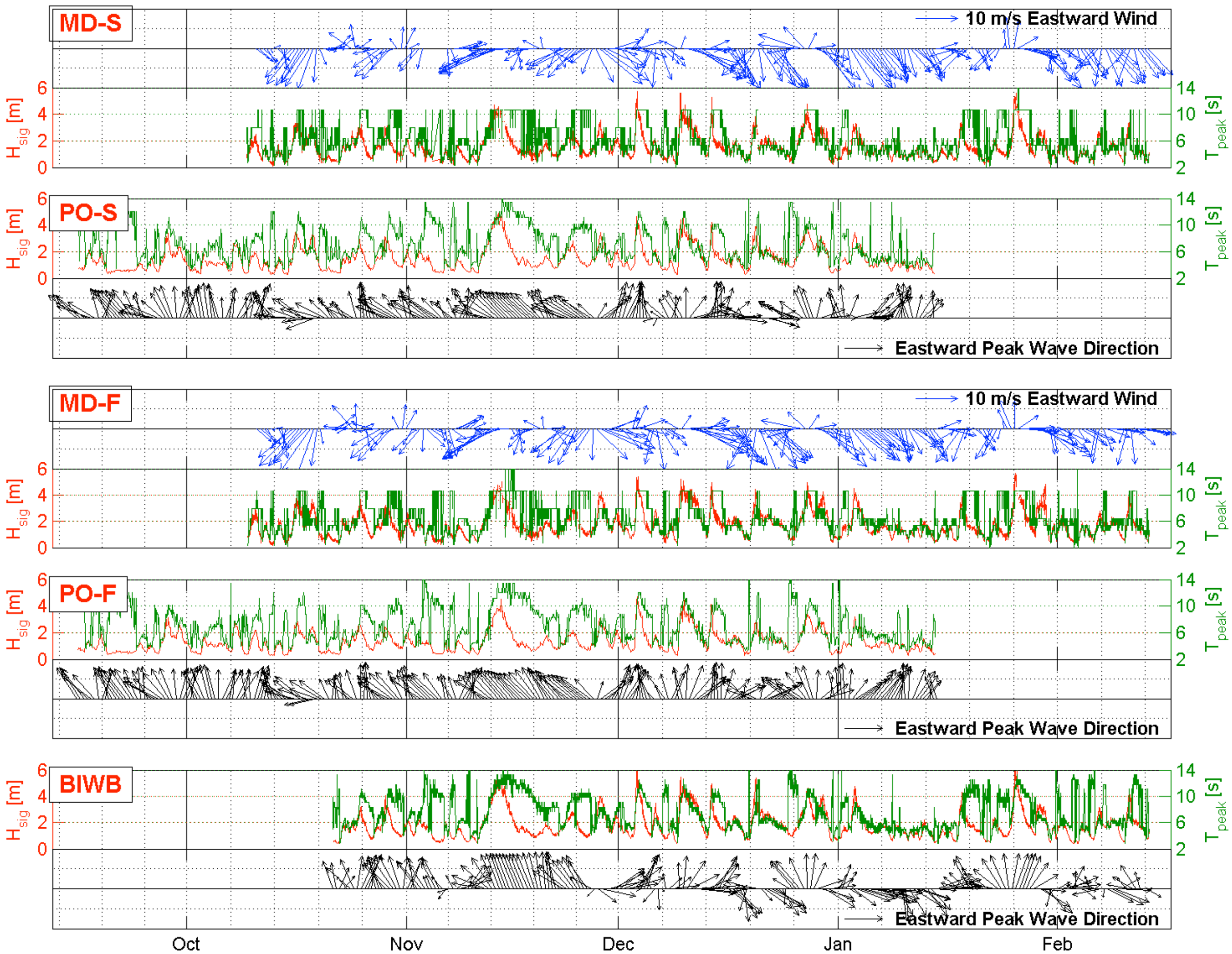

Figure 63. Wave parameters and winds, five sites, Fall/Winter.

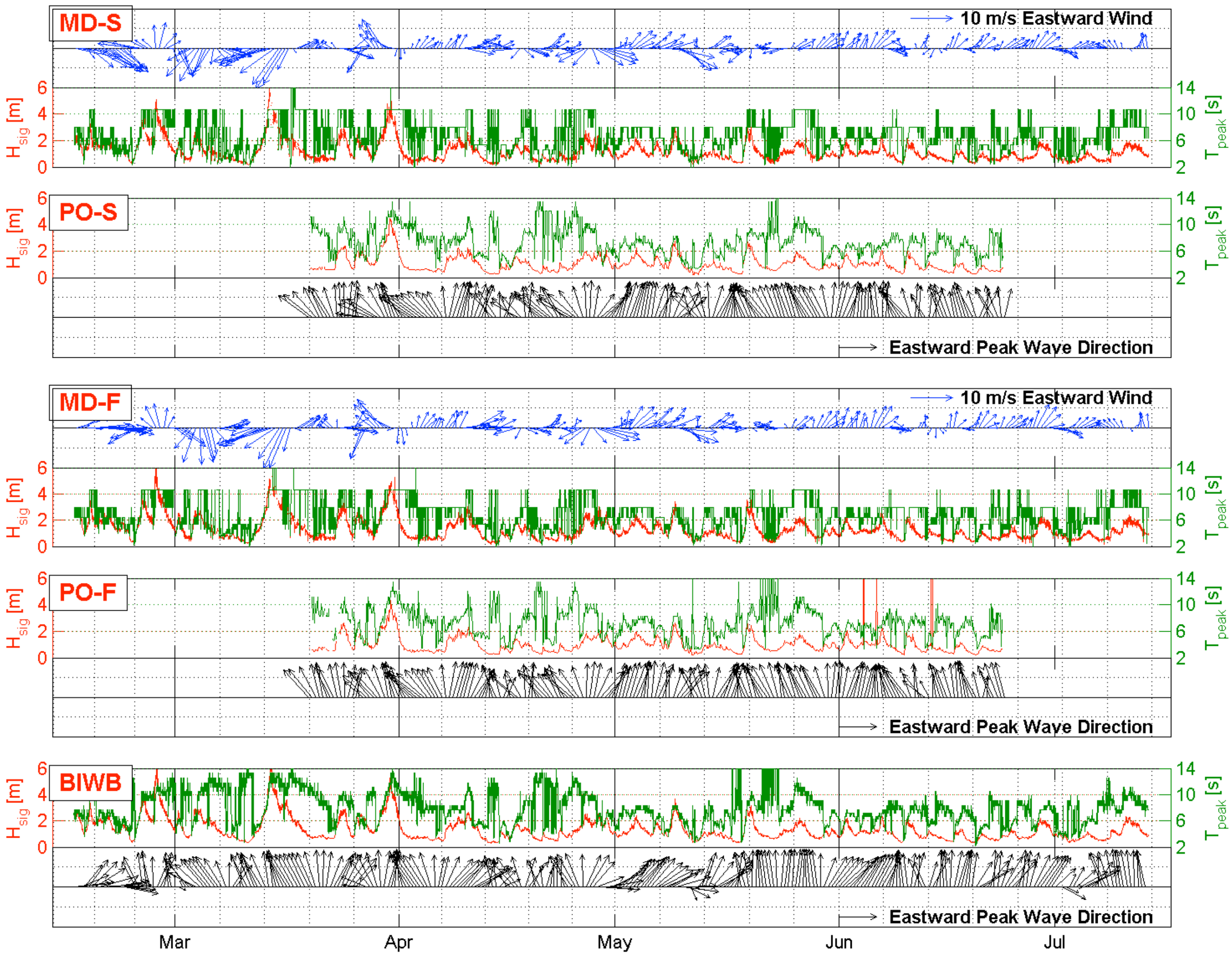

Figure 64. Wave parameters and winds, five sites, Spring/Summer.

This page intentionally left blank.